D 2014

U.PORTO
FEUP FACULDADE DE ENGENHARIA
UNIVERSIDADE DO PORTO

DEVELOPMENT OF NON-CONVENTIONAL CASTING PROCESSES

RUI JORGE DE LEMOS NETO

TESE DE DOUTORAMENTO
DOUTORAMENTO EM ENGENHARIA MECÂNICA
FACULDADE DE ENGENHARIA DA UNIVERSIDADE DO PORTO

Acknowledgments

There were many people and entities who scientifically, financially and emotionally contributed to the realization of this thesis. It is therefore with great pleasure that I express my sincere gratitude to them.

To my late father, wood patternmaker for 49 years, who taught me the foundry fundaments and life values, namely that work is the basis of the life.

To Professor Ana Reis, Assistant Professor at the Faculty of Engineering of Porto who is a big friend and was the main driving force and the first responsible for the presentation of this thesis

To Professors Jorge Lino, Associate Professor at the Faculty of Engineering of Porto University, and Professor Teresa Duarte, Assistant Professor at the Faculty of Engineering, for the motivation and tireless support. I also thank the confidence that always placed in my work, but above all, I thank the friendship always demonstrated.

To Professor Antonio Torres Marques, Full Professor at the Faculty of Engineering of Porto, the numerous attempts, often frustrated, immovable and constantly renewed to take this work forward.

To Professor António Barbedo de Magalhães, Professor Emeritus already retired, my true master and great friend, the tireless attempts to get me to take this work forward and the unshakable confidence that for 34 years always placed in me.

To all my students, especially the ones who intervened in these teamwork the kindness with which they heard me, and especially what they taught me.

To my family, the incentives they gave me, the patience when they were deprived of my company and especially how joyfully they faced the formalization of this work, probably more than me.

To INEGI, INEGI managers and whole team, particularly foundry team, I express my gratitude for the availability, knowledge and sharing determinant ideas for the implementation of this work. I also thank the kindness and warm words of support always given to me.

To the Zollern and Comandita company, his General Manager Virgilio Oliveira and large whole team involved in the R&D projects, for putting the challenges, believing in INEGI and funding the projects.

To the entities that financially funded the R&D Projects that supported this research work: SAESCT-PII&DT/1/2011 Structural Program co-financed by CCDRN and QREN; TOOLING EDGE Mobilizer Project co-financed by ADI and QREN; HYPERTURB, COMPINTEGRA and COMTICAST Co-Promotion Projects co-financed by ADI and QREN; AEROVAC and MEDCAST Individual Zollern Projects co-financed by IAPMEI and QREN.

Abstract

Despite the big interest of reactive titanium alloys and titanium aluminides, due to the enormous benefits brought to the automotive, aircraft and aerospace industry by the introduction and components in these alloys for medium to high temperature applications, the processing of these alloys is still of high complexity and difficulty.

In this work, innovative processes have been developed for melting and pouring of these alloys. These developments also tackled the problem of the reactivity with refractory shells used in the investment casting of titanium alloys and titanium aluminides, as well as the rheological behavior of refractories used in the manufacture of shells for nickel alloys.

In this context, new solutions for melting and pouring titanium alloys using initially ceramic crucibles and at the end the cold skull induction melting were developed.

The first solution promoted high overheating and high filling capacity of the molds but did not guarantee the melting with acceptable contamination of conventional titanium alloys. The second solution aimed to decrease the oxygen content of titanium alloys caused by metal-refractory reactions during melting in ceramic crucibles. Nevertheless, the cold crucible solution imposed restrictions to overheating that decreased filling capacity. The global solution consisted on the development of a system using cold crucible and counter gravity with differential pressure pouring to overcome thickness limitations.

Furthermore, ceramic crucibles for casting applications of titanium aluminides and other reactive alloys have been investigated, namely its chemical formulations and manufacturing techniques. Moreover, these alloys (i.e., titanium alloys and titanium aluminides) are highly reactive in the liquid state, which lead to the formation of a hard and cracked layer rich in interstitial elements such as oxygen on the surface of the castings products, as a result of the chemical reduction of ceramic shells's "facecoat" by liquid titanium, called "α-case".

Within this work, an extensive study of the chemical formulations of face coats of ceramic shells for casting a particular gamma titanium aluminide was performed. In

opposition to conventional titanium alloys, it was demonstrated that liquid TiAl do not react very much with zirconia and zircon based slurries

Regarding fluidity, best filling capacities were obtained with coarser “face coat” flour, centred at ≤200 mesh, probably due to its better permeability.

Cheapest common compositions like zircon (SZ) can be used to obtain TiAl castings but about 0.3mm thickness must be removed by some finishing processes like chemical milling.

Best compositions for face coats shells are based on Y_2O_3 (AY and AAFY). In these cases, if necessary, the thickness to remove will be around 0.2 mm.

A good and economically solution can be obtained using medium price zirconia based face coats (AFZr) which can be improved using some low cost fine yttria not fused (AFZrYC).

Future work must be accomplished in order to confirm grain size influence on permeability and fluidity, study of cooling conditions before remove the castings from the controlled atmosphere furnace, in order to confirm the influence of thermal effect of air on surface hardening of the castings.

To support developing process, computational tools were used within the research group, which entails appropriate numerical models and digital systems. These advances, along with experiments and measurement operations, have speeded up the whole process of development regarding mold architecture.

Lastly, and taking advantage of the knowledge obtained in investment casting of titanium alloys, a methodology for the design and manufacture of custom-fit titanium prostheses based on the medical images manipulation has been developed. The proposed approach for manufacturing metallic prostheses has also been applied with success to produce extra-oral soft-tissue prostheses in silicone.

Keywords: Non-conventional casting processes, Melting and pouring of reactive alloys, Ceramic formulations, Numerical tools, Custom-fit titanium prostheses, Extra-oral soft-tissue prostheses in silicone.

Resumo

Apesar dos enormes benefícios trazidos para a indústria automóvel, aeronáutica e aeroespacial pela introdução de peças e componentes em ligas reativas de titânio e aluminetos de titânio para solicitações a altas temperaturas, o seu processamento é de elevada complexidade e dificuldade.

Neste trabalho, foram desenvolvidos processos inovadores para a fusão e vazamento destas ligas. Estes desenvolvimentos também abordaram o problema da reatividade com carapaças refratárias utilizadas na fundição de precisão de ligas de titânio e aluminetos de titânio, bem como o comportamento reológico dos refratários utilizados no fabrico de carapaças para ligas de níquel.

Neste contexto, novas soluções para a fusão e vazamento de ligas de titânio foram estudadas utilizando inicialmente cadinhos cerâmicos e por último cadinhos frios de fusão por indução. A primeira solução promoveu um elevado sobreaquecimento e um aumento da capacidade de enchimento dos moldes, todavia não garantiu a fusão de ligas de titânio convencionais com uma contaminação aceitável. A segunda solução destinou-se a diminuir o teor de oxigénio nas ligas de titânio causado por reações refratário-metálicas durante a fusão em cadinhos cerâmicas. No entanto, a solução de cadinho frio impôs restrições de sobreaquecimento, o que fez diminuir a capacidade de enchimento. A solução global consistia no desenvolvimento de um sistema utilizando cadinho frio em contra-gravidade com pressão diferencial de vazamento para superar as limitações da espessura.

Além disso, cadinhos cerâmicos para aplicações de fundição de TiAl e outras ligas reativas têm sido investigados, nomeadamente as suas formulações químicas. Em adição, estas ligas (isto é, ligas de Ti e TiAl) são altamente reativas no estado líquido, o que leva à formação de uma camada dura e frágil rica em elementos intersticiais, tais como o oxigénio, na superfície dos produtos fundidos como um resultado da redução química do "face coat" das carapaças cerâmicas por titânio líquido, a chamada α-case.

Neste trabalho, foi realizado um amplo estudo das formulações químicas de “face coat” de carapaças cerâmicas para a fundição de uma determinada liga γ-TiAL.

Contrariamente ao que acontece com as ligas de titânio convencionais, demonstrou-se que os aluminetos de titânio no estado líquido não reagem tanto com barbotinas baseadas em zircão e zircónia.

Relativamente à colabilidade, a melhor capacidade de enchimento das moldações foi obtida para o caso de "face coats" de granulometria mais elevada centrada em ≤200 mesh, provavelmente devido à sua maior permeabilidade.

As soluções económicas de "face coats" de zircão podem ser usadas para a fundição de aluminetos de titânio, mas a camada superficial endurecida de 0,3mm deve ser removida por processos de acabamento como a maquinagem química.

As melhores formulações em termos de reatividade foram conseguidas com carapaças com "face coats" baseados em farinha de ítria, usando com ligantes produtos orgânicos ou misturas com alumina fumada. Neste caso a espessura contaminada a remover será de apenas 0,2mm.

Uma solução razoável e económica consiste na utilização de farinhas de custo médio de zircónia ou zircónia misturada com ítria chinesa (ítria química não fundida de baixo custo).

Devem ser realizados no futuro trabalhos no sentido de confirmar a influência da granulometria das farinhas das cerâmicas do "face coat" na colabilidade das ligas, bem como de confirmar a influência do arrefecimento das peças fundidas fora do forno ao ar no seu endurecimento superficial.

Os desenvolvimentos realizados ao longo deste trabalho foram suportados por ferramentas de apoio baseadas em modelos numéricos e sistemas digitais. Estes métodos computacionais avançados combinados com experiências e operações de medição permitiram acelerar todo o processo de desenvolvimento no que diz respeito à arquitetura das moldações.

Por último, e tendo em conta o conhecimento obtido em fundição de precisão de ligas de titânio, foi desenvolvida uma metodologia para o projeto e fabrico de próteses de titânio à medida, com base na manipulação de imagens médicas. A abordagem proposta

para o fabrico de próteses metálicas tem igualmente sido aplicada com sucesso no desenvolvimento e produção de próteses de tecidos moles extra-orais em silicone.

Palavras-chave: Processos de fundição não-convencionais, Fusão e vazamento de ligas reativas, Formulações cerâmicas, Ferramentas numéricas, Próteses de titânio à medida, Próteses de tecidos moles extra-orais em silicone.

Table of contents

List of Tables

Chapter II

Subchapter 2

Chapter III

Subchapter 3

Chapter IV

Subchapter 3

Subchapter 5

List of Figures

Chapter II

Subchapter 2

Chapter III

Subchapter 2

Subchapter 3

Chapter IV

Subchapter 2

Subchapter 3

Subchapter 4

Subchapter 5

1

Introduction

1. Motivation and Goals

Since 2004 the author of this work has been dedicated to the development of non-conventional casting processes for the production of turbocharger components such as aluminium and titanium alloys impellers, titanium aluminides turbines, nickel super alloys for aircraft turbo reactors combustion chamber heat shields and other components in a very close collaboration with the company Zollern & Comandita Portugal (ZCP).

All these studies led to important R&D projects, which consisted in the development of non-conventional processes absent in Portugal and/or with small or none expression in worldwide. Some of these have included an industrial implementation at ZCP. The projects started to be in the area of vacuum and low-pressure counter-gravity casting of aluminium alloys for turbocharger impellers by using hybrid moulds of cooled copper plate and plaster moulds, followed by vacuum/controlled atmosphere casting of titanium alloys, nickel super alloys and finally titanium aluminides.

Among all these R&D projects, the following can be highlighted:

TURBOCAST, **FUNDIMP** and **VABIMP**: Development and implementation of aluminium alloy vacuum and low-pressure counter-gravity casting processes for turbocharger impellers by using moulds, which are in plaster for the impeller fans and in copper cooled plate for the back massive part of the wheels. These processes resulted in a new plant in ZCP. Silicone patterns technology, equipment for casting plaster moulds with vacuum and vibration, striping presses, plaster mould production lines, melting and casting equipment and finally heat treating equipment were developed under the coordination of the author's work and fully manufactured in Portugal both for development and after further improving for industrial applications.

COMTICAST, **COMPINTEGRA** and **HYPERTURB**: Development of casting processes for titanium alloys impellers and nickel alloys and titanium aluminides for turbines. These processes were developed at INEGI and implemented in ZCP that since 2013 is producing nickel alloys components and meanwhile established a laboratory for special ceramic coatings for titanium aluminides process development.

AEROVAC: Development and implementation of a casting process for the production of nickel super alloys heat shields for the combustion chamber of turbo reactors. This process is implemented in ZCP for industrial small scale production.

All these projects began at INEGI with typically 4/5 collaborators from ZCP working at INEGI that afterwards moved to company in order to implement these processes.

TOOLING EDGE and **MEDCAST**: Development of casting processes for cranio-maxillofacial, hip and knee prostheses in titanium and cobalt chromium alloys. The casting process of chromium-cobalt alloys for prosthetic knees, whose development has exclusively been made by ZCP, is currently being implemented for industrial production and the development of the casting process of titanium alloys is as well under development centred at INEGI.

As a result of the secrecy that usually characterizes these applied industrial research projects with companies, during this period the author of the work did not publish significative papers, specifically on these issues. However, having arisen from the development of this work several projects and MSc dissertations that were done under the guidance of the author (see list of supervisions of MSc dissertations).

Taking into account the know-how and experimental facilities acquired in the development of casting processes of titanium alloys for turbochargers impellers, the knowledge in silicone processing, titanium casting and investing in a specific software for medical images manipulation an effort was made to extend the scope of applications, namely into the medical field, particularly in development of methodologies for the design and casting of custom-fit prostheses. The developed approach of design and moulds processing for wax injection demonstrated applicability in the manufacture of extra-oral soft tissue silicone prostheses, whose results are also part of this thesis.

The main objectives of the work presented throughout this thesis are:

- Development of vacuum controlled atmosphere melting and pouring processes for Ti alloys, Ni alloys and TiAl;

- Development of chemical formulations for ceramic moulds and crucibles for investment casting and induction melting of reactive alloys, such as Ti, Ni and TiAl;
- Optimization of mould layouts, rapid tooling and casting processes based on the development of numerical models and experimental validation;
- Development of design and manufacture methodologies for the casting of custom-fit titanium prostheses and vacuum casting of silicone for soft-tissue prostheses.

2. Structure of the thesis

This PhD thesis is organized in five chapters, namely (I) Introduction, (II) Investment casting of reactive alloys, (III) Enhancement of pouring processes using numerical tools and experimental analysis, (IV) Design and manufacture of custom-fit prostheses and (V) Conclusions.

Chapter I comprises an Introduction to the thesis and it includes the Motivation and Goals of the presented work, as well as the Structure of the thesis.

The main challenges associated with the investment casting of reactive alloys are expressed in Chapter II. This chapter deals with two topics: the development of melting and pouring techniques and the development of ceramic crucibles and ceramic shells formulations. The achieved developments on this last theme are synthetize in a research paper entitled "*Influence of ceramic shells face coat composition on the reactivity of TiAl castings*", which has been submitted to a peer-reviewed journal.

Chapter III focuses on the enhancement of pouring processes using numerical tools and experimental analysis. Within this chapter, the development of computational models and experimental validation approaches for supporting design and casting operations is presented. The outcomes of this study are presented throughout two research papers, which have been submitted to peer-reviewed journals. The first article deals with aluminium alloys and is entitled "*Modelling feeding flow shrinkage related defects in aluminium castings*". The other paper is related to titanium aluminides and is entitled "*Numerical and experimental research of γ-TiAl turbine produced by investment casting melted using a vacuum furnace*".

Chapter IV describes a methodology for design and manufacture of custom-fit prostheses, as well as some clinical applications. The achieved developments are presented as a set of four articles reported in conference proceedings and scientific publications. The first article is entitled "*Digital-based engineering tools for the tailored design of medical implants*" and describes in detail the adopted methodology for the design of custom-fit implants. The second and third articles present two applications of metallic prostheses, namely an artificial hip stem (in the "*Custom hip prostheses by*

Integrating CAD and casting technology") and a cranio-maxilofacial prosthesis (in the "*A framework for custom design and fabrication of cranio-maxillofacial prostheses using investment casting*"). The last research paper reports the application of the developed methodology of design and manufacture of custom-fit prostheses to the production of soft-tissue prostheses. This article is entitled "*An engineering-based approach for design and fabrication of a customized nasal prosthesis*" and describes the production of a silicone prosthesis of a nose.

Finally, the main conclusions of the present work and some suggestions for future research are expressed in Chapter V.

II

Investment casting of reactive alloys

1. Melting and pouring of reactive alloys

Investment casting of reactive alloys (titanium alloys, titanium aluminides, invar, nickel superalloys, magnesium alloys and cobalt chromium alloys among others) under the vacuum/controlled atmosphere melting and casting conditions, mould layouts and ceramic shells formulations are key variables for success of castings.

Control of the atmosphere of the melting and pouring processes, to minimize the metal atmosphere reactions is a crucial item to ensure minimal contamination of melts as well as the success in filling thin and complex parts using gravity casting and differential pressure casting. In vacuum induction melting (VIM) with ceramic crucibles the formulation and structure of crucibles are determinant for the molten metal contamination among other.

The formulation of the ceramic shell determines the metal refractory reactivity, the thermal shock resistance, permeability, dimensional stability and easy of processing of the moulds. The castings skin, the hot cracking susceptibility is also controlled by the ceramic shells with a significant impact on the properties and costs of the final component.

This chapter is divided in two areas identified above:

- Development of melting and pouring processes (Section 2.1)
- Development of formulations of the ceramic shells (Section 2.2)

In Section 2.1, a brief summary of the work done is presented as some developments are industrial property of the company Zollern & Comandita Portugal.

In Section 2.2, it is presented a historical overview of the work undertaken, the developments in the chemical formulations of ceramic shells for reactive alloys and a research paper on this topic submitted to a peer-reviewed journal.

1.1. Development of melting and pouring processes

The use of conventional titanium alloys and the newer intermetallic titanium aluminides has been noticed as an increasing demand in several engineering fields. These industrial areas recognize the numerous advantages of these alloys that present themselves as the ideal solution for many applications. Despite major markets continue to be elitist as aerospace and medical, new processing methods of these metallic alloys have been studied in order to make these materials accessible to broader applications.

In order to increase the know-how of casting technology for the manufacture of turbocharger impellers in Ti-based alloys, a commitment to investigate and develop a process for the production of components in these materials was performed. The main objective was to develop a ceramic crucible vacuum induction melting and pouring system considering moulds and crucibles, allowing pouring titanium alloy under conditions of low atmospheric contamination with high enough temperatures to facilitate the filling the thin walls of these impellers. Thus, activities of melting and casting in vacuum/controlled atmosphere systems were carried out

1.1.1. Development and implementation of a ceramic crucible vacuum/controlled atmosphere furnace

Within this subsection it is described the development of a melting and pouring furnace for titanium and other reactive alloys, targeting the production of thin wall components (0.5-0.6 mm thickness). The designed solution is a ceramic crucible vacuum induction melting furnace that uses a power source of 200KW 50KHz with capacity for differential pressure gravity pouring using 2 chambers in the vertical position: a superior fixed melting chamber and a moveable pouring chamber. The moulds are placed in the inferior chamber that is closed for the pouring. Inferior chamber can have the same pressure of the above chamber for simple gravity casting or can have a slightly inferior pressure aiming to achieve differential pressures in order to increase the filling capacity

This furnace presents some innovative concepts solutions that are:

- Furnace modularity possible to be in the future used with other configurations;

- Flexibility in terms of pouring solutions;
- High frequency power source with low electromagnetic stirring particularly helpful for low density and very reactive alloys in order to minimize erosion and reactions and metal projections;
- System compaction compared with commercial solutions with tilt pouring and big capacities;
- High security avoiding danger of water leaks near to melting like with copper crucibles;
- High monitoring with records of vacuum evolution in the in two chambers, power, temperature allowing total automatic operation for high repetitively insensible to human errors.

The design of this furnace is described in detail in (Martins, 2008), master dissertation developed under the guidance of the author of this work. The manufacture of furnace structure and double wall vacuum chambers and collectors was produced by the company M. J. Amaral and the instrumentation was assured by INEGI.

This furnace was designed and implemented during 2008 to 2010. For this task, an extensive work had been done targeting the production of ceramic crucibles by means of wax and silicone molds and the development of ceramic formulations with high mechanical strength at high temperatures, high thermal shock strength and high chemical inertia. However, the reactivity problem was not solved and all conventional titanium alloys melted with this system were contaminated with about 0,25% oxygen from ceramics, promoting low ductility to the castings. The great success of this work was discovered later, in 2012, when it was demonstrated that the system worked very well with less reactive titanium aluminides allowing us to have less than 0,1% oxygen in the castings. Another particularity of this furnace was that, unless vacuum pumps, valves and sensors, it was entirely produced in Portugal at company M.J.Amaral, which acquired knowledge and new competences that allow them to supply two furnaces for the company ZCP, which has been working with low operational costs and without any maintenance problems.

This furnace has an important and decisive role in the technological progress of INEGI that pushed it for further projects in the field of reactive alloys, such as Compintegra, Tooling Edge, Hyperturb and, recently, Medcast.

Regarding ZCP, its two furnaces are now being used for producing nickel alloys turbo reactors heat shields, waste gate components for turbochargers and Inconel turbines for turbochargers, as well as are being used for the more recent developments on titanium aluminides casting process.

1.1.2. Development and implementation of a cold skull levitation melting and pouring chamber

After the bad results in terms of melt contamination of the first solution of ceramic crucible melting process, new developments were imposed. The main goal was the development of a new solution using a cold skull induction melting process in order to minimize the oxygen contamination resulted by the chemical reduction and erosion of the ceramic crucible. Because the original design was based on the necessity of futures changes, the modularity allowed us to change the system in about three hours. The cold crucible was acquired to the patent owner, namely the French company CFSYS.

The new version of the furnace encompasses double wall cooled vacuum chambers, which were also produced by the company M.J.Amaral. The design and assembling of this new furnace allows for obtaining castings of conventional Ti6Al4V completely according to the specifications, with an oxygen level bellow to 0.2% and expected limitations of thicker wall thickness when compared to those ones possible using ceramic crucibles.

With this solution and a reasonable operating repetitiveness, INEGI and ZCP were in position to accept new challenges as conditions to develop the casting process of thicker components in Ti6Al4V, namely in Tooling Edge and Medcast projects. This last project aims to provide to the ZCP the possibility to produce titanium and cobalt chromium knee prostheses.

The design of this furnace is described in detail in (Silva, 2010), master dissertation developed under the guidance of the author of this work.

1.1.3. Development and implementation of a cold skull melting with contra gravity pouring chamber

Taking into account the limitation of low thickness (from the previous developments) and having as guarantee an acceptable oxygen contamination, new solutions were explored based on the counter gravity process, patented by Hitchiner and Daido. This option was taken being aware since the beginning of the patents existence.

Using available public patents of cold crucibles, the author started a project of developing techniques for manufacturing and repairing cold crucible by means of controlled atmosphere brazing techniques, because no supplier of this kind of components has been identified. Before advancing to the final solution, it was required to solve an important issue, namely the plunging tube for pouring after melting the alloys. This special tube was designed in order to be able to be immerged in a Ti6Al4V melt at high temperatures. The tubes were developed using a maximum refractoriness slurry made of calcia stabilized zirconia binded with fumed alumina stuccoed with alumina sand, and finished with inert yttria slurry. Even though not truly tested, under real conditions, some experiments of plunging at high temperature demonstrated that the designed solution works well. These good outcomes allowed us to go forward on the development of the new furnace with a vacuum aspiration system for the contra gravity casting in order to surpass the anterior limitation of low thickness. The big complexity of this new solution was the movement of the pouring moveable chamber that must go up when the pouring starts. This technical problem was solved by using flexible stainless steel welbows existing in the market for high vacuum applications.

The design of these concepts is described in detail in (Andrade, 2011) and (André, 2011), master dissertations developed under the guidance of the author of this work. Besides, complementary work of support to the design and manufacture was perform by the author and the INEGI team. Due to lack of time, the implementation of this new system

was never been done. Indeed, there was no time to rest because of the requests to work in the two previous versions for casting of super alloys and titanium aluminides. Multi-version designs are very interesting concepts, although sometime the field requirements make impossible its practical application. It was concluded that it would have been better to invest in another power source, structure, vacuum pumps and complimentary equipment.

1.1.4. Development of ceramic formulations for reactive alloys

Even though the benefits brought to the aerospace and automotive industries by the use of titanium alloys and titanium aluminides, such as high strength at high temperatures, the investment casting of these materials is still complex. These alloys reacts with ceramic shells at pouring temperatures, generating a hard and cracked superficial layer rich in interstitial elements (e.g., oxygen) named "α-case". This contaminated layer, which is the result of the reduction of the ceramic face coat with liquid metal, must be removed by chemical milling in majority of the cases.

The work done in this field began in 2007 considering only the reactivity between the casted metal and the face coat of the shells. These casting experiments were performed at the facilities of IFIMUP (Instituto de Física dos Materiais da Universidade do Porto), because, at that time, INEGI did not have the melting's facilities currently available. In the beginning of these studies, the ceramic formulations were based on calcia, yttria and magnesia stabilized zirconia slurries binded with ammonium zirconium carbonate, colloidal yttria and zirconia acetate, respectively.

The first outcomes, published in (Duarte, 2008), reported very hard α-case layers. Despite this, the obtained results worked as an extra motivation and a driving force for further developments.

Thus, the work continued with very cheap and fine grain size chemical yttria from China (5€/kg). After the approval of the COMTICAST project in 2008, the well-known fused yttria (150€/kg) were finally purchased from the relevant supplier Treibaker Industrie

AG. At this moment, the research idea was to concentrate efforts in a really promising solution.

Rui Félix in this MSc thesis (2008), under the supervision of the author of this work, demonstrated by means of casted cranio-maxillofacial prostheses that colloidal silica binder does not work very well with yttria flours, promoting an incontrollable slurry viscosity that increases till the level of complete inefficiency is reached (it is required too much water to compensate the continuous raise of viscosity). Nonetheless, this solution works despite it presents some lack of permeability.

The real solution only appear in 2010 but only for silicone patterns where there are no wax. With this solution of fugitive organic binder, the slurries were fully stable and economic, but they do not support wax melting and infiltrating followed by vaporization in the flash firing process. The bolilerclave technique of dewaxing was tested and not considered as an option because the high tendency for yttria hydrolysis, which must be confirmed in near future since there is still some doubts about this issue. The solution was definitively achieved at the end of 2012, but not reported as it is a property right of ZCP.

Regarding the production of nickel alloy heat shields for turboreactors, the main problem was not the reactivity but the slurry fluidity and rheology. This problem was unsolved for 3 years in Hollenzollern, the mother house of ZCP in Germany, despite the experience and competence of this company. The problem consists of excess of slurry flux inside the intervals between pins (7000 pins of 1 mm diameter x 3 mm length in a 200 x 50 mm plate). This problem was solved by using an abnormal water based high viscosity slurry that is currently being used to produce industrial components. However the resolution of this complex problem was done by means of not one but three solutions: two solutions based on alcoholic hydrolysed triorthoethilsilicate binded slurries and finally the referred one that is environmental friendly. The first two solutions were discarded, because it must be banned from industrial solutions taking into account security and hygiene concerns of alcoholic solvents.

The solutions for these problems were accomplished based on the knowledge acquired by the team of block ceramic moulding and developed during the PhD of Teresa Duarte

in 1998 under the help of the author of this work and his knowledge on the influence of grain size distribution and its effect on slurry behaviour. Vibration and vacuum was used in preliminary developments, but after all stages a normal process was defined. This solution is considered an important milestone of the author of this work as the result allows for the entrance of ZCP into the competitive market of aerospace suppliers.

Relevant and challenging problems were solved, despite the lack of scientific reports or papers as a result of the impossibility to publish in peer-reviewed journals for sake of confidentiality issues. Indeed, it is very difficult to present an investment casting problem without describing the process conditions and showing the casted confidential products.

Within this chapter, a paper entitled “Influence of ceramic shells face coat composition on the reactivity of TiAl castings” is encompassed (section 2.2). In order to not compromise the confidentiality agreement, only part of the problem is presented. This is not an easy task as some problems and solutions must be hidden. The standardized test specimen was designed in order to simulate simultaneously for the casting of conventional titanium alloys for impellers and titanium aluminides for turbines.

Influence of ceramic shells face coat composition on the reactivity of TiAl castings

Article submitted to a peer-reviewed journal

***R. Neto**, T. Duarte, J. Lino Alves and T. Barrigana*

2. Influence of ceramic shells face coat composition on the reactivity of TiAl castings

2.1. Introduction

Titanium is a low density element (4.5 g/cm^3, about 57% of iron) of improved properties with the addition of alloying elements. Some titanium alloys were developed with the aim of reducing or no reacting with the surrounding tissue implants due to an oxide film formed on their surface. The increasing use of this material is mainly due to its relatively low elastic modulus (100 GPa), higher biocompatibility and superior corrosion resistance, when compared to conventional stainless steel or cobalt - chromium alloys employed in medical area. These are attractive features responsible for the introduction of pure titanium (α CpTi), later α+β alloy (Ti6Al4V), also used in aeronautical applications and automobiles, and recently titanium aluminides (Rocha, 2010).

Titanium aluminides (γ-TiAl) are intermetallic alloys (formed by two metals with different crystal structures) whose development was created by the need for materials to work at high temperature applications, such as aerospace or automotive, with good mechanical properties and lighter weight than the common nickel superalloys, which are the mostly used for high temperature environments. Due to their attractive properties, such as high melting point (around 1600 °C), low density (3.9-4.2 g/cm^3), high specific strength (0.14 MPa.m^{3}kg^{-1}), high stiffness (100-145 GPa), good oxidation resistance and good creep behaviour at elevated temperatures, these alloys are potential candidates for several applications (Clemens and Smarsly, 2011).

Among the future high temperature applications of greater commercial interest one can include turbines for turbochargers to be used in gasoline direct injection passenger cars and mass production of turbines for diesel engines turbochargers (Tetsui, 2011). They are in competition with nickel superalloys for this practical application, only losing on the cost of raw materials (460 €/kg for commercial gamma titanium aluminide Met PX and 7 €/kg for superalloys) and manufacturing difficulties (Kothari *et al.*, 2012). Nowadays some TiAl alloys can be ordered at about 100 €/kg.

As a material that allows service temperatures of about 800 °C (for some turbine applications can withstand temperatures up to 1000 °C, maintaining high mechanical strength in the region of 800 °C), these materials have earned an increasing interest since the 80s (Leyens and Peters, 2003). The main properties of conventional Ti and TiAl alloys are shown in Tables 2.1 and 2.2.

Table 2.1 - Properties of several commercial titanium alloys (Titanium Information Group, 2012).

ASTM Grade	Alloy composition	Tensile strength min. (MPa)	Yield strength min. (MPa)	Young modulus (GPa)
4	Pure Ti	550	480	105
5	Ti-6Al-4V	895	825	114
6	Ti-5Al-2,5Sn	825	795	110
20	Ti-3Al-8V-6Cr-4Zr-4Mo (Beta C) aged	1170	1105	102

Table 2.2 - Ti aluminides and nickel superalloys, HC – compact hexagonal, CCC – body centred cubic, CFC – face centred cubic crystal structures (adapted from Magalhães, 2012).

Properties	Titanium	Titanium alloys	Ti3Al (α)	TiAl (γ)	Nickel superalloys
Crystalline lattice	HC	HC/CCC	HC	Tetragonal face centered	CFC
Density (g/cm3)	4.5	4.1-4.7	3.7-3.9	3.7-3.9	8.3
Young modulus at RT (GPa)	100-105	96-117	100-145	160-176	206
Yield strength at RT (MPa)	270-600	380-1150	700-990	400-650	800-1200
Ductility at RT (%)	20	10-25	2-7	1-5	3-50
Ductility at elevated temperature (%/ °C) *when available	12-50	10-50	10-20 (660 °C)*	10-60 (870 °C)*	20-80 (870 °C)*

From the analysis of Tables 2.1 and 2.2 it can be concluded that the major disadvantages of titanium aluminides are the reduced ductility, derived from the small number of intermetallic slip systems of the crystal structure (tetragonal face centred), and the low yield strength (400-650 MPa). One way to improve the ductility is through the addition of alloying elements that increase the number of slip systems (Magalhães, 2012).

Precision casting, lost wax and investment casting are synonyms given to the foundry manufacturing process that can produce parts of complex shapes difficult to obtain by machining processes (Sopcak, 1986). Figure 2.1 shows a schematic summary of the investment casting process that can be described as follows:

1. CNC machining of a mould for wax injection. Alternatively it can be created a CNC machined or additive manufacturing model, and obtain a mould to produce the model in wax by filled resin casting;
2. Injection of a wax model with the final shape of the part (compensated with the shrinkage);
3. Construction of a "tree" of models with wax (including feeding and gating systems);
4. Coating the "tree" with a suitable refractory slurry which will resist to high temperatures and reproduce every detail of the model. This part of the process involves dipping into a slurry, subsequent stuccoing with ceramic particles and drying, and repeat this operation until a shell with an adequate thickness is obtained;
5. Flash firing of the wax model: the whole model and shell are heated to temperatures that cause wax melting, leaving a "negative" in refractory material;
6. Sintering the shell at elevated temperature, if necessary, giving it the best properties for casting, and pre - heating the shell;
7. Pouring the metal into the shell, using the selected casting technique;
8. Solidification, cooling and knock-out of the shell, followed by cutting the gating and feeding system;
9. Finishing the part.

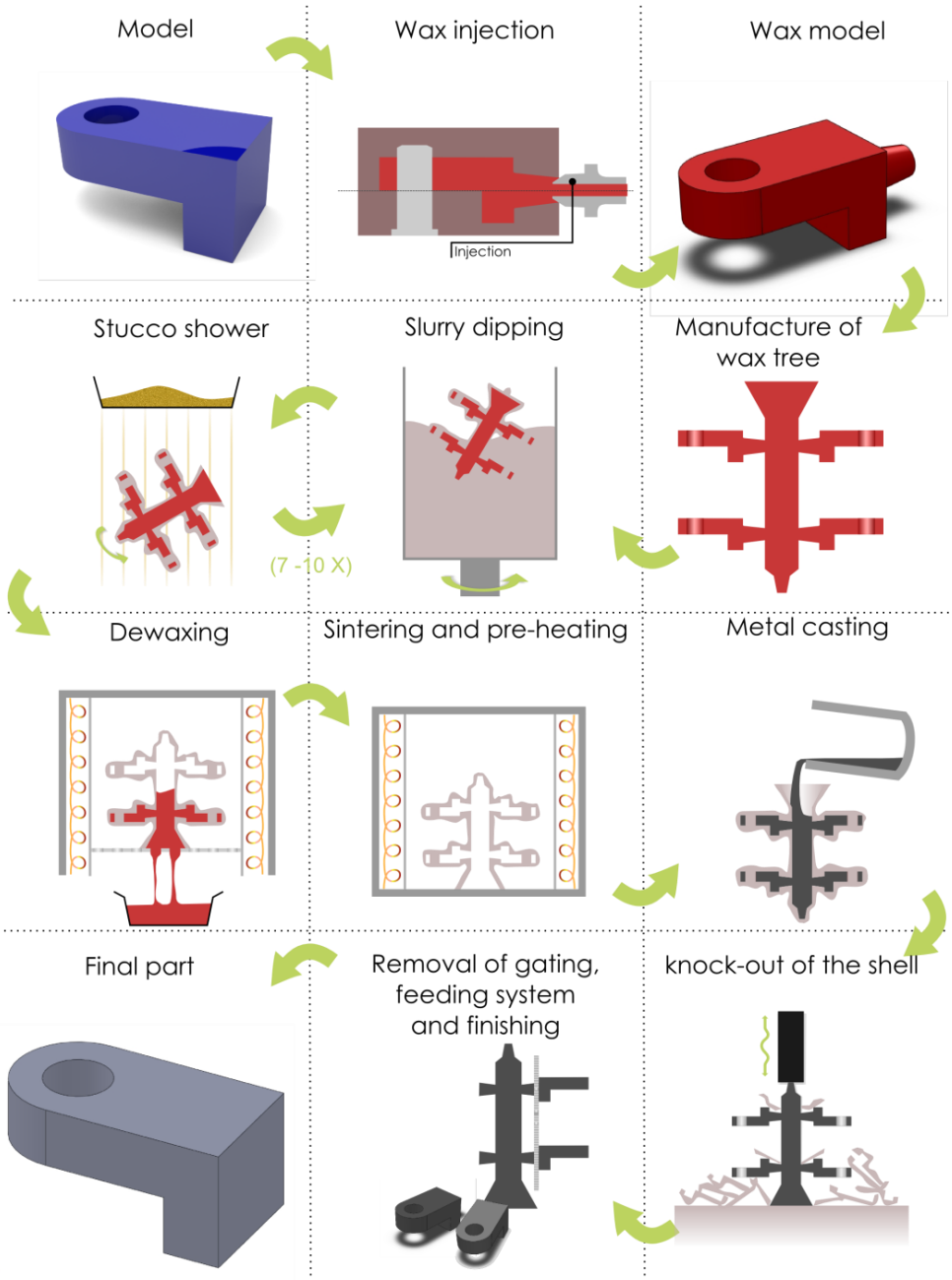

Figure 2.1 - Main steps of the investment casting process.

The ceramic shells used in investment casting are made by sequential application of ceramic coatings. Each coating is a thin layer of ceramic slurry (ceramic flours, for example ≤ 74µm (≤ 200 mesh), with a binder), followed by stuccoing with a shower fine particles (for example 125-250 µm). Figure 2.2 shows a possible composition of a ceramic shell, and Figure 2.3 exhibits the relative position of the materials in the shell. It is important to note that the backup layers follow the same manufacture procedure as those of face coat, but with changes in the composition and stucco particle size, using cheaper and coarser ceramic materials.

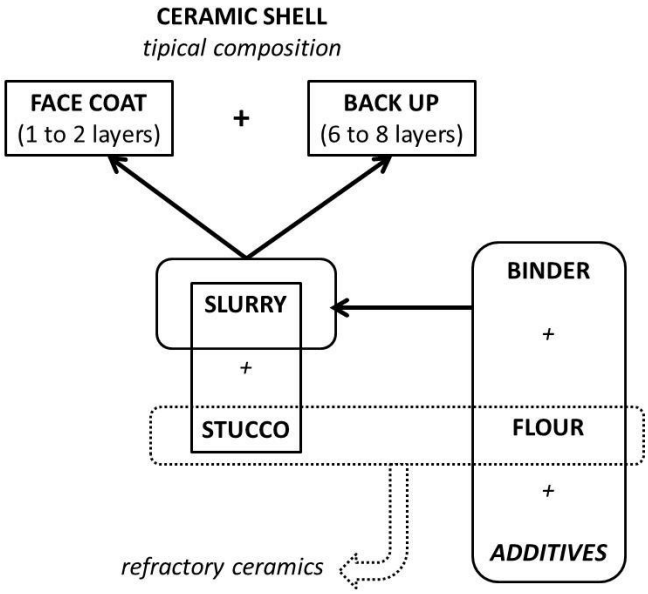

Figure 2.2 - Generic composition of a ceramic shell for investment casting.

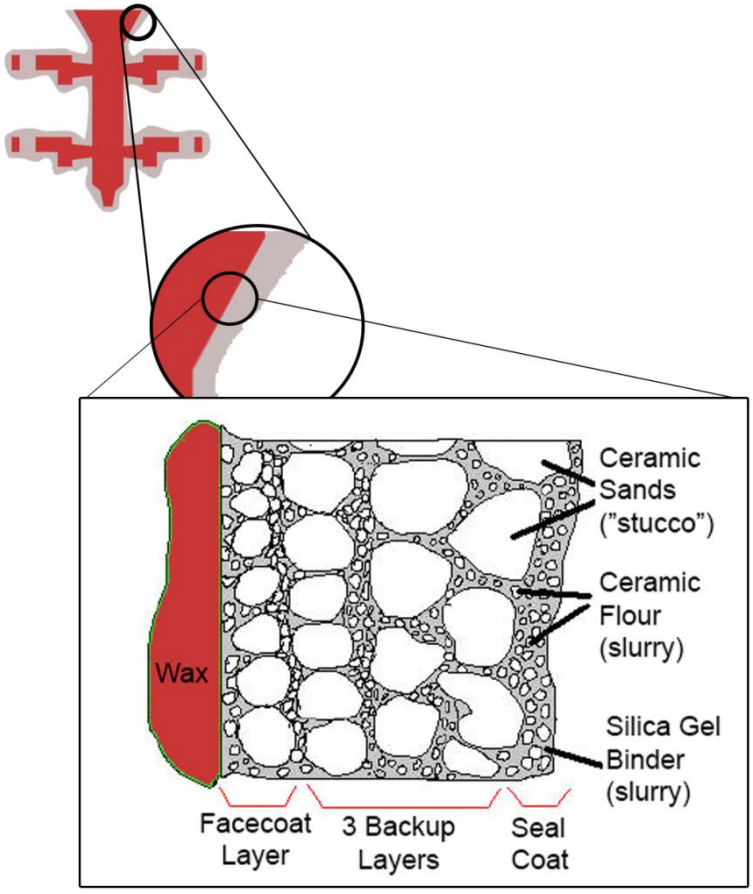

Figure 2.3 - Generic composition of a ceramic shell for investment.

Due to the nature of the casted alloy, some aspects must be considered when defining the constitution of a successful ceramic shell (Pattnaik *et al.*, 2012):

1. Green strength to ensure wax removal by heating without warping, destroying or loosing properties;
2. Strength to withstand the metalostatic pressure of casted alloy;
3. Resistance to thermal shock to avoid fracture during casting;
4. Chemical inertia to avoid reduction of the metal;
5. Permeability to allow air to escape through the walls during pouring of the molten metal;
6. Collapsibility to avoid cracking of components during cooling (Jones and Yuan, 2003);
7. Thermal conductivity to keep uniform heat transfer and adequate cooling through the metal walls.

In order to be able to obtain shells which meet the highest possible number of the previously mentioned requirements, the choice of ceramic materials must be focused on the following (Felix, 2008):

- Free energy of formation;
- Melting / softening temperature;
- Thermal properties;
- Availability / cost.

Traditionally, refractories for casting titanium alloys and titanium aluminides are zircon ($ZrSiO_4$), alumina (Al_2O_3), calcia (CaO), magnesia (MgO), stabilized zirconia (ZrO_2-X, X being other compound) and yttria (Y_2O_3). With non-reactive alloys, vitreous silica (SiO_2) and aluminosilicates are also used (Guntlin *et al.*, 2012).

One of the major challenges/difficulties in lost wax casting of titanium and titanium aluminides is their high reactivity in the liquid state with the ceramic shells. Figure 2.4 presents a summary of the Ellingham diagram for oxides suitable to be used as face coat in investment casting. All oxides (MgO, CaO and Y_2O_3) below the Ti-TiO_2 line, at the casting temperatures about 1400 – 1500 °C are potential candidates.

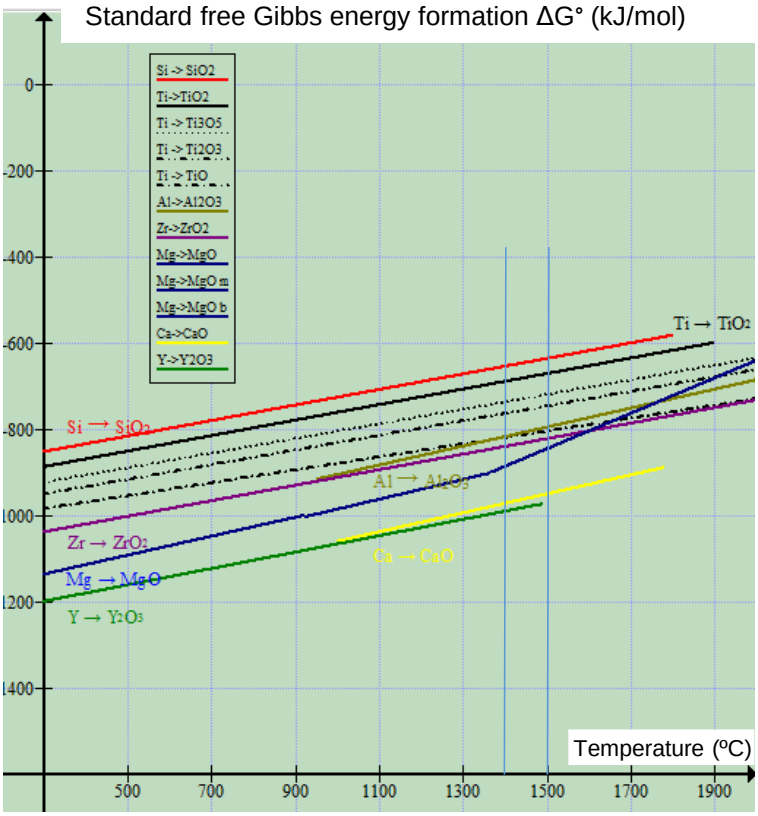

Figure 2.4 - Ellingham diagram for the more common oxide formation occurred in investment casting (Turkdogan 1980).

Table 2.3 presents the main thermal properties of the different ceramics used in shells and presented in Figure 2.4.

Table 2.3 - Thermal properties of different ceramic materials (Barrigana, 2013).

Ceramic	Thermal expansion coefficient (x 10-6K-1) 20-1000 °C	Thermal conductivity (Wm-1 K-1) 20-26 °C	Free Gibbs energy formation, ΔGO (kJ/mol O2)	Softening temperature (°C)
Zirconia – ZrO2	10.0	2.5	-743 (a 1900 K)	2010
Yttria – Y2O3	8.1	8.0 – 12.0	-989 (a 1469 K)	1855
Alumina – Al2O3	8.0	28.0 – 35.0	-711 (a 1900 K)	1540
Silica – SiO2	0.5 – 0.8	1.2 – 1.4	-610 (a 1685 K)	1280
Magnesia - MgO	9.0 – 12.0	30.0 – 60.0	-684 (a 1900 K)	2100
Calcia - CaO	15.2	30.0	-899 (a 1756 K)	1950
Zircon - ZrSiO4	4.5	8.0	-	1815

The melting temperature of the titanium aluminides (γ-TiAl), 1460-1500 °C (Appel *et al.*, 2011), determines the temperature range to analyse in Ellingham diagram (see Figure 2.4) and compare the free energy of oxides formation. As shown in Figure 2.4, the lines related to the free energy of oxide formation in the lower part of the diagram means that the reaction is thermodynamically more stable.

With a softening temperature of 1855 °C, above the melting temperature of the alloy TiAl and larger Gibbs Free energy than all oxides that could be used in the ceramic shells (-989 $kJmol^{-1}$ at 1469 K), yttria is undoubtedly the most promising refractory material for face coat in terms of reactivity. Its use in ceramic shells only began to be more common in the last 15 years because, despite its potential, there were enormous difficulties in producing an yttria-based slurries which did not gelify prematurely, preventing parts production in large series. In 1993, Horton used successfully face coat yttria slurries, applying colloidal silica as a binder and with the addition of hydroxide ions. This procedure avoided premature gelling of the slurry (Pattnaik *et al.*, 2012).

Different combinations of binders, flours particle size and manufacturing techniques have conducted to the current state of art of ceramic shells, where yttria is the ideal ceramic with the lowest reactivity, as described by Altindis *et al.* (2011).

Guntlin *et al.* (2012) studying the "investment casting" of titanium aluminides, claims an Y_2O_3 formulation face coat and Al_2O_3 as a successful back-up, with minimal oxygen contamination (300 to 500 ppm by weight), in shells and crucibles for VIM (vacuum induction melting). They refer the existence of fused yttria due to a reaction - dissolution process of the face coat with the liquid metal, but the effect of the presence of yttrium inside the part was not studied. Duarte *et al.* (2008) also concluded that yttria face coats result in almost no "α-case" presence in Ti6Al4V casts.

However, as suggested by Altindis *et al.* (2011), for industrial use in investment casting, further research is still demanded to improve the stability and longevity of yttria ceramic slurries and thereby improve the mechanical strength and inertia of the shells.

Yttria slurries in industrial environment are still a concern due to the availability/cost. China is the rare earths largest exporter of todays' world. The exploitation of resources in the early '80s and the opening of frontiers to the exportations led many countries (India, Brazil, South Africa and USA) who extracted rare earths, to cease this activity because they were unable to compete with the prices and abundance of Chinese resources. Since the beginning of the XXI century, China decreased the extraction of rare earths, mainly by environmental causes, increasing prices and forcing consumers to find alternatives to rare earths (Voigt, 2012).

Researchers worldwide are currently focused on developing alternative cheaper ceramic formulations with similar or lower reactivity than the yttria ones. In 2012, Cheng *et al.*, published the article "Formation Mechanism of “α-case” on Titanium Investment Cast Parts", where they not only further study the “α-case” formation mechanism, but also proposed a slurry formulation with titanium powder. Cheng *et al.* (2012) refer the difficulties of working with a slurry prone to premature gelling and containing an expensive oxide such as yttria. So, the new goal is the development of a stable face coat slurry, with a long life, minimum cost and a reasonably chemical inertia with titanium aluminides (Cheng *et al.*, 2012).

The ceramic slurry usually consists of a major portion of highly refractory materials with a binder. The role of binder is providing a link among the refractory ceramic particles and promoting enough strength to withstand the mechanical and thermal stresses during the shell preparation and use. Basically, there are two natures and two types of binders used in investment casting (Pattnaik *et al.*, 2012):

- Aqueous dispersions (inorganic nature) colloidal solutions such as colloidal silica, colloidal zirconia, colloidal yttria and colloidal fumed alumina (nano-sized solid particles in aqueous phase);
- Alcoholic dispersions (inorganic nature) such as ethyl silicate;
- Polymeric dispersions (organic nature) such as acrylate polymers;
- Hybrid nature dispersions: mixing dispersions of organic and inorganics (such as zirconium acetate modified with polyacrylamide polymer) (Chen et al., 2011).

2.2. Experimental Procedure

Although the literature is abundant relative to standard test samples for investment casting, experimental work with thin sections parts with complex geometries are uncommon. In this work, the experimental studies were conducted considering the necessity to simulate simultaneously both turbines and impellers turbochargers manufacturing process. The standard test sample designed by us for this work was

machined in an aluminium alloy 7075 (see Figure 2.5) and it measures about 40 mm (diameter). This part was used to obtain a resin filled with aluminium powder mould for wax injection. The wax was injected at 68-70 ^{o}C with a 6 bar pressure, using a release agent without silicone to prevent silicon contamination.

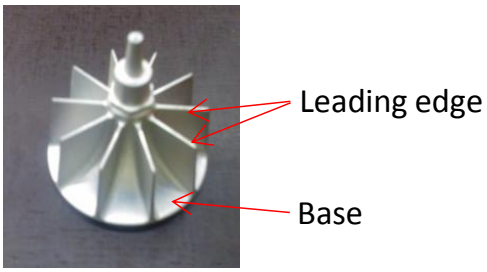

Figure 2.5 - Standard test sample machined in an aluminium alloy 7075.

The leading edge of the wax turbine blade were measured with a digital calliper to control dimensional variations during the whole manufacturing process (wax and final metallic part). Figure 2.6 shows measurements in these two parts.

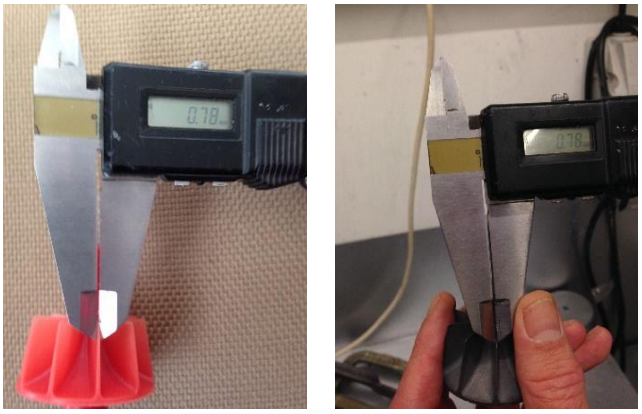

(a) (b)

Figure 2.6 - Measurement of reference values for: a) the leading edge of the blades, and b) turbine base.

The wax parts were welded in a tree (gating and feeding system) for investment casting (see Figure 2.7).

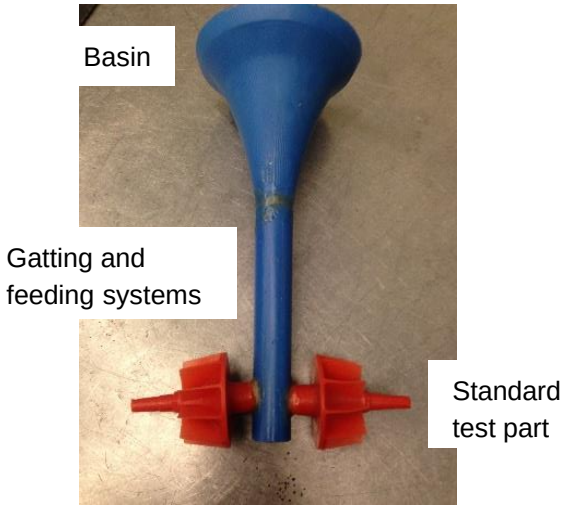

Figure 2.7 - Wax test samples in the tree ready for investment casting.

After this step, shells with different compositions were manufactured using the materials indicated in Tables 2.4 and 2.5. Each tree was degreased, washed in water and dried. Then they were dipped in the slurry during 30 s, air drying for 1 minute and stuccoed in a rain fall during 10 s. This sequence was repeated twice, to create the face coat.

The backup was done using 5 layers of fumed alumina binder, alumina flour and alumina stucco, or silica binder, zircon flour (or fused silica) and aluminosilicates stucco (Duarte *et al.*, 2009).

Table 2.4 – Binders properties.

	Organic	**Fumed Alumina**	**Colloidal Silica**
Reference	A	AF	S
Type and binder nature	Polymeric dispersion, organic nature	Aqueous dispersion, inorganic nature	Aqueous dispersion, inorganic nature
Solids content (%)	47	40 - Al2O3	30 - SiO2
Density (g/cm3)	1.06	1.39	1.21
Medium size of aggregates (µm)	Not available	0.08	0-0.10
Cost (€/kg)	2.5	18.0	5.0

Table 2.5 – Summary of slurries face coat (FC) composition.

	Binders	**Flours**	**Stucco**
AY	A	50% fused yttria - ≤ 200 mesh and 50% fused yttria - ≤ 325 mesh	yttria 125-250 µm
AAFY	A+AF	Fused yttria - ≤ 200 mesh	yttria 125-250 µm
AFZr	AF	6% yttria stabilized zirconia - ≤200 mesh	4% CaO stabilized zirconia - 150-300 µm
AFZrYC	AF	6% yttria stabilized zirconia - ≤ 200 mesh, and 10%	4% CaO stabilized zirconia -

		fine chinese yttria 3-7 µm	150-300 µm
SZ	S	zircon ≤ 250 mesh	zircon 70-125 µm
SAlT	S	50% fused alumina -200 mesh, 50% fused alumina 0-30 µm, Ti powder 45 µm	fused alumina - 106-150 µm

The dewaxing was done in a flash fire furnace at 1000 ^{o}C for 2 h. The shells with yttria (AY and AAFY) were also sintered at 1400 ^{o}C for 2 h (Duarte *et al.*, 2009).

The chemical composition and main properties of the TiAl ingot alloy used in this study are indicated in Table 2.6.

Table 2.6 –Main properties of the γ-TiAl alloy (Barrigana, 2013).

Alloy	**γ-TiAl (TiAl GFe)**
Chemical composition (% weight)	33.5Al – 4.8Nb – 1.0Cr – 0.2Si and O<0.5
Chemical composition (% at.)	48.1Al – 2.0Nb – 0.7Cr – 0.3Si and O<0.5
Melting temperature (°C)	1460
Hardness (HV)	268-281
Density (g/cm3)	3.9 – 4.2
Thermal conductivity (W.m-1.K-1)	22

TiAl alloy was melted in a semi levitation cold copper crucible induction furnace, with a maximum power of 100 kW. The shells were preheated at 1150 °C and placed in the furnace chamber, which was cleaned twice with argon. First vacuum at $7.5x10^{-2}$ mbar, second one at $5x10^{-2}$ mbar, and argon injection up to 100 mbar.

After melting and pouring (1640 °C, overheating around 180 °C), and cooling for 2 min inside the furnace, the chamber was opened and the shells allowed to cool to room temperature.

Shells were knocked-out and blasted with corindon sand (see Figure 2.8). The parts were then cut and measured to know if they are filled or not.

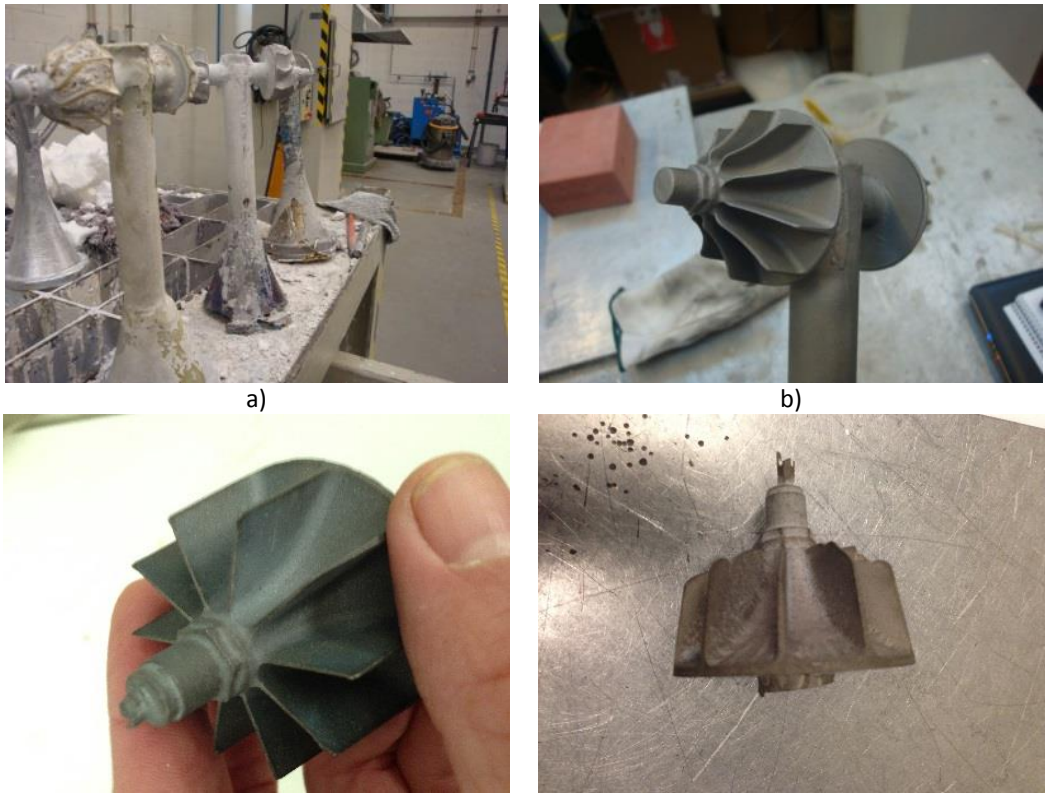

a) b) c) d)

Figure 2.8 - Casted metallic tree: a) after knock-out and b) after corindon blasted; Casted parts: c) complete filling and d) incomplete filling.

From each tree component, different samples were removed for metallographic analysis and microhardness measurement, as described in Figure 2.9. Samples were embedded in cold epoxy resin and polished in accordance to standard metallographic procedures for titanium alloys.

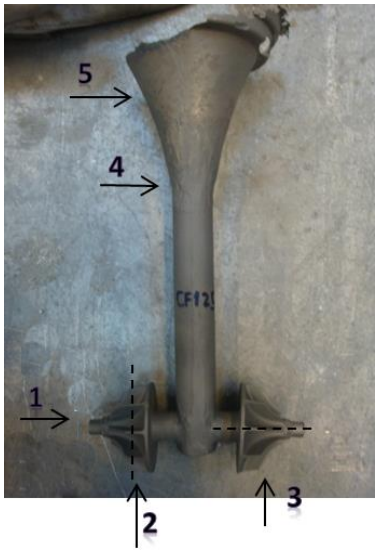

Figure 2.9 - Location of samples used in micro hardness and microstructural characterization.

Medium microhardness (0.05 kgf) was determined starting from the surface, at the following distances: 0.02; 0.07; 0.12; 0.20; 0.5 and 1 mm. The profiles were obtained in 5 polished (1 µm finishing) cross sections (longitudinal, transversal riser/feeding channel, transversal top of riser, transversal base and transversal leading edge) of each sample (see Figure 2.9).

Optical analysis was performed in an Olympus microscope PMG3. SEM/EDS analysis was done in a High Resolution (Schottky) Environmental Scanning Electron Microscope with X-Ray Microanalysis and Electron Backscattered Diffraction Analysis: Quanta 400 FEG ESEM/EDAX Genesis X4M. Samples were coated with a C thin film, by vapour deposition, using a JEOL JEE – 4X Vacuum Evaporator equipment. Each image contains a data bar with the most important analysis conditions.

2.3. Results and Discussion

Sample standard tests in TiAl were obtained using different face coat shells compositions as mentioned in the experimental conditions (see Table 2.5). Not only the pouring temperature but also different face coats affect the alloy fluidity when filling the shell. To test the fluidity of the TiAl alloy in these face coat materials, the thickness of the castings were measured.

Wax parts were measured to check the dimension accuracy. All parts present a leading edge thickness of the turbine blade of 0.78 mm, and a turbine base with 0.80 mm, as shown in Figure 2.6. Figure 2.10 shows the values measured on the metallic samples test produced with the different shells slurries face coat composition and the estimated thickness value (0.8 mm). The results of table 2.10 shows that the coarser flours of ≤200 µm of face coats promotes high fluidity turning easy the filling of thin zones, probably due to higher overall shells permeability, but these results must be confirmed in posterior works.

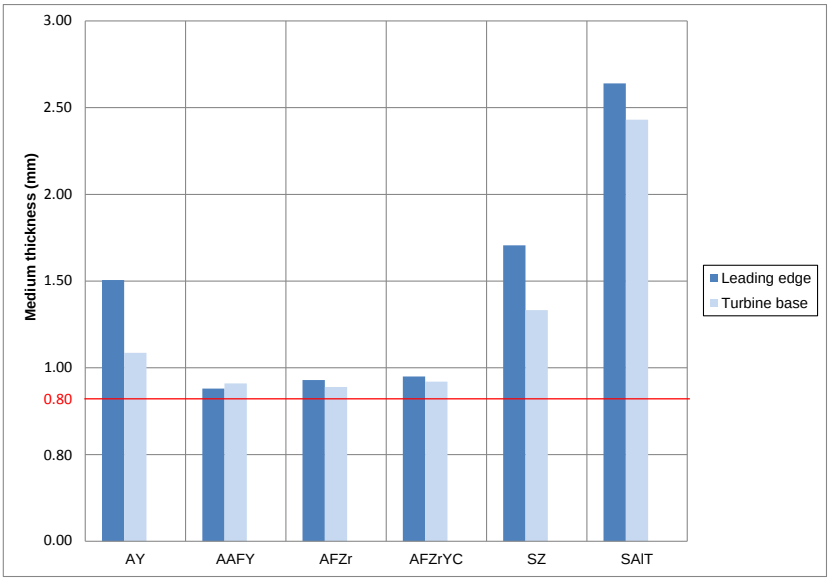

Figure 2.10 - Medium thicknesses of the metallic turbines leading edge and base obtained with different shells slurries face coat composition.

Castings made in shells with face coats AY, SZ and SAIT demonstrated low fluidity because metal did not fill the entire fans. Castings made in shells AAFY, AFZr and AFZrYC exhibited good fluidity because metal reproduced the original dimensions of leading edge and turbine base.

Microhardness profiles were obtained in 5 polished cross sections of each sample as described previously. Figure 2.11 and Table 2.7 show the medium microhardness evolution from the surface until 1 mm depth. Figure 2.10 also presents a horizontal line of 280 HV representing the microhardness of TiAl alloy (before casting) experimentally obtained.

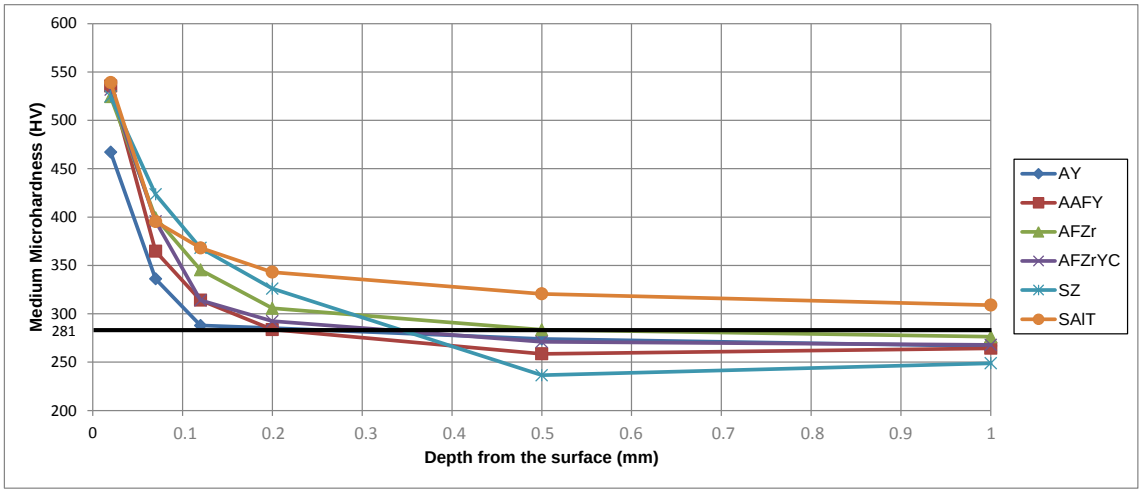

Figure 2.11 - Medium microhardness evolution from the surface to a 1 mm depth of the 6 casting obtained from the shells tested.

Table 2.7 –Microhardness values (HV) of all samples.

		Medium microhardness (HV)					
Shell Code	**Shell Code**	**AY**	**AAFY**	**AFZr**	**AFZrYC**	**SZ**	**SAIT**
Depth from the surface (mm)	0.02	467	535	524	532	525	539
	0.07	336	365	399	396	423	395
	0.12	288	314	345	314	368	368
	0.20	285	284	306	292	326	343
	0.50	274	259	284	271	236	321
	1.00	267	264	276	268	249	309

As one can see the surface hardness is identical for all materials (524-539 HV), except for AY condition which promotes a softer "α-case" (467 HV).

Y_2O_3 (AY) is the less reactive face coat with a hardened zone of about 0.1 mm. This result is in accordance with the literature and Elingham diagram. Y_2O_3 with inorganic binder fused alumina (AAFY) is also a good solution in terms of reactiveness.

Less expensive face coat shells composed by yttria stabilized zirconia (YSZ) and YSZ with 10% fine cheap yttria (AFZr and AFZrYC), slightly more reactive than Y_2O_3 are still a good solution for the face coat composition.

At 0.5 mm thickness the microhardness is already with values equal or lower than the ingot alloy, except for the SAIT condition, which even at 1 mm is harder (309 HV), as result of an strong reaction with face coat.

All the samples obtained using the shells presented in this work exhibit similar behaviour, which means that zirconia, yttria and even zircon (SZ) are equal possibilities for the face coat.

Considering the hardness values obtained it is possible to determine an "α-case" thickness around 0.2-0.3 mm, except for SAIT, who present even at 1 mm a 309 HV value, higher than the alloy before casting (280 HV).

Figure 2.12 shows optical images of the casted samples obtained with the different face coats shells (see Table 2.5).

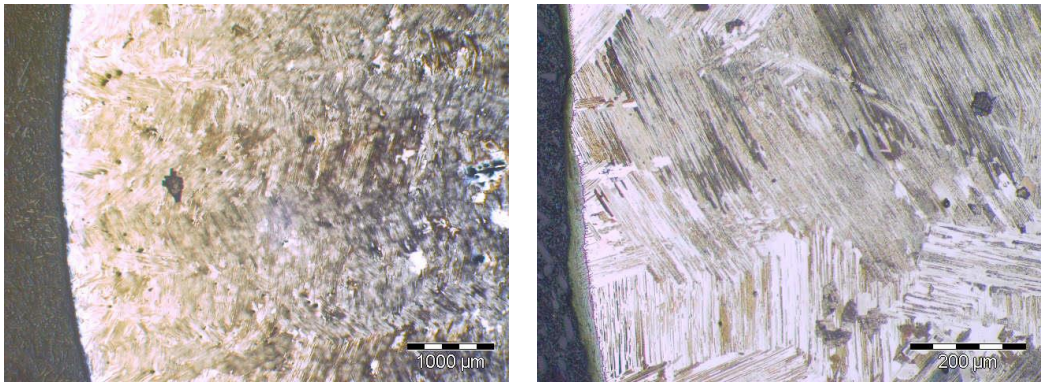

a)

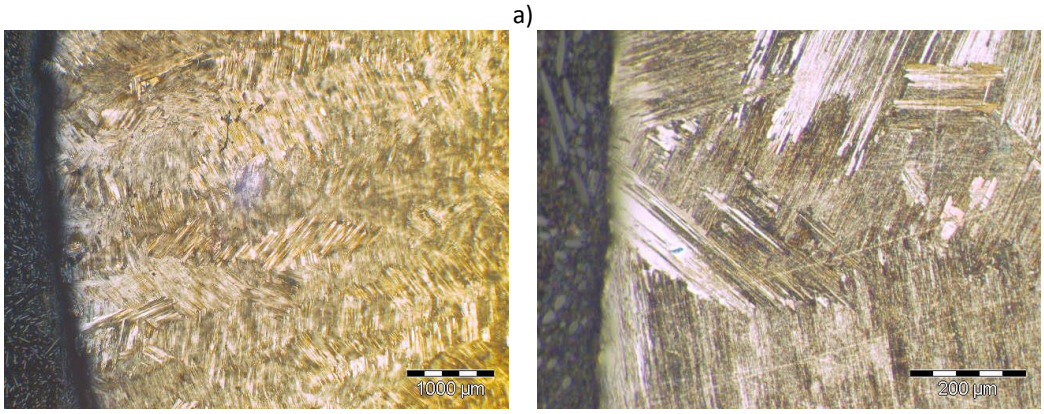

b)

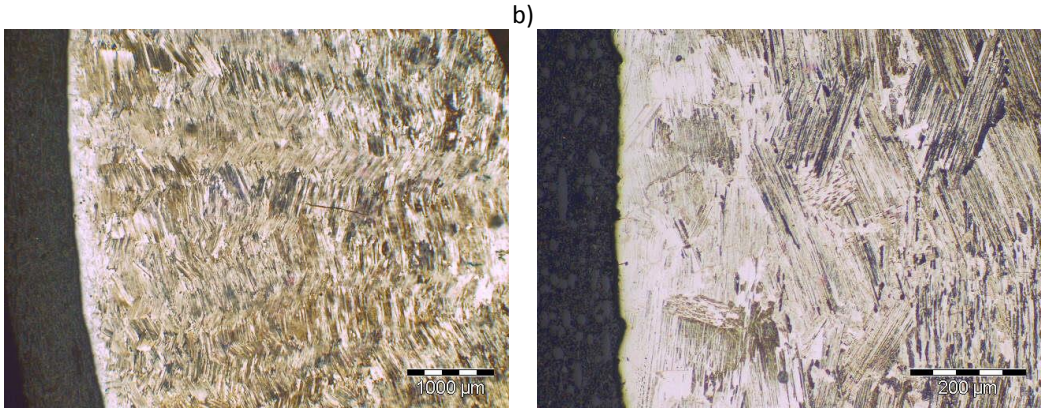

c)

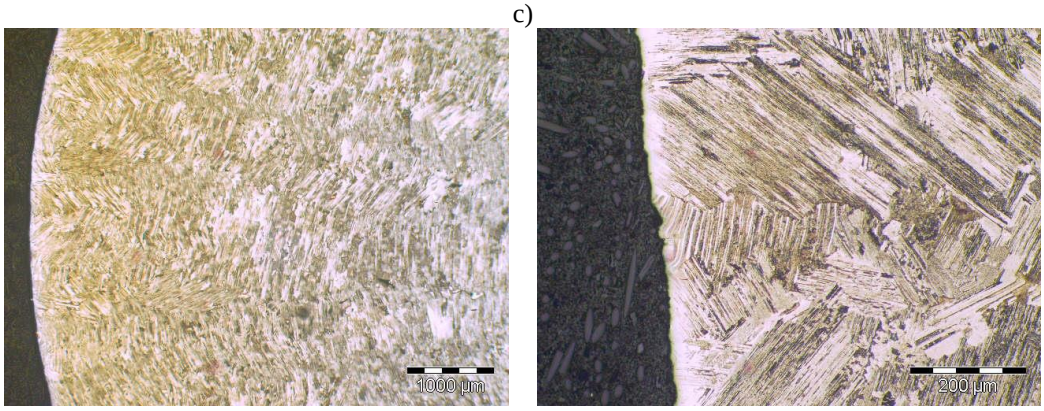

d)

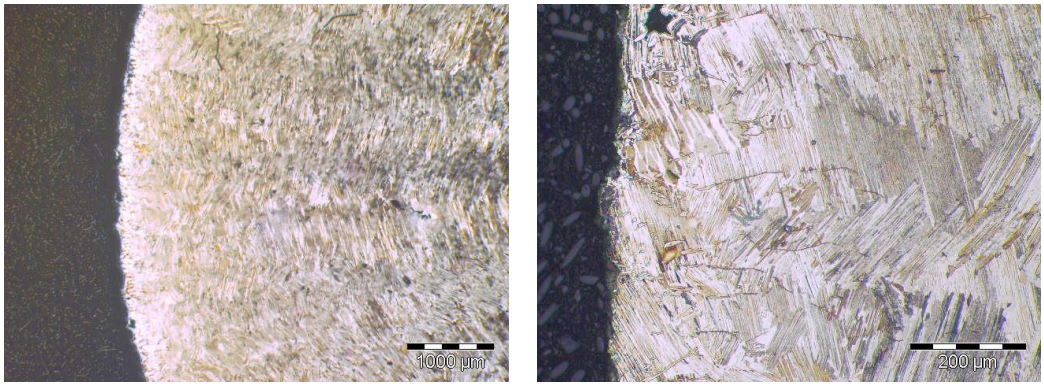

e)

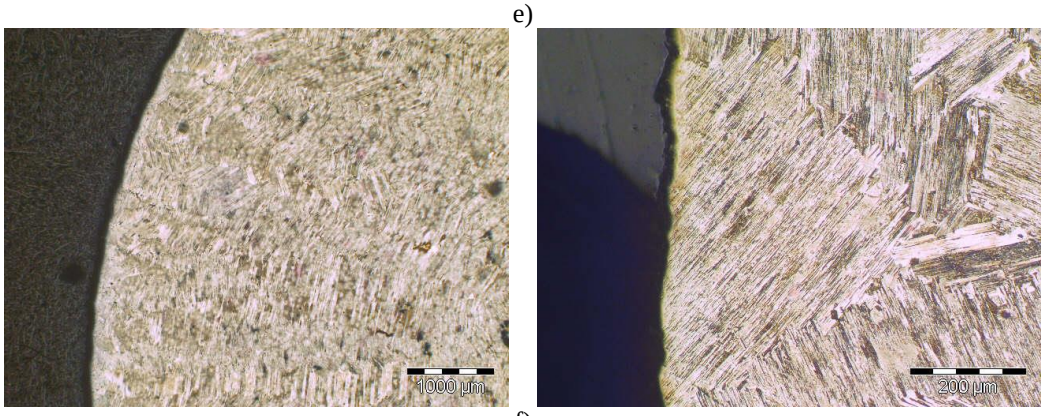

f)

Figure 2.12 - Optical microstructures of the samples produced with the different face coats (see table 2.5 for details): a) AY, b) AAFY, c) AFZr, d) AFZrYC, e) SZ and f) SAIT.

Although the different microhardness values, resulting from the distinct face coat shells compositions, no significant differences on the TiAl microstructures were obtained, between surface and interior, with no typical microcracked "α-case" layer in any sample.

The existence of the hardened layer was probably promoted by an earlier removing of the castings from the controlled atmosphere furnace (ASM, 1998).

Figure 2.13 shows the more representative SEM microstructures, indicating regions A and B, 200 µm apart where X rays spectrums were obtained. The value of 200 µm was chosen in order to determine if the microhardness differences were related with the chemical composition or microstructure.

a)

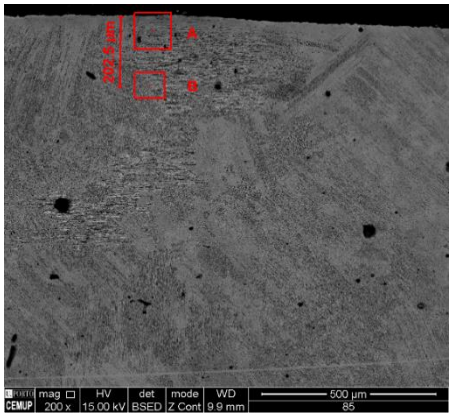

85	Chemical Composition wt%			
AY	Al	Nb	Ti	Cr
A	33.91	5.44	59.06	1.59
B	33.54	6.14	58.89	1.43
Ingot Alloy	34.54	5.32	59.86	0.28

b)

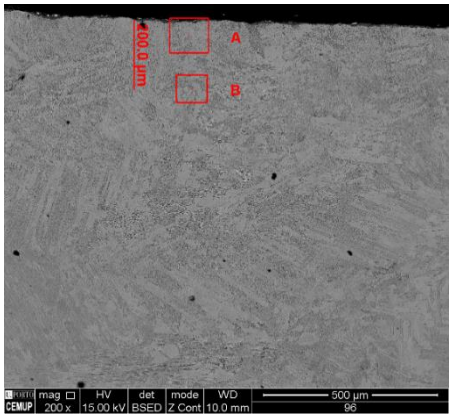

96	Chemical Composition wt%					
AAFY	Al	Nb	Ti	Cr	O	Y
A	34.73	4.83	57.95	0.93	1.42	0.14
B	36.16	4.53	58.09	1.22	0.00	0.00
Ingot Alloy	34.54	5.32	59.86	0.28	0.00	0.00

c)

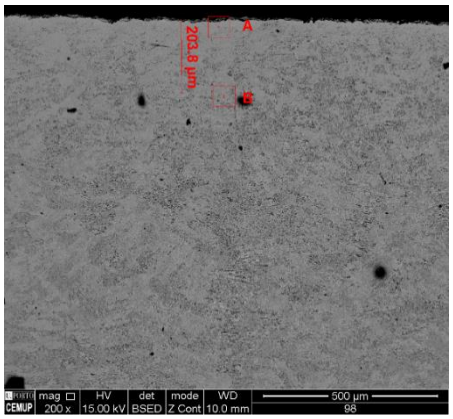

98	Chemical Composition wt%			
AFZr	Al	Nb	Ti	Cr
A	37.05	5.50	56.27	1.18
B	34.91	5.29	58.45	1.35
Ingot Alloy	34.54	5.32	59.86	0.28

d)

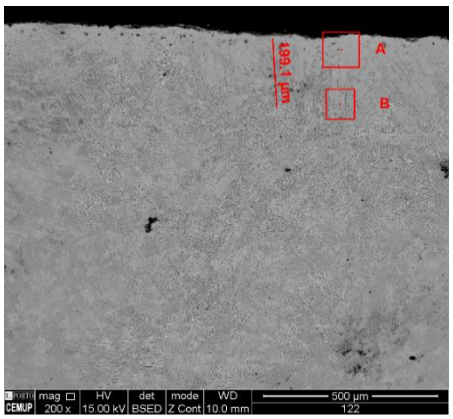

122	Chemical Composition wt%				
AFZrYC	Al	Nb	Ti	Cr	Zr
A	36.93	4.79	55.20	1.18	1.90
B	34.90	5.09	58.81	0.77	0.43
Ingot Alloy	34.54	5.32	59.86	0.28	0.00

e)

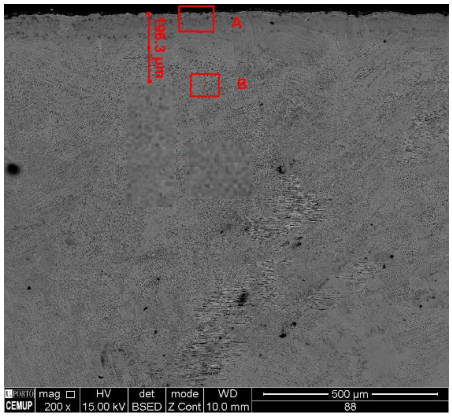

88	Chemical Composition wt%				
SZ	Al	Nb	Ti	Cr	Si
A	33.73	4.58	59.83	1.41	0.45
B	34.81	6.47	57.25	1.24	0.23
Ingot Alloy	34.54	5.32	59.86	0.28	0.00

f)

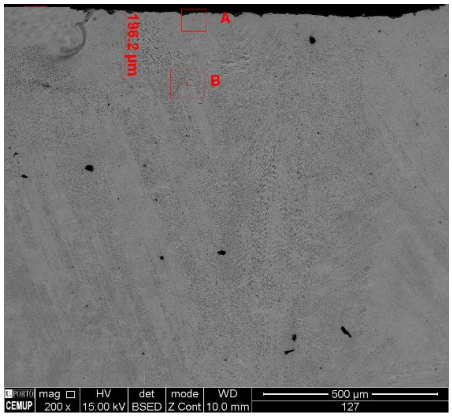

127	Chemical Composition wt%				
SAIT	Al	Nb	Ti	Cr	Si
A	32.97	10.86	54.52	0.97	0.68
B	31.06	12.74	54.54	1.49	0.17
Ingot Alloy	34.54	5.32	59.86	0.28	0.00

Figure 2.13 - SEM microstructures of the metallic TiAl samples produced with the different face coats with the locations where chemical composition was determined: a) AY, b) AAFY, c) AFZr, d) AFZrYC, e) SZ and f) SAIT.

These SEM/EDS analysis were made in order to try to find some differences between surface and interior of castings to justify the microhardness values obtained. In all samples tested no significant microstructural differences between surface and interior were detected.

Castings obtained from SAIT and SZ shells compositions exhibits some Si rich zones which cause can be from the reaction with silica of the binder.

Samples obtained from AFZrYC shells presents some Zr rich zones mainly at the surface (see region A on Figure 2.13d) that can be explained by the reduction of ZrO_2 by liquid metal. If alumina is reduced it is not detectable because de ingot alloy has Al.

Castings obtained from AY and AFZr face coats did not show any significant contamination on surface or interior.

In castings obtained from AAFY some Y was found near surface probably due to contamination from the shell face coat due to the lower sintering temperatures used.

2.4. Conclusions

Regarding fluidity, best filling capacities were obtained with coarser face coat flour grain size ≤ 200 mesh, probably due to its better permeability.

Cheapest common compositions like SZ can be used to obtain TiAl castings but about 0,3mm thickness must be removed by some finishing processes like chemical milling.

Best compositions for face coats shells are based on Y_2O_3 (AY and AAFY). In these cases, if necessary, the thickness to remove will be around 0.2 mm.

A good and economically solution can be obtained using zirconia based face coats (AFZr) which can be improved using some low cost fine yttria not fused (AFZrYC).

Future work must be accomplished in order to confirm: flour grain size distribution influence on permeability and fluidity of TiAl, study processability, friability and determine cooling conditions before remove the castings from the controlled atmosphere furnace. We believe that a significant part of surface hardening of castings is due to air contamination of hot metal surface after removing of the castings from the argon atmosphere.

References

Altindis, M., Hagemann, K., Polaczek, A.B., Krupp, U., 2011. Investigation of the effects of different types of investments on the "α-case" layer of Ti6Al7Nb castings. *Adv. Eng. Mater.* 13(4), 319-324. http://dx.doi.org/10.1002/adem.201000264. doi: 10.1002/adem.201000264

Andrade, J., 2011. *Desenvolvimento de um forno para fusão em cadinho frio e vazamento em contra-gravidade.* MSc Dissertation, Faculty of Engineering of University of Porto.

André, G., 2011. *Desenvolvimento do processo de fusão e vazamento de ligas de níquel e aluminatos de titânio*. MSc Dissertation, Faculty of Engineering of University of Porto.

Appel, Fritz, Paul, J.D.H., Oehring, M., 2011. *Gamma Titanium Aluminide Alloys*. Willey-VCH, Weinheim, Germany.

ASM, 1998. Casting. In: *ASM HandBooks OnlineTM*, Vol. 15, access online on 20-11-2013, URL: HTTP://PRODUCTS.ASMINTERNATIONAL.ORG/HBK/INDEX.JSP

Barrigana, T.G., 2013. *Estudo da reatividade de ligas de titânio e aluminetos de titânio fundidos com os refractários de carapaças cerâmicas*. MSc Dissertation, Faculty of Engineering of University of Porto, Porto, Porto.

Chen, Y., Xiao, S., Tian, J., Xu, L. and Chen, Y., 2011. Effect of particle size distribution on properties of zirconia ceramic mould for TiAl investment casting. *Trans. Nonferrous Met. Soc. China* 21, s342-s347. doi: 10.1016/s1003-6326(11)61603-8.

Cheng, X., Sun, X.D., Yuan, C., Green, N.R., Withey, P.A., 2012. An investigation of a TiAlO based refractory slurry face coat system for the investment casting of Ti–Al alloys. *Intermetallics* 29, 61-69. doi: 10.1016/j.intermet.2012.05.005.

Clemens, H., Smarsly, W., 2011. Light-Weight Intermetallic Titanium Aluminides – Status of Research and Development. *Adv. Eng. Mater.* 278, 551-556. doi: 10.4028/www.scientific.net/AMR.278.551.

Duarte, T.P., Neto, R.J., Félix, R., Lino, F.J., 2008. Optimization of Ceramic Shells for Contact with Reactive Alloys. *Mater Sci Forum* 587/588, 157-161.

Duarte, T.P., Neto, R.J., Félix, R., Lino, F.J., Rodrigues, B., Barbosa, T., 2009. Manufacturing Ceramic Shells for Casting Titanium Components. IRF 2009 – *3rd Conf. on Integrity, Reliability and Failure*, Porto, Portugal, 20-24 July.

Guntlin, R., Aguilar, J., Kattlitz, O., Stoyanov, T., Tiefers, R., Jana, S., 2012. State of the art development in investment casting to face the challenges of the new generation of aero engine components. WCIC - *13th World Conference on Investment Casting*. Kyoto, Japan, 15-18 April.

Jones, S., Yuan, C., 2003. Advances in shell moulding for investment casting. *J. Mater. Process. Technol.* 135(2-3), 258-265.

Kothari, K., Radhakrishnan, R., Wereley, N.M., 2012. Advances in gamma titanium aluminides and their manufacturing techniques. *Prog. Aerosp. Sci.* 55, 1-16. doi:10.1016/j.paerosci.2012.04.001.

Leyens, C., Peters, M., 2003. *Titanium and Titanium Alloys - Fundamentals and applications*. Willey-VCH, Weinheim, Germany.

Magalhães, Á., 2012. *Desenvolvimento do processo de fundição de turbinas para turbocompressores em aluminetos de titânio*. MSc Dissertation, Faculty of Engineering of University of Porto, Porto, Portugal.

Martins, B., 2008. *Desenvolvimento de um forno de indução para fusão e vazamento de ligas de titânio ti e outras ligas reativas com reprodutibilidade*. MSc Dissertation, Faculty of Engineering of University of Porto, Porto, Portugal.

Pattnaik, S., Karunakar, D.B., Jha, P.K., 2012. Developments in investment casting process - A review. *J. Mater. Process. Technol.* 212(11), 2332-2348. doi: 10.1016/j.jmatprotec.2012.06.003.

Rocha, B., 2010. *Desenvolvimento do processo de produção de próteses em ligas de Titânio*. MSc Dissertation, Faculty of Engineering of University of Porto, Porto, Portugal.

Silva, L.P., 2010. *Desenvolvimento de um forno para fusão em cadinhos frios e optimização das arquitecturas de moldações por simulação numérica*. MSc Dissertation, Faculty of Engineering of University of Porto, Porto, Portugal.

Sopcak, J.E., 1986. *Handbook of Lost Wax or Investment Casting*. Gem Guides Book Co., California, USA.

Tetsui, T., 2011. Manufacturing technology for gamma-TiAl alloy in current and future applications. *Rare Metals* 30(S1), 294-299. doi: 10.1007/s12598-011-0288-3.

Titanium Information Group, 2012. DATA SHEET No 19 Titanium Alloys. UK.

Turkdogan, E.T., 1980. *Physical Chemistry of High Temperature Technology*. Academic Press.

Voigt, K., 2012. *China cuts mines vital to tech industry*. CNN, online access on 06-06-2013, URL: HTTP://EDITION.CNN.COM/2012/08/08/BUSINESS/CHINA-RARE-EARTH/

III

Enhancement of casting processes using numerical tools and experimental analysis

1. Computational methods for numerical simulation of casting processes

With the continuous development of materials and manufacturing technologies for complex components with a high-level of geometrical and mechanical specifications have been produced by metal casting. Indeed, several advanced materials are used in foundry targeting to meet all the current technical requirements. For instance, in automotive industry the main goal is to fabricate casting products with quality by using a minimal quantity of material (*i.e.*, lightweight components).

In general, the empiric and conventional methods are time-consuming and requires many resources. The most critical task is the design of the net-shape part and its gating system. An enrichment of this task is crucial to get a casting with high-quality. It is predicted that 90% of casting defects resulted from design errors, being only 10% related to manufacturing problems.

The computational tools of numerical simulation provide a great support on the enhancement of the design phase as it allows to analyse the manufacturing process and to predict the defects that can result from this process. A finite element-based study of a casting process entails two steps: the filing and solidification simulations. The application of this analysis on the prediction of the final casting product permits to determine the main causes of eventual defects in the component, whether it results from the design process, the filling system or any other reason. This technique allows for an enhancement of the design project, as well as the manufacturing process before the component to be produced.

Regarding the casting process, various physical phenomena are involved, such as fluid flow and heat transfer. The computational modelling of these complex phenomena is only possible by using efficient and accurate numerical tools able to provide reliable predictions of the process.

Two scientific papers, which use numerical methods to simulate casting processes, are included within this chapter. The aim of these studies is to improve the reliability of the results by changing design and process conditions before starting the production. In the

first article, entitled "*Modelling feeding flow related shrinkage defects in aluminium castings*", the development of a solidification model for Al-Si alloys is presented based on process defects. This model entails several phenomena interactions, namely heat transfer, solidification and fluid dynamics (feeding flow and free surfaces). The main goal of this analysis was to obtain a model more close to reality in order to predict the casting defects related to the physical phenomena straightly involved. Using this proposed model, it is possible to predict a set of features of the final casting products: porosity by surface initiation, external porosity and internal porosity by nucleation.

In the second paper, entitled "*Numerical and experimental research of γ-TiAl turbine produced by investment casting melted using a vacuum furnace*", describes the development of an advanced model for filling and solidification simulation of γ-TiAl investment casting. This study permits to obtain an accurate model that works as a supporting tool on the enhancement of the γ-TiAl investment casting process and helps the engineer on the development of an optimized strategy for the design and manufacturing.

Regarding this topic, the role of author was focused on three key stages: i) the definition of the physical phenomena to be included in the numerical models, ii) the design of experimental test to be performed for validation purposes, and iii) the analysis of the preliminary results and, hence, the development of solutions for the model's redesign and adjustment.

Modelling feeding flow related shrinkage defects in aluminum castings

Article published in Journal of Manufacturing Processes, vol. 14(1), 2012, pp. 1-7.

A. Reis, Z. Xu, R.V. Tol and ***R. Neto***

2. Modelling feeding flow related shrinkage defects in aluminium castings

2.1. Introduction

Recently, due to the development of computer technology, an effort is done to predict casting defects directly as a consequence of the physical phenomena that are involved. A modelling approach based on an improved description of the physical processes has become a more realistic practical and straightforward option. Shrinkage related defects result from the interplay of phenomena such as fluid flow, heat transfer with solidification, feeding flow and its free surfaces, deformation of the solidified layers and so on.

Many attempts have been made to model shrinkage related defects. However, common models do not take into account feeding flow and therefore zone searching based on the solid fraction is needed. Coupling heat transfer, feeding flow and mass conservation into shrinkage defects, is an important approach. The first model that took into account feeding flow dates back to the early 1D analytic work of Piwonka and Flemings (1966). This early analytical work formed the basis of a category of models based upon Darcy's law. Darcy's law relates the flow through a porous medium to the pressure drop across it. Kubo and Phelke (1985) were the pioneers in presenting a 2D numerical model by coupling Darcy's law to the equations of continuity estimating the fluid flow. Other 2D models were presented by Zhu and Ohnaka (1990) and Huang and Berry (1993). In terms of 3D models, Bounds *et al.* (2000) presented a model that predicts macroporosity, misruns, and pipe shrinkage in shaped castings. Later, Sabau and Viswanathan (2002), Pequet *et al.* (2002) and Carlson *et al.* (2003) also present 3D models that included the concept of pore nucleation and growth.

This paper proposes a model to explicitly calculate shrinkage defects as a result of deficiency in feeding flow. A 3-D numerical problem that illustrates the ability to compute internal and surface interconnected defects is presented and compared with experimental results.

To date no methodology has been proposed to quantify the extent of shrinkage porosity, coupling internal (cavities) and external (surface connect or surface depression) shrinkage defects which occur when solidification shrinkage cannot be compensated by feeding flow. There are no validation experiments that are suitable for this model regarding the factor that determines whether shrinkage porosity is either internal or surface connected or both.

2.2. Modelling

The model solves the coupled macroscopic conservation equations for mass, momentum, and energy. It also takes into account different morphologies in solidification when calculating feeding flow and the pressure drop in the liquid as a result of cooling and solidification.

2.2.1. Continuum equations

Considering that the solid is not moving and there is no deformation, the average mass conservation equation can be written as:

$$\frac{\partial \rho}{\partial t} + \nabla \rho_l \vec{u} = 0 \tag{1}$$

where *u* denotes the liquid velocity vector, and *ρ* is the temperature and fraction solid dependent density. Comparing with the body force and source terms, the convection and diffusion of momentum have a small contribution during feeding. Therefore, they are omitted in the momentum equation. The velocity field during cooling and solidification in the casting is determined by:

$$\frac{\partial \rho \vec{u}}{\partial t} = -\nabla \mathrm{P} + \rho \vec{g} + S \tag{2}$$

where *P* is pressure and $\rho \vec{g}$ is the body force. It is assumed that when solidification starts, the solid particles adhere and form a cohesive immobile network. Liquid metal

flows through the network and the resulting pressure drop is calculated from the Darcy equation. This is represented in the model by adding a momentum sink "S".

$$S = -K\rho\vec{u} \tag{3}$$

where K is the permeability of the solid skeleton. K reflects the resistance of the solidified structure to the feeding flow. K depends on the amount of solid fraction and the way of solid fraction is distributed, e.g. the way of the material solidifying on a microscopic scale has been deduced here from the Ergun equation, see van Tol (1998):

$$K = C_{drg}\frac{1}{1-f_s}\left(\frac{f_s}{1-f_s}\right)^2 \tag{4}$$

where f_s is the solid fraction, C_{drg} [1/s] is a parameter of the solidification morphology.

K reflects the resistance of the already solidified metal to the feeding flow. K, in this model, the permeability function is dependent on the amount of solid fraction, f_s, and of the permeability coefficient K_0.

$$K = K_0\frac{{f_s}^2}{(1-f_s)^3} \tag{5}$$

where K_0 is the permeability coefficient that is typically the function of a characteristic dimension and solidification morphology.

The proposed model has two stages, before and after coherency:

- in first stage, $f_s < f_{coeh}$, mass feeding will take place and the melt is considered to behave as a slurry. K_0will take the value found in section, $K_0 = 2.8E^{-10}$ (Reis, 2008);
- in second stage after coherency, $f_s > f_{coeh}$, the permeability coefficient is set to a 10 times smaller value (decreasing the permeability). The value adopted for K_0 isotropic is $2.8E^{-11}$, which corresponds to using the secondary arm spacing as a characteristic dimension.

For surface elements a special boundary condition that takes into account columnar solidification from surface to the transition to equiaxed, d_{tran} (Reis, 2008) is used. In this region permeability is set to 100× lower than the isotropic permeability in the normal direction to free surface, i.e. parallel to surface flow.

Considering $\vec{n}$ as the normal vector to the free surface and *{1}* as the unitary vector the new permeability $[K]^n$ can be written as:

$$[K]^n = 10E^2[K]\vec{n} + [K](\{1\} - \vec{n}) \quad \text{if} \quad f_s > \frac{f_{coh} \cdot t_{crt}}{\vec{n}} \begin{Bmatrix} dx \\ dy \\ dz \end{Bmatrix} \tag{6}$$

Permeability model:

$$[K] = 2.8E^{-10}\frac{(1-f_s)^3}{f_s^2} \quad \text{if} f_s < f_{coeh} \tag{7}$$

$$[K] = K_0\frac{(1-f_s)^3}{{f_s}^2} \quad \text{if} f_s > f_{coeh} \text{ and equiaxed} \tag{8}$$

$$[K] = [K_0]^p\frac{(1-f_s)^3}{{f_s}^2} \quad \text{if} f_s > f_{coeh} \text{ and columnar}$$

The temperature and solid fraction are calculated by the energy conservation equation:

$$\frac{\partial}{\partial t}(\rho H) + \nabla(\rho H\vec{u}) = k\nabla^2 T \tag{9}$$

The enthalpy H is defined as:

$$H = \int_{T_0}^{T} c_p dT + H_L \tag{10}$$

with $H_L = (1 - f_s)L$, where L is the latent heat, $c_p$is the specific heat and k is the thermal conductivity.

The profile of any free surface (external or internal) is described by an F function. This function is similar to the function used in VOF method for free surface tracking. In this method, the fluid is represented by a step function. Since this function must be conserved as it is convected with the fluid, the time dependence of F is governed by the following:

$$\frac{\partial F}{\partial t} + \nabla F\vec{u} = 0 \tag{11}$$

Physically $\partial F/\partial t$ represents the amount of liquid that flows from the free surface element to compensate shrinkage. When averaged over the cells of a spatial mesh, the average value of F in a cell is equal to the fractional volume of the cell filled by the metal.

It should be stated here that, in a normal application (filling calculations), the only component of the F function is liquid metal. In the present model the value F can be composed by liquid metal and by a solid component if the solidification has already started. Consequently F value is at least equal to the value of the solid fraction, this means that if a pct is already solid, only the remaining liquid, "L" in Eq. (12), can be used in feeding shrinkage. A unit value of F corresponds to a full cell; a zero value corresponds to an empty cell.

$$L = (1 - f_s) - \frac{\partial F}{\partial t} \tag{12}$$

When the amount of liquid in a cell, "L", reaches zero there is no more liquid metal in this free surface element and the surrounding cells with $F = 1$ are activated as free surface continuing feeding the casting enlarging the empty volume. This means that at least one neighbour of a surface cell is a full element, $F = 1$, and the feeding velocities are always from inside to outside. Only in free surface elements that have a full neighbour, the term $\partial F/\partial t$ is calculated and it is always negative (inside to outside).

2.2.2. Numerical method

In this research, we did not use any finite element analysis software. In fact we used the finite volume method to solve the governing equations. Up to now no commercial software can simulate the phenomenon perfectly. This is purely original research work,

we developed the core code to solve the problem. But we used Experto-ViewCast to deal with pre-processing and pro-processing.

The finite volume method is used to discretize the governing equations. A structured orthogonal mesh is employed to discretize the mould and the casting. A staggered grid serves to discretize the governing equations for fluid flow calculation. The Semi-Implicit-Method for Pressure Linked Equations, SIMPLE method, described in detail by Patankar (1980) is used to handle the velocity and pressure coupling for the equations. The velocity field is calculated from the momentum and continuity equations at each time step using the updated properties of each volume element, such as solid fraction, density, and permeability. For every time step, the temperature distribution, used to calculate solid fraction, was obtained by solving the energy equation. Next the properties of each volume element were updated again. Iteration is continued until the continuity equation is satisfied. The movement of the free surface is evaluated by using the velocity field. An adapted free-surface algorithm Xu (1993) has been developed to describe the external and internal shrinkage defects. An element becomes a free surface depending on its pressure and solid fraction. At each time step, if the conditions of $P <$ P_{atm} and $f_s < f_{s\,crit} = 0.3$ in any of the outside layer elements are satisfied, this element becomes a free surface element. Also for internal elements, the condition of pore nucleation $P < P_{crit}(T) = P_{atm} \times (1 - (T_l - T)/(T_l - T_s))$ is tested. If this happens this element will be treated as a free surface element that can act as a feeder. The material properties used in the calculations are taken from Reis (2008).

2.2.3. Shrinkage defects formation

The governing equations are solved to obtain the temperature, fraction solid, melt pressure and feeding velocity throughout the casting. Before the start of solidification, unrestrained liquid feeding occurs. Liquid contraction in the casting will be fed by the highest part of the system due to gravity, resulting in “pipe shrinkage”. When the solidification starts at the outer shell of the casting, the pressure in the liquid begins to drop due to flow resistance caused by formation of solid crystals. As long as the pressure

in outside layer elements, besides the top part, drops to the atmospheric pressure they also become free surface elements that can feed the solidifying casting to compensate the metal contraction. In those elements that are emptying of liquid, the pressure is forced to the atmospheric pressure. This will result in external shrinkage defects, also called “caved surfaces”.

Once feeding path becomes obstructed by solid or partially solid material the liquid pressure quickly drops and when it reaches a critical value, $P_{crit}(T)$, a pore can nucleate and grow to account for the mass deficit resulting in an internal shrinkage defect. The internal pressures which act on pore elements must exceed all of the external forces that tend to make it collapse. As long as the pressure is larger than the critical pressure, the amount of porosity that forms is determined from the continuity equation. In this way it is not necessary to search the connected zones to feed shrinkage and the shrinkage distribution will automatically emerge by the calculation.

2.3. Results and Discussion

When designing the geometry for the test case the idea has been to reproduce a real casting condition, while maintaining the geometry as simple as possible. With a simple geometry we can better identify the variables directly enrolled in shrinkage feeding. Also the choice of the geometry has been related with being prone to different types of shrinkage defects as to illustrate the features of the developed model. Figure 2.1 shows the proposed geometry.

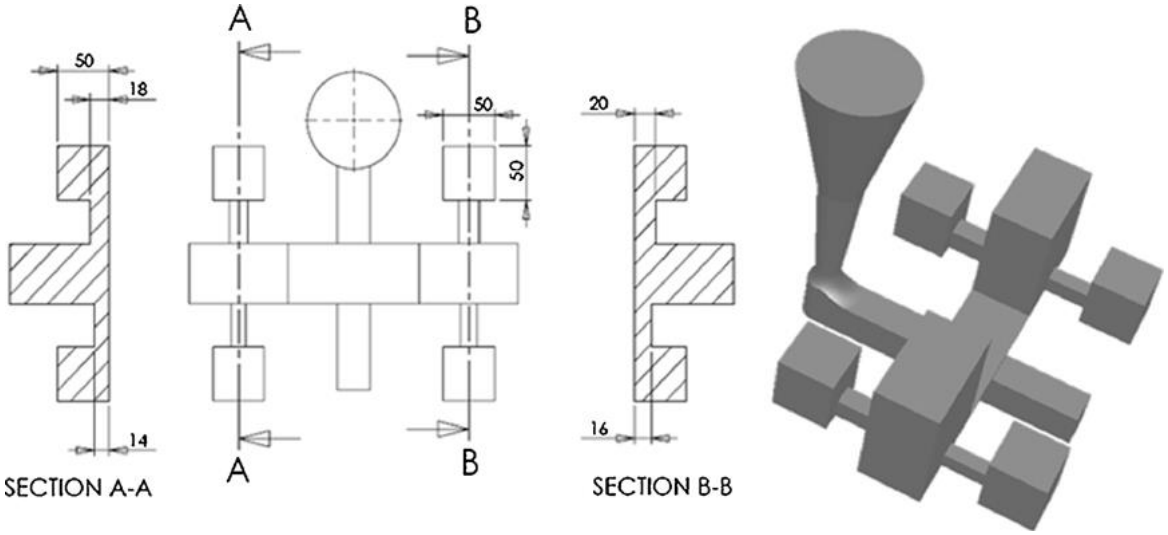

Figure 2.1 - Designed geometry, top view and two sections views A–A and B–B and 3D model.

In this paper results for short freezing, AlSi12 and long freezing alloy, AlSi7, are presented. A comparison is made between numerical and experimental. Experimentally obtained cooling curve is shown in Figure 2.2.

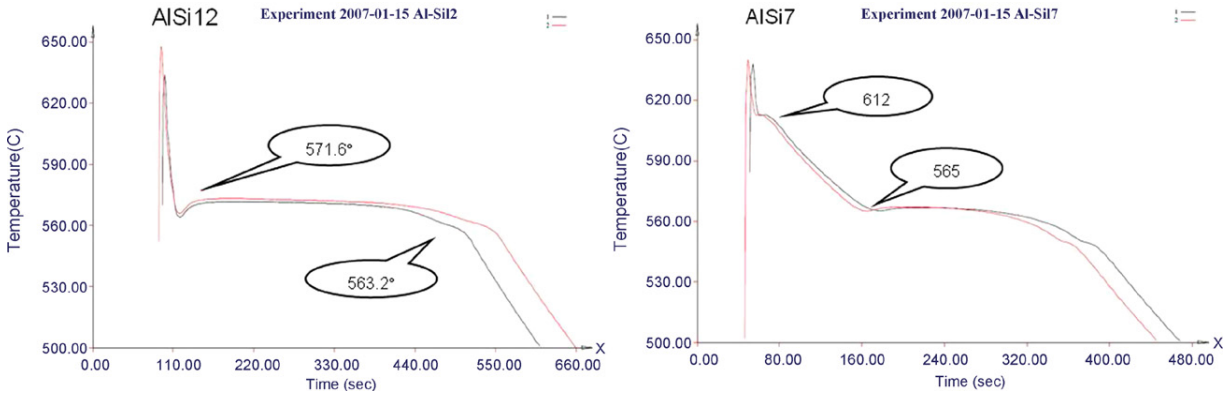

Figure 2.2 - Experimental cooling curve for AlSi12 alloy and AlSi7.

2.3.1. Experimental results

The metal was poured at 700º C. Before being poured the alloys were out-gassed. The out-gassing treatment was performed by the addition of 0.3NaCl + 2.5$AlFe_3$. To guarantee repeatability, two castings were poured at the same time. The samples were cut and polished.

Figure 2.3 presents results for the long freezing alloy, AlSi7, showing in detail the 14 mm and 18 mm neck connected part defects: surface sink and surface connected defect found in the re-entrant angle. Results obtained with short freezing alloy, AlSi12 are

presented in Figure 2.4 (14–18 mm neck section). These views show that the defects are surface connected porosity, i.e. surface started. As expected, due to freezing characteristics the short freezing material AlSi12 and the long freezing AlSi7 presented a very different behaviour. In short freezing alloys the surface connected porosity was much more visible and concentrated in a single cavity while in long freezing alloy the surface connected porosity had a much more complex shape in the form of an interdendritic cavity. Other clear evidence was the surface sinking that was mainly visible in the long freezing material. It was important to clarify the nature of the defects, since it was not immediately evident the nature of defects found in the long freezing alloy. When sectioned, the porosity resembled a mass of separate pores in regions separated by dendrites, and therefore could be mistaken for isolated interdendritic porosity instead of a single cavity.

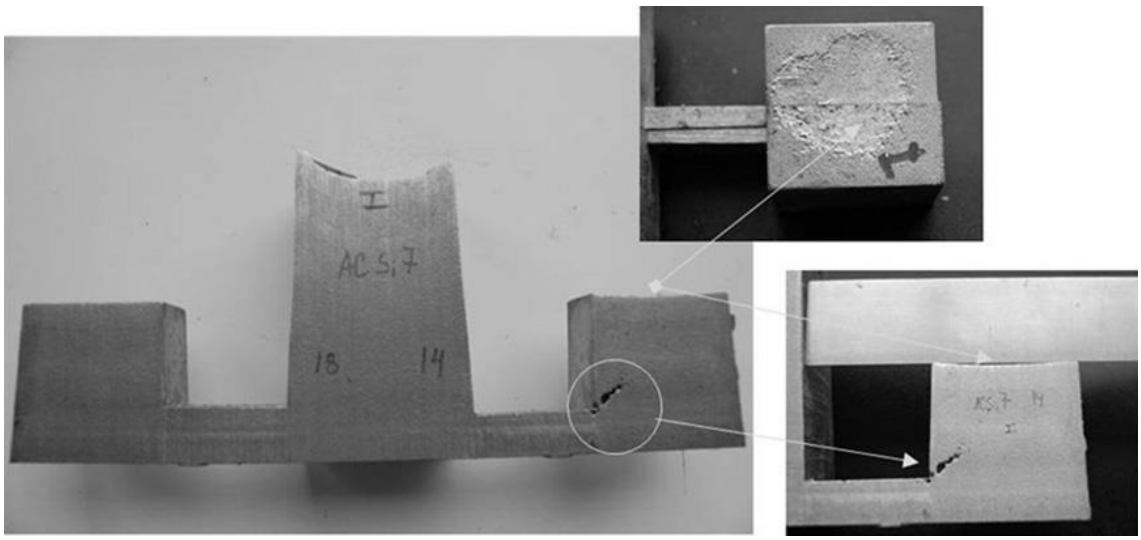

Figure 2.3 - Detail views from 14 mm section, showing the surface sink and surface connected porosity, AlSi7.

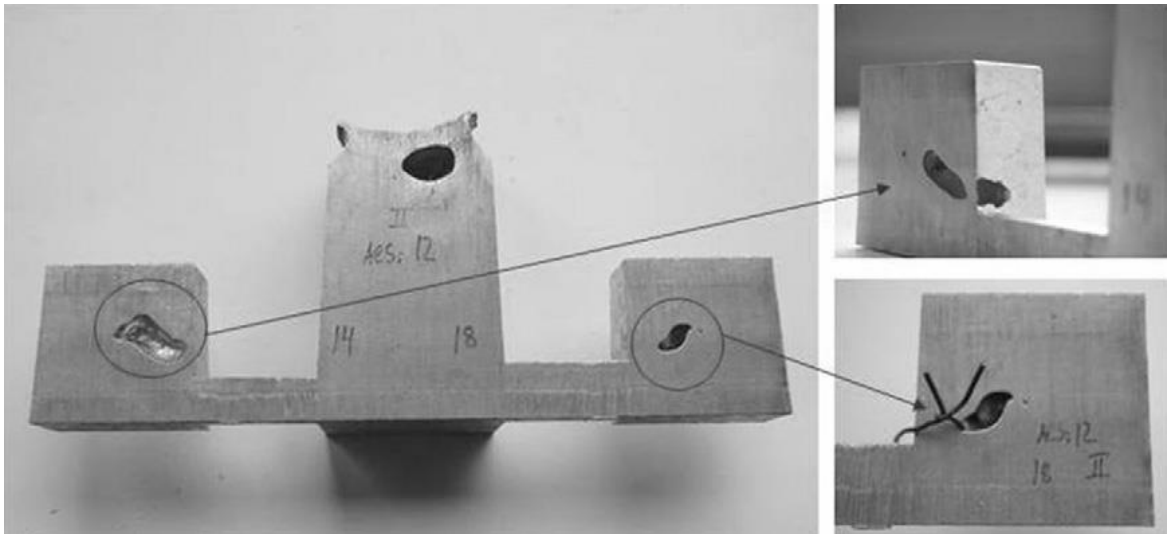

Figure 2.4 - Detail views from AlSi12, short freezing, section 14 mm and 18 mm, showing the surface connected porosity.

2.3.2. Numerical and experimental comparison

To adequately represent the geometry, a finite-volume mesh of 231.770 total elements was used. 19.330 were metal elements and 212.440 were sand elements (Figure 2.5). When considering the long freezing material, AlSi7, as the neck solidifies, the path, between the feeder and the part, becomes obstructed resulting in the pressure drop in the part. Initially, sinking of the top surface is observed, resulting in a sloped top surface, Figure 2.6(a). Eventually the top surface will be solidified and feeding from this surface stops. Pressure will continue dropping until any other surface element equals the outside pressure. By then, if these elements are still liquid enough, they can freely move to compensate shrinkage as in the re-entrant angle elements causing the growth of an interdendritic porosity (Figure 2.6(b)).

The finial shrinkage distribution is given in Figure 2.7.

When considering a short freezing material, the outside layer quickly solidifies and it is difficult to feed through a free surface movement. Only hot-spots on surface, at the corner between casting and neck, are liquid enough to feed the part. This surface connected porosity was much more visible and concentrated in a single cavity. Due to shrinking, the pressure in the inner part quickly drops resulting in internal, or surface connected shrinkage porosity.

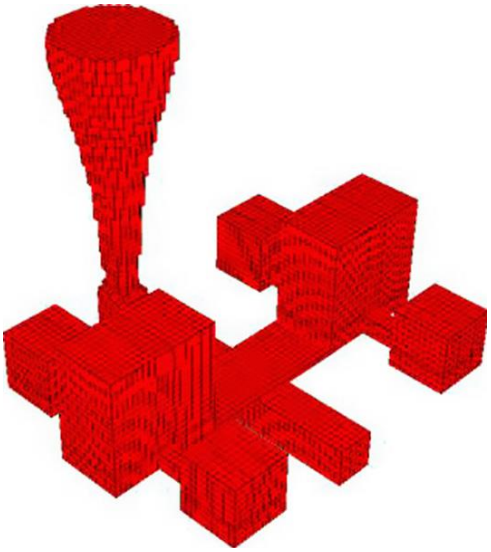

Figure 2.5 - Geometrical model and mesh of finite volume.

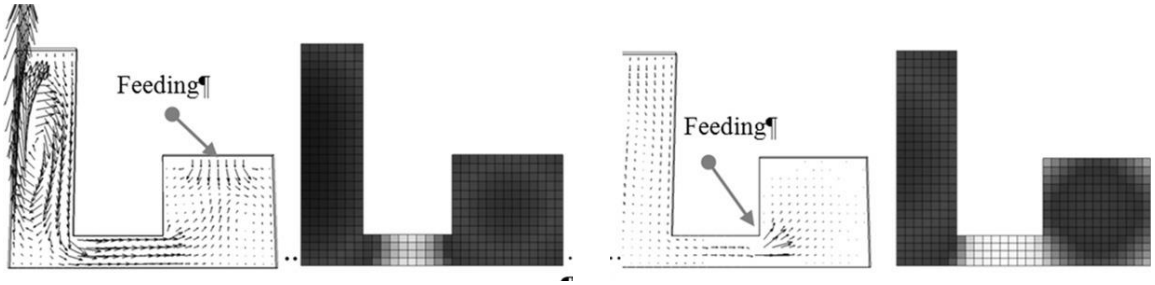

a) b)

Figure 2.6 - Feeding velocity field and solid fraction for AlSi7 with neck size of 14 mm a) 25% average solid b) 40% average solid.

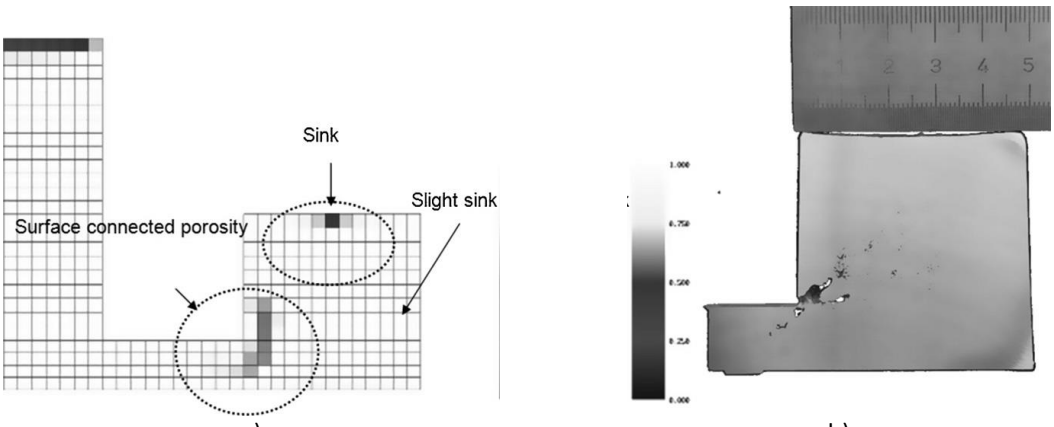

a) b)

Figure 2.7 - Shrinkage defects distribution for AlSi7 with neck size of 14 mm: a) simulation b) experiment.

A detailed comparison between simulated and experimental shrinkage defect for neck size 14 mm is shown in Figure 2.8. From the experimental and simulated results, it is

obvious that in order to obtain a sound casting, the neck size for a short freezing material is much bigger than for a long freezing material.

As the size of neck increases, simulated the amount of defects in the part decreases, which is in correspondence with reality as shown in Figures 2.9 and 2.10.

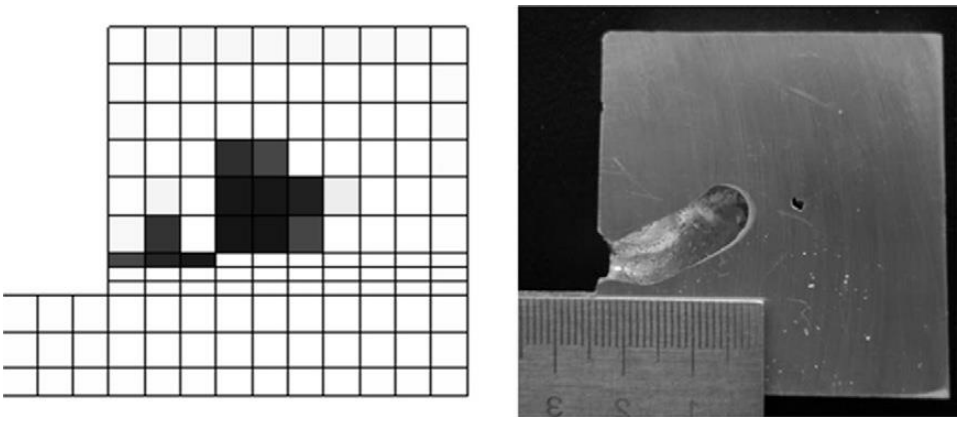

Figure 2.8 - "Caved surfaces" shrinkage defect for AlSi12 neck size 14 mm.

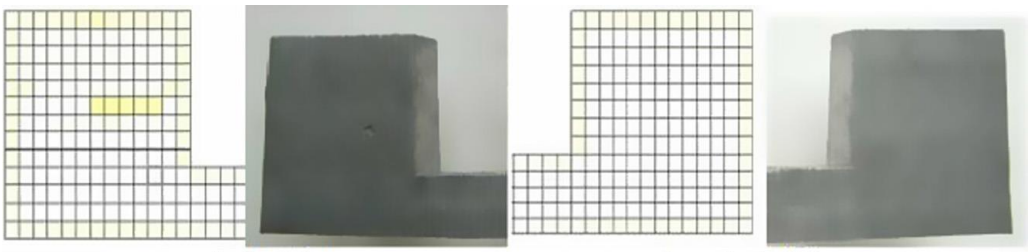

a, neck size 16mm b, neck size 18mm

Figure 2.9 - Shrinkage defect for AlSi12 neck size 16 mm and 18 mm.

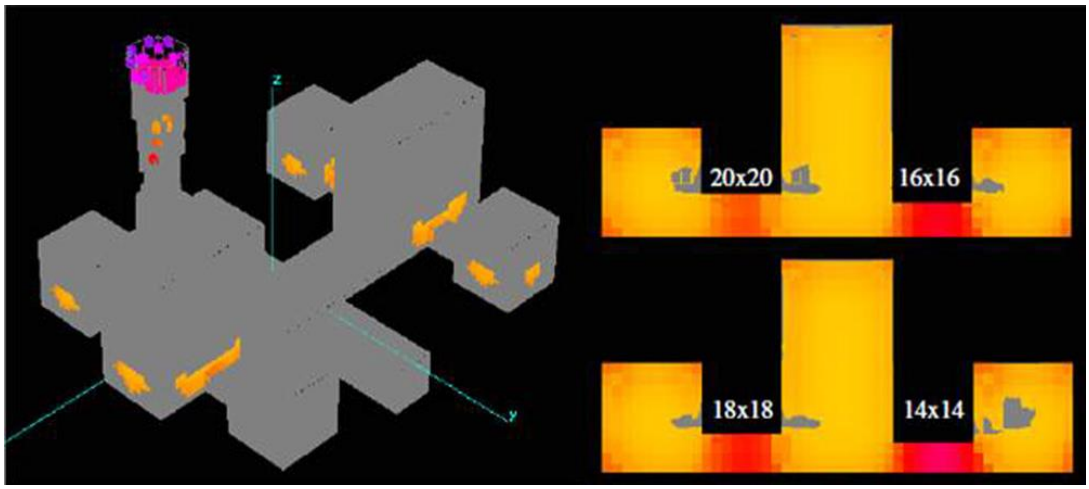

Figure 2.10 - Shrinkage defect for the complete model.

2.4. Conclusions

This model and corresponding validations have been applied to AlSi alloys. In this model different types of defects can be predicted: porosity by surface initiation, external porosity and internal porosity by nucleation. As expected, due to freezing characteristics the short freezing material AlSi12 and the long freezing AlSi7 presented a very different behaviour.

Internal porosity by surface initiation was found in both short and long freezing alloys, although having different appearance. In the long freezing alloy AlSi7, what seems to be a series of separate interdendritic pores, is in reality a single interconnected pore with a highly complex shape. On the other hand, the short freezing alloy AlSi12 reveals a single and evident cavity. Numerical results showed that in the long-freezing-range alloy this type of defect occurred at a late stage in solidification, when developing the dendritic mesh (higher solid fraction-less permeability). This means that drawing liquid from the nearby surface becomes easier than drawing liquid from the more distant feeder. The point from which liquid may be drawn can be any surface and a random point in a surface. However, in the short freezing alloy, the initiation site begins at the surface and is much more localized. Surface sinks (top and side) were found in long freezing alloys. They were particularly evident when the path from the feeder was smaller. This means that the lowering in internal pressure happened very soon and leads to an inward movement of the external surface of the casting, since it was not solid enough to resist the pulling due to pressure drop. If the movement is severe and localized it constitutes a defect known as a ‘sink’ or a ‘draw’. The expected shrinkage features were well described by the present model and illustrate the capability of the “defect” model to predict the shrinkage defects of interest to the foundry industry. The model gives the correct trend in predicting the location, extent, and nature of the shrinkage porosity defects.

The way to avoid the shrinkage defect is to make the riser neck larger. In this way it will form a direct solidification and makes the feeding path open. The current method can also simulate this situation.

References

Bounds, S., Moran, G., Pericleousm K., Cross, M., Croft, T.N., 2000. A computational model for defect prediction in shape castings based on the interaction of free surface flow, heat transfer, and solidification phenomena. *Metall. Mater. Trans.* 31B, 515–527.

Carlson, K.D., Lin, Z., Hardin, R.A., Beckermann, C., Mazurkevich, G., Schneider, M.C., 2003. *Modeling porosity formation and feeding flow in steel casting*. In: Stefanescu *et al.* (Ed.). Modeling of casting, welding and advanced solidification process X, 295–302.

Huang, H., Berry, J.T., 1993. Evaluation of criteria functions to minimize microporosity formation in long-freezing range alloys. *AFS Trans*, 669–675.

Kubo, K., Phelke, R., 1985. Mathematical modeling of porosity formation in solidification. *Metall. Mater. Trans.* 16B, 359–366.

Patankar, S.V., 1980. *Numerical heat transfer and fluid flow*. CRC Press.

Pequet, Ch., Gremaud, M., Rappaz, M., 2002. Modeling of microporosity, macroporosity, and pipe-shrinkage formation during the solidification of alloys using a mushyzone refinement method: application to aluminum alloys. *Metall. Mater. Trans.* 33A, 2095–2106.

Piwonka, T.S., Flemings, M.C., 1966. Pore formation in solidification. *TMS AIME Trans*. 236, 1157–1165.

Reis, A., 2008. *Numerical modelling of shrinkage defects induced by the feeding flow in aluminium castings*. PhD thesis, University of Ghent, Belgium.

Sabau, A.S., Viswanathan, S., 2002. Microporosity prediction in aluminium alloy casting. *Metall. Mater. Trans.* 33B, 243–255.

van Tol, R., 1998. *Mould filing of horizontal castings*. PhD thesis, University of Delft, Nederland.

Xu, Z.A., 1993. *Fluid flow and thermal analysis during mould filling and solidification of castings*. PhD thesis, University of Ghent, Belgium.

Zhu, J.D., Ohnaka, I., 1990. Computer simulation of interdendritic porosity. In: Rappaz *et al.* (Eds.) *Aluminum alloy ingots and casting, modeling of casting, welding, and advanced solidification processes* V, 435–442.

Numerical and experimental research of γ-TiAl turbine produced by investment casting melted using a vacuum furnace

Article submitted to a peer-reviewed journal

***R. Neto**, N. Song, S. Wu and A. Reis*

3. Numerical and experimental research of γ-TiAl turbine produced by investment casting melted using a vacuum furnace

3.1. Introduction

Gamma titanium aluminides (γ-TiAl) represent a good substitute for traditional heat-resistant steels and Ni-based superalloys for high-temperature structural applications, mostly in those areas where the combination of low density, high tensile properties, creep strength and corrosion resistance, associated with superior strength-to-weight ratio are demanding such as military and aerospace industries (Gomes *et al.,* 2008; Noda, 1998; Renjie *et al.*, 2010; Tetsui, 2001). These attractive properties of titanium aluminides were outweighed for over a decade in the 1990s due to the existing difficulties on its processing and machining at room temperature (Kothari *et al.*, 2012). Currently, the production of TiAl-based alloy parts is increasing as a result of deeper understanding of titanium aluminides microstructure, deformation mechanisms, and advances in microalloying, as well as the development of new and cheaper processing techniques than those used so far (Kothari *et al.,* 2012; Renjie *et al.*, 2010). The interest of the automotive's industry on producing next-generation engines with these light-weight heat-resistance materials is speeding up these developments and promoting further advances on γ-TiAl processing (Aguilar *et al.,* 2011; Renjie *et al.*, 2010). The weight reduction of low-pressure turbines (LPT) and turbocharger turbine wheels by using intermetallic γ-TiAl based alloys is expected to contribute to the improvement of its turbo-lag and to reduce fuel consumption as well as significantly decrease CO_2 emissions and noise in motor vehicles (Clemens and Mayer, 2013; Noda, 1998).

Mitsubishi was the pioneer on the implementation of TiAl turbocharger wheels in their Lancer Evolution 6 sports car. Afterwards, the production of wrought processed high-performance γ-TiAl valves for racing car application has started. Only few years later, an US aero engine manufacturer announced the initiation of investment cast γ-TiAl blades in the LPT. General Electric has already equipped the last stage(s) of the low-pressure turbine (LPT) of the so-called GEnX jet engine with cast TiAl blades (Clemens and Mayer, 2013).

In spite of the advantages brought to automotive and aerospace industries by using TiAl-based alloys, one of the major problems that is holding back the manufacturing of engine components with these alloys is their processing. There are two main approaches to produce turbocharger turbines, namely powder metallurgy and casting process Powder metallurgy is hard to apply for turbocharger manufacturing due to its poor soundness and weldability (Sung and Kim, 2007). From the viewpoint of cost-effective process, investment casting could be regarded as an economic net-shape technology for TiAl alloys (Sung and Kim, 2007). Investment casting (also known as 'lost wax casting' or 'precision casting') has been a widely used process and is known for its ability to produce components of excellent surface finish, and dimensional accuracy. It is recommended for making castings of complex and nearnet shape geometries, where machining may not be possible or too wasteful (Pattnaik, 2012). However, investment casting of TiAl components is a long and complex process requiring very close control and strict documentation in order to achieve the required qualification for production of castings (Aguilar *et al.*, 2011). Thus, it is clear that processing of TiAl-based alloys requires further developments in order to establish a reproducible and reliable manufacturing route able to produce robust and quality acceptable aero-engine components at an acceptable cost (Aguilar *et al.*, 2011; Clemens and Mayer, 2013; Wu, 2006). This assumption motivates the present work that aims to study the production of a TiAl turbine by investment casting. In order to predict the investment casting process and take conclusions about the adopted manufacturing route, computational simulations are carried out. There are a wide range of commercial codes available for metal casting simulation. Sung and Kim (2007) utilized Magmasoft® to perform some investigations on castability of TiAl turbocharger turbine using several casting parameters. Within this study, Procast® software is applied to simulate the filling and solidification processes. The unknown thermo-physical variables for computational modelling are determined by the experiment of TiAl alloys' casting. In order to avoid contamination by oxidation, a vacuum crucible is used. A comparative study between experimental and numerical results is presented. The microstructure of TiAl alloy under different solidification speed is analysed, as well as its microhardness.

3.2. Experimental method

For this study, a turbine is designed in SolidWorks® (Dassault Systèmes SolidWorks Corporation, Waltham, MA). This engine component is appropriate to investigate the filling and solidification processes as it has a complex geometry with both curvature and thin wall parts. In this work, the thinnest part of the component is the turbine blade tip with approximately 0.4 mm.

Following, the wax pattern is formed. Due to the highly curved surfaces of the turbine, a milled master turbine wheel is made to produce the wax mold. Figure 3.1a illustrates the milled master turbine wheel and Figure 3.1b shows the wax pattern of the turbine.

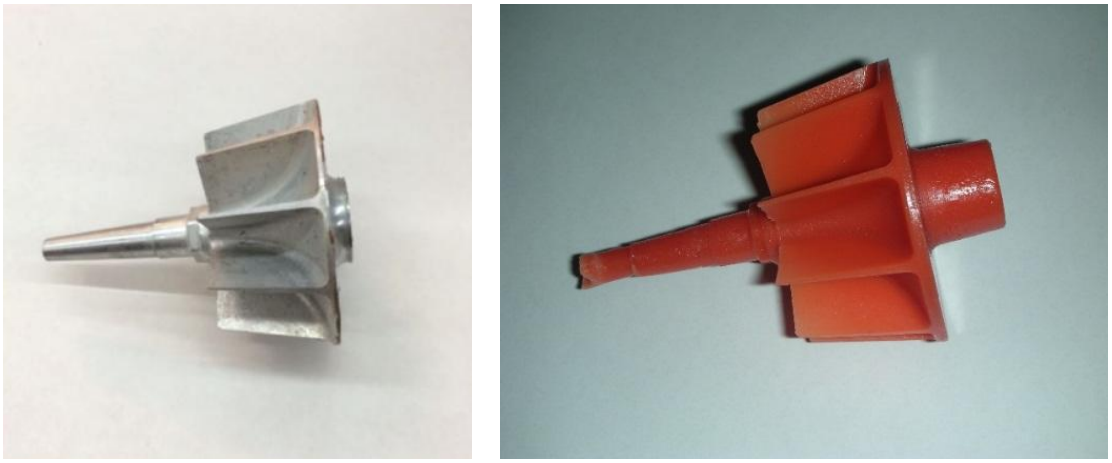

a) b)

Figure 3.1 - Designed turbine: a) Milled master part and b) Wax pattern.

After the formation of the wax patterns, they are gated together to a wax sprue (Figure 3.2a). Then, the sprued pattern is invested with ceramic or refractory slurry, which is then solidified to build a shell around the wax pattern (Pattnaik, 2012). Ceramic shell moulds are produced by covering the wax clusters with ceramic materials. This is achieved by dipping the cluster in ceramic slurry followed by sanding. The ceramic slurry provides a smooth surface while sand gives strength to the shell. This process is repeated several times between drying intervals until a defined shell thickness is achieved (Aguilar et al., 2011). The ceramic shell plays a key role in oxidation of the castings. Researchers have done a lot of work on this aspect (Renjie *et al.,* 2010; Sung and Kim, 2005). Although, as reported by Gomes et al. (2008), until now no refractory material was found to be absolutely inert against TiAl alloys and some interactions between the alloy and the crucible/mould materials always occurred during melting and

casting, leading to metal contamination. Taking into account the Gibbs free energy of formation, Kostov and Friedrich (2006) found that Y2O3 presents the most negative value among common metallic oxides, suggesting that it is a suitable material to be used as crucibles/moulds for melting and casting of TiAl alloys. Based on this study, an Yttria-based ceramic slurry is used to produce the front layers of the mould (also now as face coat) in order to fabricate a TiAl alloy product with lower oxidation problems (Aguilar *et al.*, 2011). It is considered a face coat of 2 mm thickness. For the back-up layers (also now as backup coat), alumina is used and a 5 mm thickness is considered. Fig. 3.2b and 3.2c illustrates the face coat shell and backup coat shell, respectively. From Fig. 3.2 it can be seen that the pouring basin is also showed during wax and shelling process. But after filling, that position usually contains no alloy.

Afterward, the ceramic shell is preheated to 1100°C before pouring. This step is necessary due to the thin wall parts of the turbine. Otherwise, the liquid alloy will freeze during filling and will cause an incomplete filling. The filling temperature of liquid is controlled to be around 1605°C.

a) b) c)

Figure 3.2 - a) Wax sprue, b) Face coat shell after dry and c) Backup coat shell.

Next, the TiAl ingot is re-melted in a special designed vacuum furnace. All the process is performed under vacuum conditions. Figure 3.3 shows the vacuum furnace used in this study.

Figure 3.3 - Vaccum furnace.

3.3. Numerical study

Computational simulations are carried out in order to predict the filling and solidification processes. This numerical study is performed in Procast® (ESI-Group, Paris).

3.3.1. Material

The testing material is γ-TiAl RNT650, being the composition and the liquidus and solidus listed in Table 3.1. The thermal parameters of the TiAl alloy are calculated in Procast®.

Table 3.1 - The composition, liquidus and solidus of the γ-TiAl RNT650 alloy.

	Al	Nb	Cr	Si	Ti	Liquidus (°C)	Solidus (°C)
γ-TiAl	48.1	2.0	0.7	0.3	balance	1505	1384

3.3.2. Initial and boundary conditions

In order to simulate the whole investment casting process with accuracy, two distinct layers are considered on generating the numerical model. The former is the face coat, which is based on Yttria material and its thickness is set to be 2 mm. The other layer is the backup coat, is made of alumina and has a 5 mm thickness. Mould materials and its

properties have a key effect on the final heat transfer pattern and, thus, they should be taken into account while modelling the heat transfer phenomena (Mould material properties, especially thermal resistance, significantly changes with a variation of temperature (Rafique and Iqbal, 2009)).

In the experimental process, no different material boundary is added between the face coat and the backup coat. Thus, the interface of these two layers is set to EQUIV in Procast®.

Due to the thin wall parts of the turbine, a very fine mesh is used. The mesh size of the turbine is set to be 0.5 mm excepting for the blade tip part, which has a mesh size of 0.2 mm. A total element number of 926302 is considered. Figure 3.4 shows the meshes of the turbine, the face coat and backup coat. The pouring position is set from the bottom of the basin and the beginning of the sprue.

According to the experiments, the inlet pouring speed is set to be 1 kg/s. For investment casting process, the radiation effect of the shell can't be ignored. Thus, the emissivity of the outer surface of the shell is considered to be a variable of the temperature.

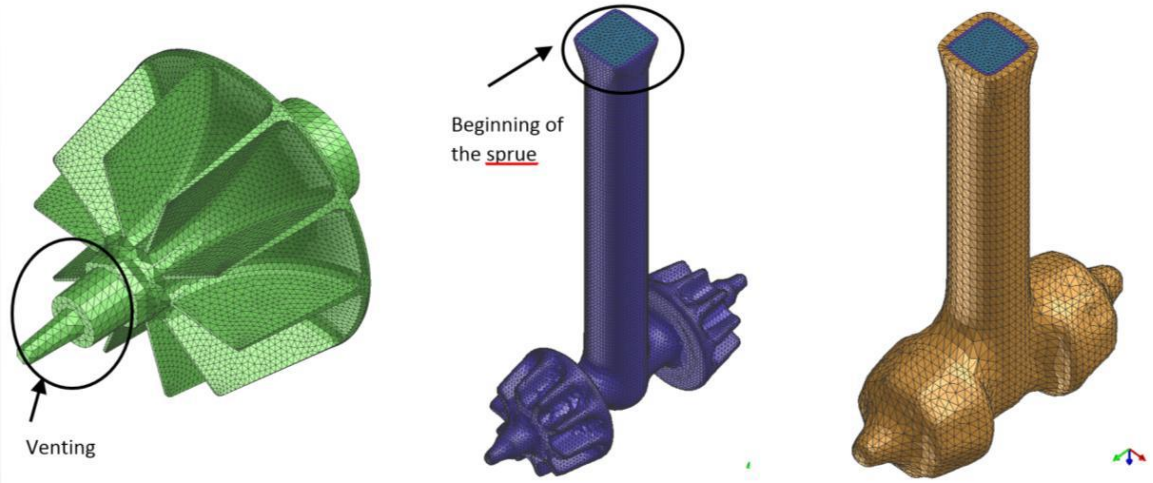

a) b) c)

Figure 3.4 - Finite element meshes: a) turbine, b) face coat and c) backup coat.

3.4. Results and Discussion

In this section, the principal results are presented and discussed, according to five analysing factors: i) the filling sequence of the blade tips, ii) the shrinkage position of the turbines, iii) the solidification speed of different positions of the turbine, iv) the microstructure of the TiAl alloy under different solidification speeds and v) the hardness of the different positions of the TiAl turbine.

3.4.1. Filling sequence of the blade tips

The simulation of the filling process allows for observing the filling situation of the turbine. Figure 3.5 shows the filling sequence of the liquid metal. From Figure 3.5 it can be seen that, for the kind of gating system used, the upper tip of the turbine is the last filling position as the gas or bubbles in the liquid are easier gathering there. This explains why for some turbines the upper tips always have unfilling problems (Jovanovid, 2005). These unfilling problems can be solved if the venting solution or the shell permeability are under proper conditions. The filling sequence has not too much influence in the filling temperature. Although, it is related with the filling speed.

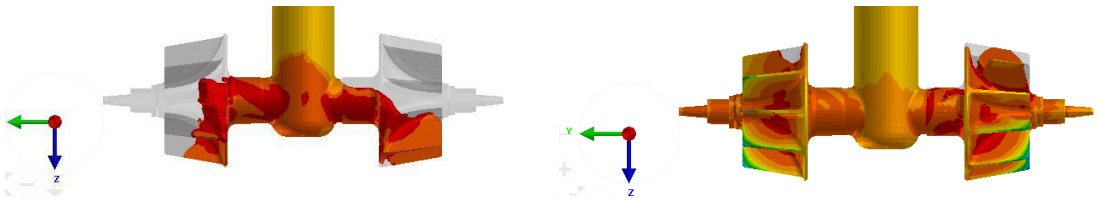

a) b)

Figure 3.5 - The filling sequence of the liquid: a) the bottom tip of the blade and b) the top tip of the blade.

Figure 3.6 depicts the velocity and temperature field during filling process. As shown in Figure 3.6a, the velocity of the liquid alloy into the turbine is around 1 m/s. By analysing Figure 3.6b, it can be seen that there is a substantial difference between the temperatures at the highest and lowest positions of the model. From this simulation, it can also be observed that immediately after filling the temperature of the tip of the turbine dropped to nearly liquidus. This outcome is valid for the turbine in study, but not for the overall turbines because the difference of thicknesses between the blade and the centre part affects significantly the solidification speed.

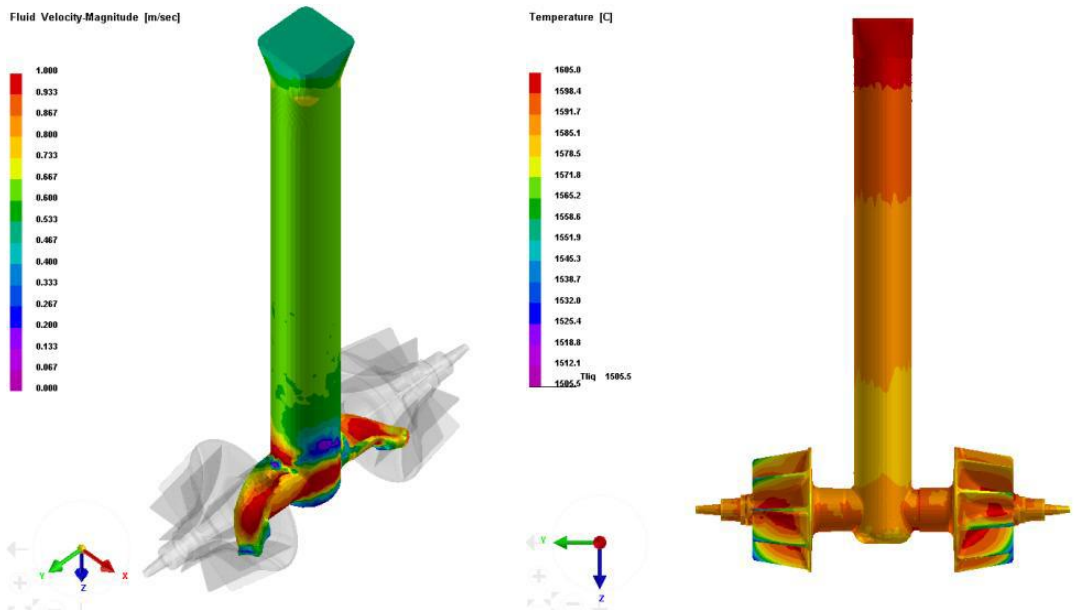

a) b)

Figure 3.6 - Velocity and temperature field of pouring process: a) the fluid velocity of the liquid into the turbine; b) the temperature field of the turbine just after filling.

3.4.2. Shrinkage position of the turbines

The shrinkage of the casting and sprue are predicted. Figure 3.7 shows the shrinkage positions of the whole gating system from both numerical and experimental aspects. By analysing Figure 3.7a, it can be seen that there is shrinkage only in the sprue. The experimental results corroborate the shrinkage position observed in the numerical model. Thus, it can be concluded that the applied sprue is suitable to feed the designed turbine.

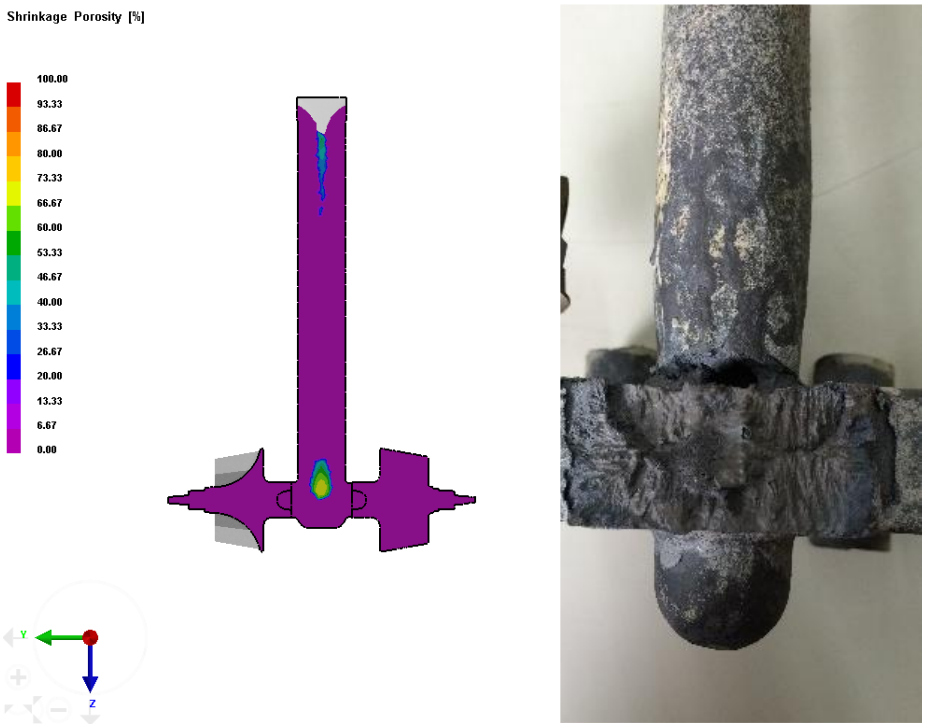

a) b)

Figure 3.7 - Shrinkage of the gating system: a) numerical and b) experimental results.

3.4.3. Solidification speed of different positions of the turbine

It is quite difficult to test the temperature change of the turbine during investment casting process, especially for the very thin blade tip position. That will require put a thermocouple inside the shell mould and preheat it, together with the shell, to more than 1000°C. To overcome this problem, computational methods are used. By numerical simulation, it is possible to predict the temperature variation in different positions of the turbine. Figure 3.8 depicts the temperature variation of four different positions in the turbine with time. Position 1 is set at the middle part of a turbine blade. Positions 2, 3 and 4 are located in the centre line of the turbine. From Figure 3.8 it can be seen that the solidification speed of the 4 positions are quite different. The centre bottom of the turbine (Position 3) is the last solidification position. The position 4 goes to the liquidus temperature zone to the solidus temperature zone in 40 seconds. But the blade (position 1) uses less than 5 seconds to solidify. Indeed, position 1 represents the location among the four that solidifies faster within 35 seconds. Turbine blade has edge-

cooling effect. This kind of solidification situation will cause different microstructures and also cause different mechanical properties of the whole turbine.

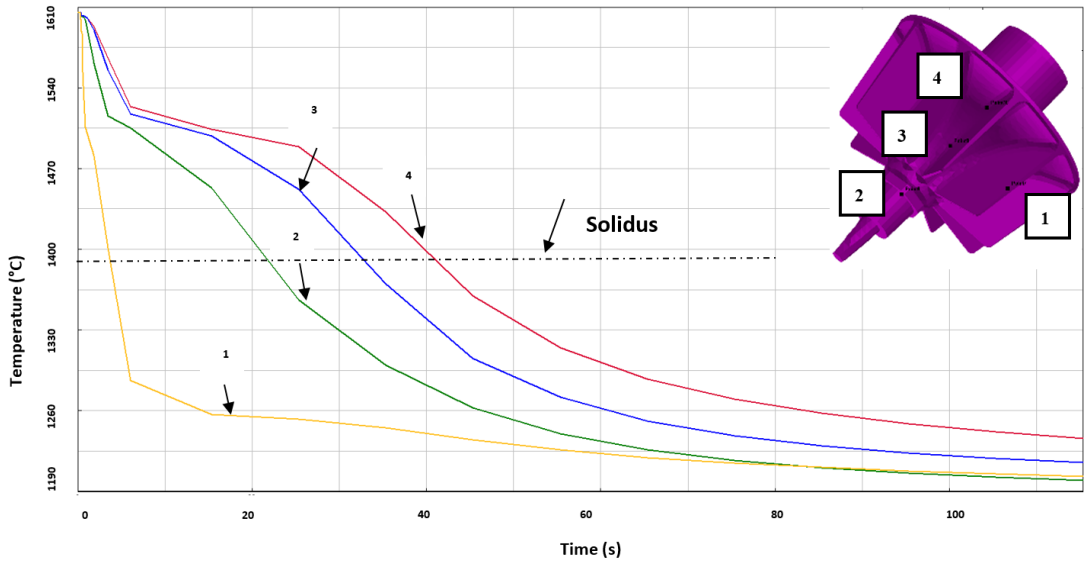

Figure 3.8 - Temperature drop VS time change of the different positions of the turbine. Blade middle (point 1), centre top (point 2), centre middle (point 3), and centre bottom (point 4).

3.4.4. Microstructure of the TiAl alloy under different solidification speeds

In this section, microstructures of distinct positions under different solidification speeds (As cast) are presented. The positions adopted for the microstructures are the considered in subsection 4.3 and illustrated in Figure 3.8. This analysis is aimed to check the influence of different solidification conditions on the formation of the microstructure. The tip of the blade is under the fast solidification speed and the microstructure of the tip is quite fine (Figure 3.9a). The inner centre of the turbine is the last solidification zone. This location has a coarser microstructure as it can be seen in Figure 3.9b-d. Thus, it is expected that, whenever exist, the defects appear firstly in the inner centre position.

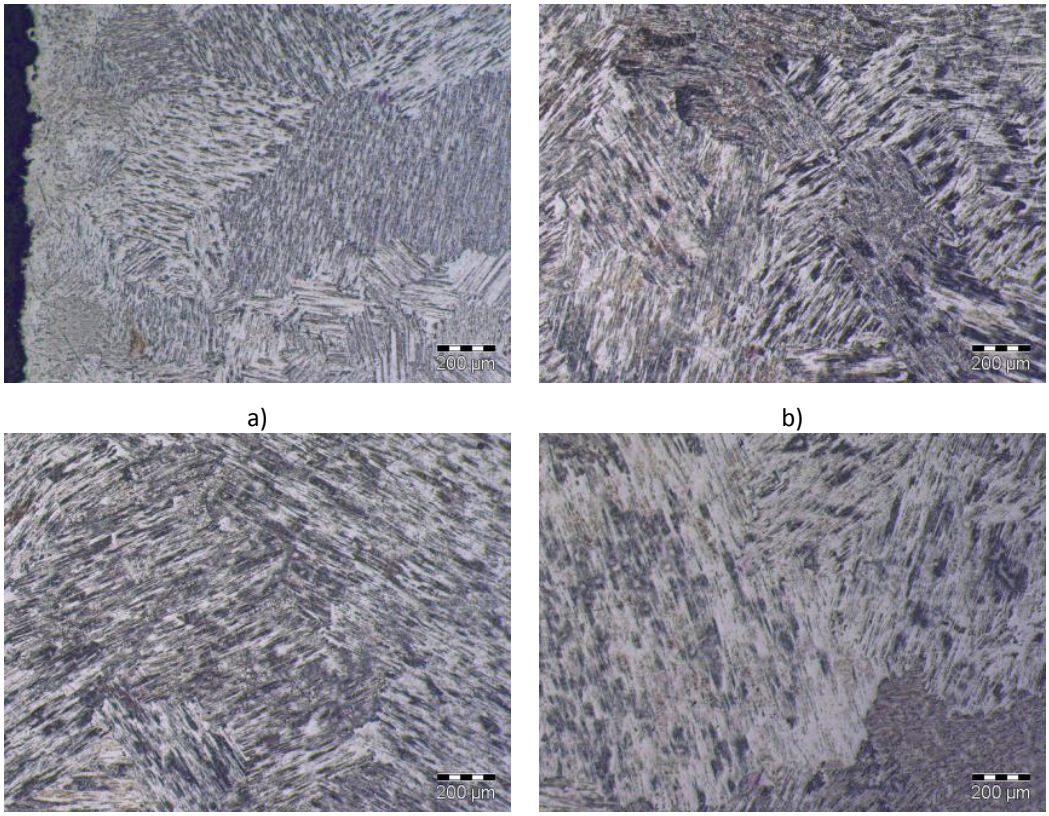

a) b)

c) d)

Figure 3.9 - Microstructures at four turbine positions: a) blade (position 1), b) centre top (position 2), c) centre middle (position 3) and, d) centre bottom (position 4).

3.4.5. Hardness of the different positions of the TiAl turbine

Hv5 hardness of 5 turbine samples are measured. The testing positions are taken along the turbine centre, according to Figure 3.8, that is 0 mm (position 2), 12 mm (position 3) and 24 mm (position 4) from the turbine top. The obtained results are plotted in Figure 3.10. By analysing Figure 3.10, it can be concluded that the hardness decreases from the top to the bottom of the turbine. This outcome confirms that the hardness of the TiAl decreases as the microstructure gets coarser.

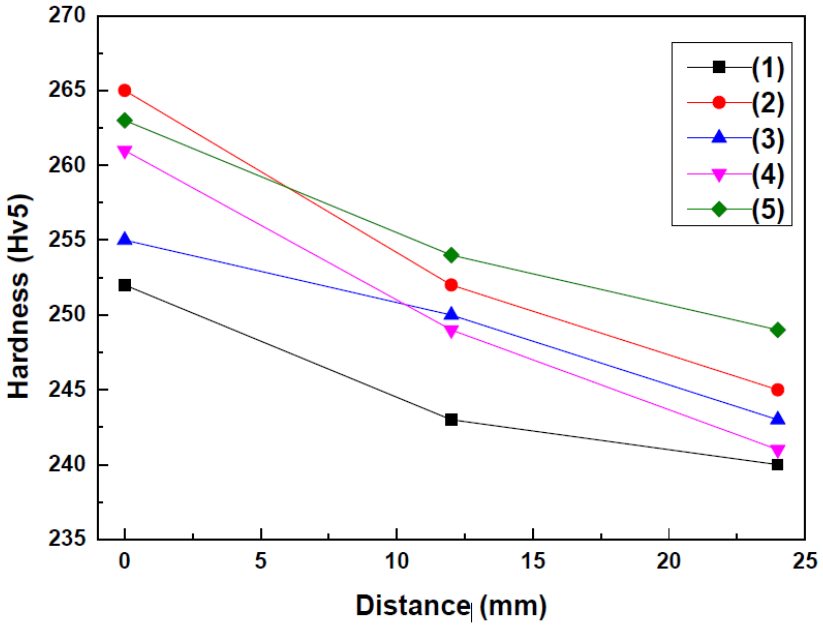

Figure 3.10 - Hardness of different positions of the turbine- centre part.

3.5. Concluding Remarks

- The vacuum furnace was successfully used to cast a TiAl turbine wheel. Numerical and experimental methods are used to analyse the filling and solidification process.
- The filling simulation reveals that the upper part of the blade tip is more able to catch gas or inclusions than the downer tips. This outcome is congruent with some casting experiments using the same gating system. The shrinkage position in the sprue predicted by numerical simulation also shows a good agreement with the experimental results.
- The microstructures of distinct positions of the turbine are different as a result of dissimilar solidification speeds. The tip of the blade presents the fast solidification position and the finest microstructure. The centre of the turbine has the coarsest microstructure because of the lower solidification rate. Further investigations are required for developing methods to refine the microstructure at the inner part of the turbine.
- The hardness at four different positions of the turbine is quite related to the corresponding microstructures.

References

Aguilar, J., Schievenbusch, A., Kättlitz, O., 2011. Investment casting technology for production of TiAl low pressure turbine blades – Process engineering and parameter analysis. *Intermetallics* 19(6), 757-761.

Clemens, H., Mayer, S., 2013. Design, Processing, Microstructure, Properties, and Applications of Advanced Intermetallic TiAl Alloys. *Adv. Eng. Mater.* 15(4), 191-215.

Gomes, F., Barbosa, J., Ribeiro, C.S., 2008. Induction melting of γ-TiAl in CaO crucibles. *Intermetallics* 16(11-12), 1292-1297.

Jovanovid, M.T., Dimčid, B., Bobid, I., Zec, S., Maksimovid V., 2005. Microstructure and mechanical properties of precision cast TiAl turbocharger wheel. *J. Mater. Process. Technol.* 167(1), 14-21.

Kostov, A., Friedrich, B., 2006. Predicting thermodynamic stability of crucible oxides in molten titanium and titanium alloys. *Comput. Mater. Sci.* 38(2), 374-385.

Kothari, K., Radhakrishnan, R., Wereley, N.M., 2012. Advances in gamma titanium aluminides and their manufacturing techniques. *Prog. Aerosp. Sci.* 55, 1-16.

Noda, T., 1998. Application of cast gamma TiAl for automobiles. *Intermetallics* 6, 709-713.

Pattnaik, S., Karunakar, D.B., Jha, P.K., 2012. Developments in investment casting process—A review. *J. Mater. Process. Technol.* 212(11), 2332-2348.

Rafique, M.M.A., Iqbal, J., 2009. Modeling and simulation of heat transfer phenomena during investment casting. *Int. J. Heat Mass Transfer.* 52(7-8), 2132-2139.

Renjie, C., Ming, G., Hu, Z., Shengkai, G., 2010. Interactions between TiAl alloys and yttria refractory material in casting process. *J. Mater. Process. Technol.* 210(9), 1190-1196.

Sung, S.Y., Kim, Y.J., 2005. Alpha-case formation mechanism on titanium investment castings. *Mater. Sci. Eng.* A 405(1-2), 173-177.

Sung, S.Y., Kim, Y.J., 2007. Modeling of titanium aluminides turbo-charger casting. *Intermetallics* 15(4), 468-474.

Tetsui, T., 2001. Application of TiAl in a Turbocharger for passenger vehicles. *Adv. Eng. Mater.* 3, 307-310.

Wu, X., 2006. Review of alloy and process development of TiAl alloys. *Intermetallics* 14(10-11), 1114- 1122.

IV

Design and manufacture of custom-fit prostheses

1. Customized medical prostheses

Over the years, the need for intervention on the prosthetic manufacturing field has been growing with the increase of life expectancy. In orthopaedics, the application of "standard" medical implants is the common option. Nonetheless, the use of these devices results very often in post-operative complications and requires complex revision surgeries. Thus, there is a rising interest in the development of customized medical implants that can provide an enhancement of the functional and aesthetical results and, consequently, improving patient's quality of life.

In this chapter, four articles are presented, which follow a straightforward and effective methodology for the development of patient-specific prostheses. This approach consists in the use of medical images, obtained from CT or MRI scans, for the 3-D reconstruction of the virtual models of patient's anatomy, enabling the 3-D modelling of the customized prosthetic CAD model. Furthermore, the fabrication process is supported by rapid prototyping and rapid tooling technologies.

In the first article, entitled "*Digital-based engineering tools for tailored design of medical implants*", a detailed description of a methodology for prosthetic design is presented. Also, in this paper, the role of this approach for pre-operative planning is emphasised.

In the following two articles, *"Custom hip prostheses by integrating CAD and casting technology"* and *"A framework for custom design and fabrication of cranio-maxillofacial prostheses using investment casting"*, a procedure for manufacturing titanium casted prostheses is proposed. The main goal consisted on the development of a method able to provide faster and cost-effective solutions for the design and fabrication of customized prostheses.

The fourth paper, entitled "*An engineering-based approach for design and fabrication of a customized nasal prosthesis*", describes a methodology for the design and manufacture of silicon-based extra-oral prostheses. The demand of these external medical devices arises from the need to improve the social and psychological quality of life, as well as aesthetical features, of patients with facial defects. Conventionally, these

prostheses are fabricated by an anaplastologist through a manual, costly and time-consuming process. The proposed approach depicted encouraging results, providing a customized prosthetic solution able to fit the anatomical features with a minimal discomfort for the patient and, also, delivering excellent functional and aesthetical results.

Digital-based engineering tools for tailored design of medical implants

Article to be published in the Proceeding of the 5th European Conference on Mechanisms Science (EUCOMES), Guimarães, September 16-20, 2014.

***R. Neto**, T. Marques, M. Marta, N. Leal, M. Couto and M. Machado*

2. Digital-based engineering tools for tailored design of medical implants

2.1. Introduction

Preoperative planning offers many benefits for patients, surgeon and remaining members of the surgical team, avoiding delays and misunderstandings. The exercise of thinking throughout the sequential steps of the surgical intervention (*i.e.* preoperative planning) allows for predicting possible problems and to develop contingency plans for achieving a successful outcome (Hak *et al.*, 2010). With the development of imaging and computer technologies, the preoperative planning has become even more present in hospitals and clinical practices. Typically, an orthopaedic surgery of a trauma clinical case is preceded by a 3-D reconstruction of the patient's anatomy based on CT scans and a preoperative planning (Lantada and Morgado, 2012). In some cases, rapid prototyping complements the preoperative planning by combining virtual training with surgical training using physical models (Deshmukh *et al.*, 2012; Suero *et al.*, 2010; Sun *et al.*, 2009).

In a broad sense, an orthopaedic surgery involves the implantation of a medical device. These implants can present a standard geometry or a tailored design. Implant customization represents a suitable solution to achieve positive results in patient comfort and adequate strength distribution, by designing the implant to fit a patient's anatomy. Also, the use of patient-specific implants increases the longevity of the implant leading to a deferment or suspension of the surgical revision intervention. The development of novel implant with a tailored design is even more important in patients who require orthopaedic reconstruction as a consequence of bone loss (e.g. osteosarcoma (Sun *et al.*, 2009)) or defect (e.g. trauma (Suero *et al.*, 2010)). This demand motivates the present study. Thus, a general framework for preoperative planning and tailored design of medical implants is outlined based on digital methods. Two distinct case-studies are considered as demonstrative examples of application.

2.2. Methods

In this section, a three-step methodology for preoperative planning and tailored design of medical implants is presented, namely *i*) data acquisition and 3-D reconstruction, *ii*) 3-D modelling and *iii*) implant design.

2.2.1. Data acquisition and 3-D reconstruction

Medical imaging techniques (e.g. MRI - Magnetic Resonance Imaging or CT - Computed tomography) are used to acquire patient's personalized data, which is usually delivered on DICOM file format. Then, a digital software is used for 3-D virtual reconstruction of patient's anatomy. For this task, MIMICS software (Materialise, Leuven) is considered. The first step of 3-D virtual reconstruction comprises to import and correctly orient the DICOM image-set. Prior to image segmentation, a filter (e.g. discrete Gaussian filter) should be applied to reduce CT noise and artifacts. The next step is the image segmentation. The usual procedure of image segmentation in MIMICS consists of combining the thresholding tool with the region growing option. Firstly, based on the image grayscale intensities, which corresponds to the use of different histogram window and level ranges, the thresholding tool is applied to isolate bone tissue from other tissues. Next, the region growing feature eliminates noise and separate structures that are not connected. The segmentation masks can be edited by using several MIMICS tools (edit mask – draw, erase, local thresholding; multiple slice edit; 3-D edit mask; Boolean operations; etc.) in order to correct connections between different bones and isolate bone surfaces. After image segmentation, the 3-D anatomical model is calculated and a virtual reconstruction of the model is accomplished.

Figure 2.1 illustrates the final result of a segmentation process in MIMICS interface described above. As shown, the software provides three sectional views of the segmented masks (coronal, axial and sagittal) and also, the resultant 3-D model of patient's anatomy (Figure 2.1, lower right corner). At this point, the 3-D virtual model is able to be analysed by the surgeon, who decides if there is any area that need further studies. Then, the STL model is imported to the software of the SL-stereolithography equipment (ViperTM SLA® System, 3D Systems® Corporation, Rock Hill – SC) and an epoxy model of the patient's anatomy is prototyped.

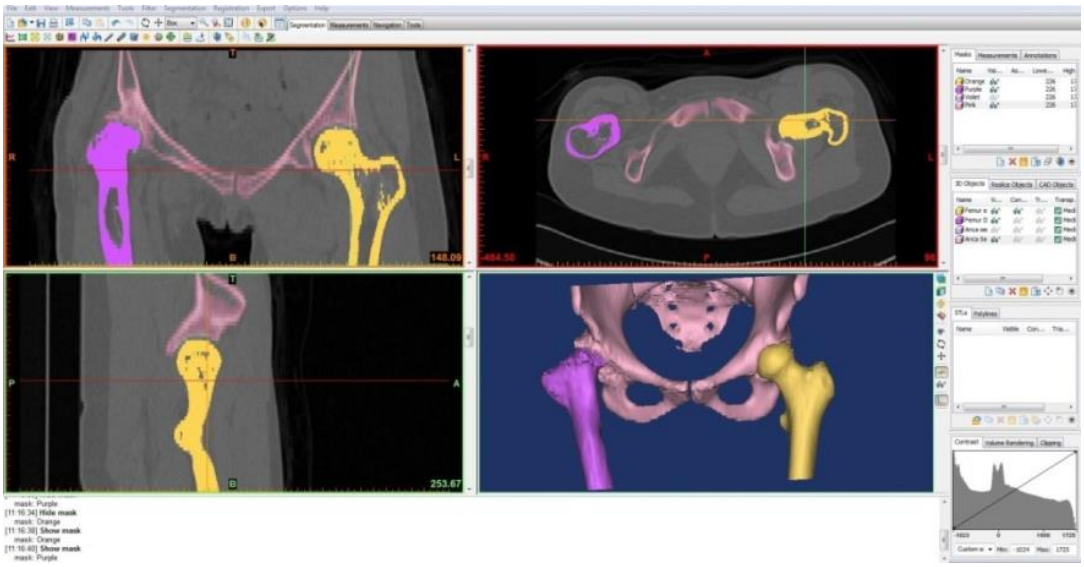

Figure 2.1 - MIMICS 16.0 interface: 3-D hip reconstruction.

2.2.2. 3-D modelling

The 3-D modelling task entails two main steps, namely an evaluation of the 3-D virtual model and a 3-D manipulation and measuring. Within 3-matic 8.0 software (Materialise, Leuven), Fix Wizard tool is used to examine and repair the 3-D virtual model in terms of inverted normals, bad edges (such as bad contours, near bad edges and planar holes), possible noise shells, and overlapping/intersecting triangles. Whenever a bone fracture exists, the anatomical position of the bones needed to be verified and realigned (Figure 2.2). Afterwards, in order to determinate the exact dimensions and contours demanded for a proper fitting between the implant and patient's anatomy, a 3-D measuring is performed. In a broad sense, the 3-D modelling task has a fundamental role in the preoperative planning, since it provides an even more realistic view of the patient's anatomy and detailed information with relevance for the clinical guidelines of the planned surgery.

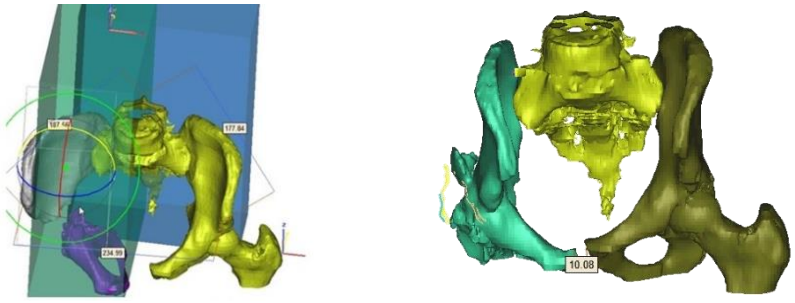

Figure 2.2 - 3-D manipulation for the alignment of sacroiliac joint.

2.2.3. Implant design

This task comprises the design project of the customized implant and it can be performed in a STL-editor (such as 3-matic). Afterwards, modelling adjustments of the implant design (for sake of manufacturing or other purposes) can be carried out in 3-matic or other CAD software (e.g. SolidWorks). It is important to mention that, prior to the implant design, the internal structure of the bony tissue, which will surround the implant, is analysed to identify the anatomical regions/points that are more appropriate for cuttings and placement of fixation systems.

For pre-validation purposes, implant 3-D models are prototyped by using SL-stereolithography techniques. The prototypes are examined for searching/checking imperfections on the geometry. Whenever geometrical imperfections are reported, one of the following measures has to be taken: *i*) edit the geometry of the implant to eliminate the detected imperfections; *ii*) restart the whole process of implant design. Thus, the implant design is an iterative process that stops with the validation of the implant geometry. The pre-operative planning is concluded when the implant is correctly positioned at the patient bone.

At this point of the project, the orthopaedic surgeon has a digital model of a patient-specific implant, which can be produced by additive manufacturing-based technologies, as well as a preoperative plan with relevant data for the clinical intervention, such as anatomical distances, implant alignment and fixation system anchorage.

2.3. Demonstrative examples of application

2.3.1. Case-study 1: Femur fracture

This case-study consisted of a triple fracture of the distal femur, resultant of a trauma accident. The patient is a Caucasian female subject with 46 years old. CT scans (Brilliance CT 16-slice, Philips Healthcare, Best) are acquired in order to get personalized data of patient's anatomy and its trauma injury defects. The resultant DICOM image-set comprises a total of 75 slices with 1.9 mm increment and a pixel size of 0.487 mm. The

first modelling step consists of importing the DICOM images to MIMICS 16.0 for image segmentation. Then, the 3-D virtual model of patient's anatomy is constructed. With the 3-D virtual model, the fractures, *i.e.* the shape and positioning of bone fragments, were analysed in detail (see Figure 2.3a).

The next step comprises to import the STL file of the 3-D model of patient's anatomy to 3-matic 8.0. Within this software, several operations of 3-D manipulation (such as rotate, move, etc.) were carried out in order to correct the position of the bones, to reduce the fractures and to ensure a correct placement and alignment of bones and its multiple fragments. Figure 2.3b shows the result of this process.

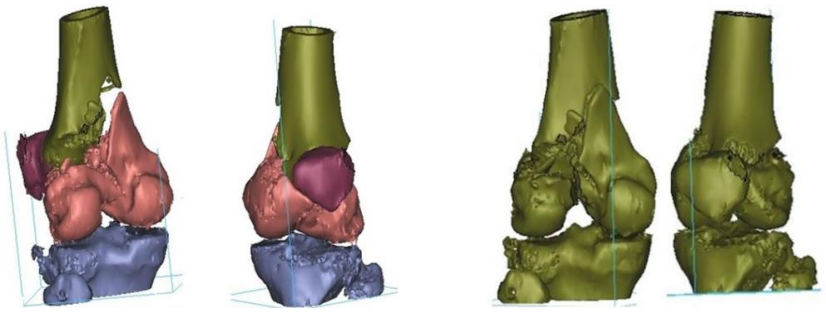

a) b)

Figure 2.3 - a) 3-D model after image segmentation; b) 3-D model after 3-D manipulation in 3-matic 8.0 (fracture reduction and correct placement/alignment of bone segments).

In order to stabilize the fractures and to keep the bone fragments aligned and in a correct position, a tailored system of implants was developed, namely a surgical plate and a set of screws. The designed plate is based on the Locking Compression Plate (LCP) commercialized by SYNTHES® (Synthes GmbH, Oberdorf) (see Figure 2.4a). This plate has a combination of locking and compression holes (Combi holes). These holes allow the surgeon to choose between conventional plating techniques, locked plating techniques, or a combination of both. Afterwards, the CAD model of the surgical plate was projected onto patient's anatomy (Figure 2.4b) in order to ensure an appropriate adjustment of the implant to patient. Within this process, some modelling operations were executed, such as surface fitting, trimming and smoothing. Following, the screws are introduced in order to lock the surgical plate in an anatomical position that will guarantee a correct alignment of the bones fragments and a stabilization of the fractures (Figure 2.4c).

Due to the complexity of this case-study (with multiple fractures in the same bone), a pre-validation of the designed implant system is required. This pre-validation process is carried out by fabricating epoxy models by means of SL-stereolithography as illustrated in Figure 2.5.

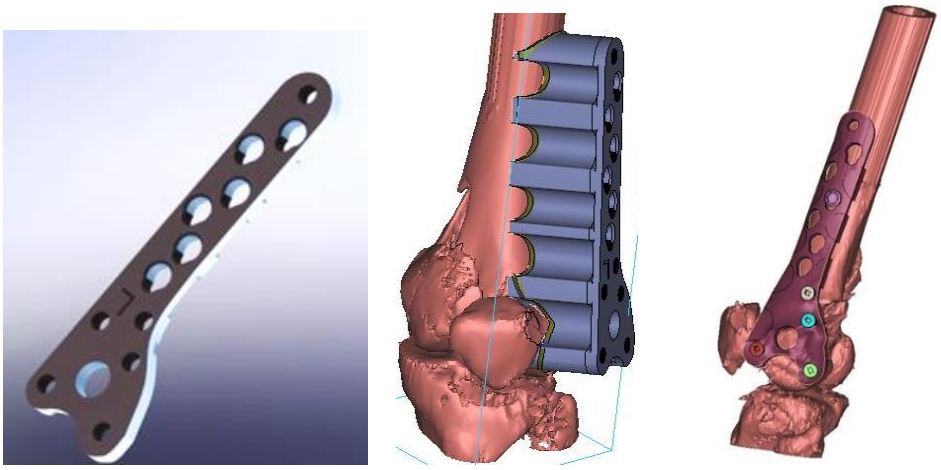

a) b) c)

Figure 2.4 - a) SYNTHES® Locking compression plate. Implant design in 3-matic: b) implant projection onto patient's anatomy; c) tailored implant system – plate and locking screws.

a) b) c)

Figure 2.5 - Prototyped models for pre-validation: a) plate; b) anterior view; c) posterior view.

2.3.2. Case-study 2: Maxillofacial deformity

The case-study 2 reports a maxillofacial deformation resulting from cancer removal. The patient is a Caucasian female with 68 years old. CT scans (Toshiba Aquilion, Toshiba Medical Systems, Japan) are acquired to obtain fundamental information about the deformation in the bone and surrounding anatomical structures. The resultant DICOM image-set comprises a total of 215 slices with 1 mm slice thickness and pixel size of 0.351 mm. Using this CT data, a 3-D model of the patient's cranium is built. Prior to the virtual reconstruction, similarly to cases-study 1, an image segmentation process is conducted.

By analysing the 3-D model, an absence of part of the zygomatic and superior maxilla bone is noticed (see Figure 2.6a). As a result, the step of 3-D manipulation is skipped as there are no bone fragments to be repositioned or aligned. For sake of comprehension of the patient's anatomy and malformation, the cranium model is prototyped using SL-stereolithography (Figure 2.6b).

Aiming to correct the internal and external appearance/function of the facial bony structure, a customized implant is developed. Within 3-matic 8.0, the missing bone area is reconstructed by means of mirror modelling tools, being other adjustments also performed (e.g. surface trimming and smoothing). Due to the importance of the maxilla in the chewing process, an extra bracket is added to the prosthesis design for supporting a future dental reconstruction (see Figure 2.7a).

Taking into account the bone density as well as the prosthesis structural stability, the anatomical points more favorable to the implant fixation are determined. SL-stereolithography is used for pre-validation of the implant design (see Figure 2.7b).

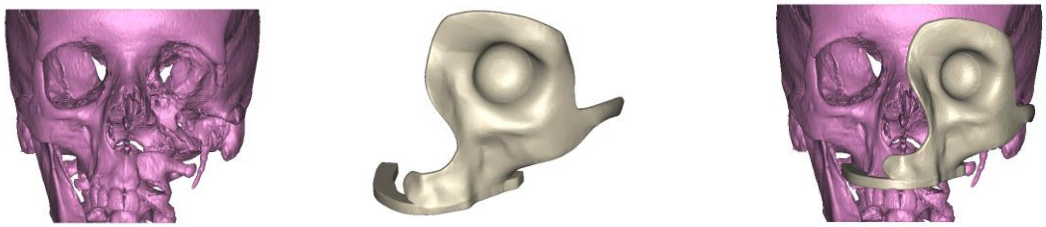

a) b) c)

Figure 2.6 - 3-D virtual models: a) cranium; b) prosthesis; c) cranium and prosthesis.

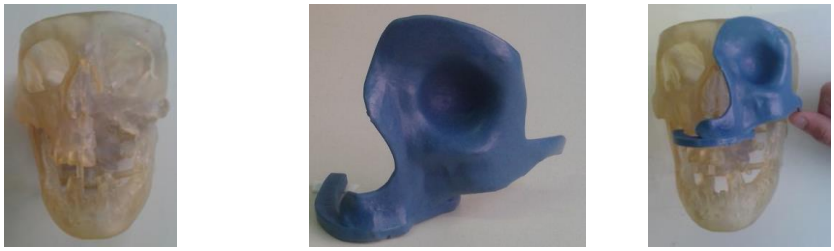

a) b) c)

Figure 2.7 - 3-D model plastic models: a) cranium; b) prosthesis; c) cranium and prosthesis.

2.4. Conclusions

Combining digital methods with preoperative planning, a framework for tailored design of medical implants is presented. This approach entails three main tasks: *i*) data acquisition and 3-D reconstruction; *ii*) 3-D modelling; *iii*) implant design.

In clinical studies, the use of patient-specific implants promotes a correct placement and fixation of the implant and ensure its longevity. Within this work, two case-studies are presented as demonstrative examples of application and a preoperative planning is outlined for each case, resulting in two customized implants. It is important to mention that the project of a novel implant design requires a pre-analysis of the internal bony structure in order to assurance the static stability and structural support of the respective orthopaedic device.

In a broad sense, the proposed methodology of preoperative planning based on digital methods offers a set of advantages for orthopaedic surgeons, such as *i*) the 3-D visualization of the injured area; *ii*) the 3-D measuring and manipulation of bone fragments; *iii*) the possibility of testing distinct treatments, *i.e.* different system of implants and surgical cuts; *iv*) the 3-D visualization of the final result, that is, how the implant will fit to patient's anatomy.

As future work, structural analyses of the designed implants using finite element methodologies are pointed out as added values for this study. Moreover, investigations on methods for automatizing the design procedure of customized implants are suggested as upcoming developments. The proposed procedure is executed by a

designer/engineer and it is reliable and accurate. Nonetheless, alternative techniques with some level of automation are preferable. Other future purpose is to investigate manufacturing techniques that meet the demand for high precision, cost-effectiveness and longevity of the orthopaedic implants.

References

Deshmukh, T.R., Kuthe, A.M., Chaware, S.M., Bagaria, V., Ingole, D.S., 2012. A novel rapid prototyping and finite element method-based development of the patient-specific temporomandibular joint implant. Comput Methods Biomech Biomed Engin. 15(4), 363-370.

Hak, D.J., Rose, J., Stahel, P.F., 2010. Preoperative planning in orthopedic trauma: benefits and contemporary uses. Orthopedics 33(8), 581–584.

Lantada, A.D., Morgado, P.L., 2012. Rapid Prototyping for Biomedical Engineering: Current Capabilities and Challenges. Annu Rev Biomed Eng. 14, 73-96.

Suero, E.M., Hüfner, T., Stübig, T., Krettek, C., Citak, M., 2010. Use of a virtual 3D software for planning of tibial plateau fracture reconstruction. Injury 41, 589–591.

Sun, S.P., Chou, Y.J., Sue, C.C., 2009. Full-Scale 3D Preoperative Planning System for Calcaneal Osteotomy with a Multimedia System. J. Foot Ankle Surg. 48, 528–539.

Custom Hip Prostheses by Integrating CAD and Casting Technology

Article published in the AIP Conf Proc 1479 (Numerical Analysis and Applied Mathematics - ICNAAM 2012), 2012, pp. 1596-1599.

*P.F. Silva, N. Leal, **R. Neto**, F.J. Lino and A. Reis*

3. Custom Hip Prostheses by Integrating CAD and Casting Technology

3.1. Introduction

Customization is the way to achieve positive results in patient comfort and adequate strength distribution by projecting prosthesis to fit a single individual (McTighe, 1999; Pieringer *et al.*, 2003; Ruyu *et al.*, 2005). Unfortunately, this tailor made parts production carries out costs that are higher than the standard prosthesis. The main reason for this is the process complexity to provide a perfect adjustment between the prosthesis and the bone. Nowadays is available in the market software applications and methods to treat DICOM (Digital Imaging and COmmunications in Medicine) files in a way that physical prototypes can be materialized. Considering this, INEGI is been using STL files to materialize models (SL Quickcast) (Rahmati *et al.*, 2010) that are converted in final functional titanium alloy parts, using the investment casting in a cold crucible with controlled atmosphere. The price reduction is one of the key factors evaluated along the project to enable the introduction of this manufacturing technology.

3.2. Method

The method presented is based on continuous technological developments with the implementation of SL Quickcast models with titanium alloys, all together aimed to decrease the cost of customization of the hip prosthesis. DICOM files obtained by MRI (Magnetic Resonance Imaging) or CT (Computed Tomography) scans are processed in a computer with Mimics and 3-matic software. The objective of both programs is to obtain a STL (Standard Template Library) file starting only with the medical images that should have the maximum definition possible (more images available from the patient exam, better the will be the definition of the bone structure). Although the programs can isolate other tissues like muscle, skin or even major vascular vessels, obviously the main focusing of the processing work is the femur and pelvis bones.

3.2.1. Images – Mimics and 3-matic Software

The Mimics can automatically interpret the orientation of the scanned images and, therefore, the orientation of the body. If the program alone cannot do this, it is possible to teach the software the right orientation of the images.

Segmentation is the next and the most import step. Using "Thresholding" feature, standard bone tissue selection can isolate the bones images from other tissues of lower density. This function can be adjusted manually, like a grey scale to improve the results and consequently reduce the noise.

Editing masks is a property that provides the opportunity to correct connections (noise) between different bones and final isolation of the bone surface.

"Region Growing" feature creates a new complete mask from a previous faulty one (with noise), but for this it needs to be completely isolated. Different colours can be applied for these final masks, enabling an easier distinction of the bone structures. Figure 3.1 shows the final steps of the isolated bone tissue and also the femur mask isolated from all other masks.

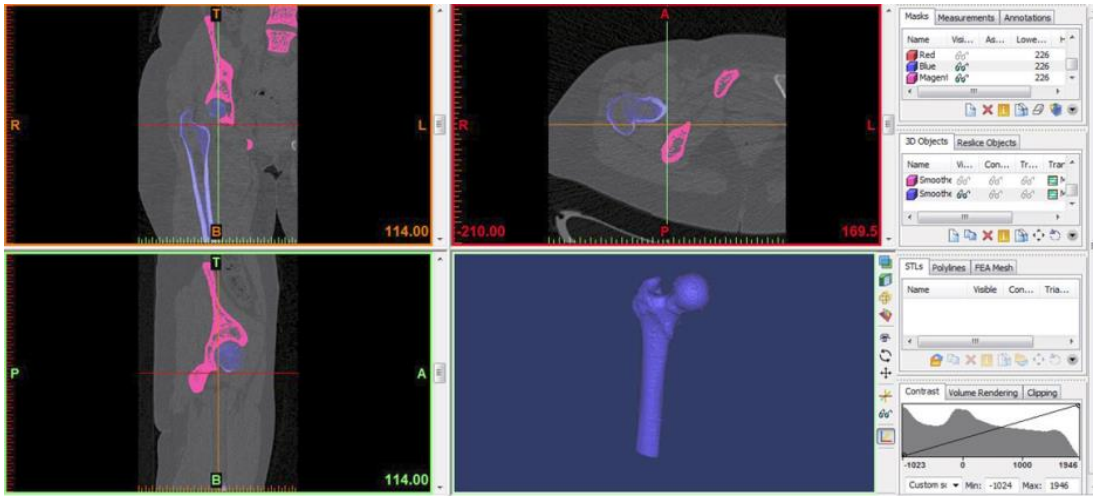

Figure 3.1- DICOM files treated in Mimics to create an isolated femur mask.

After finishing the masks in Mimics, the file is directly exported to 3-matic. The 3-matic is used to study the femur cavity and shade the various components of the part. In this case, the bone wall is eliminated to only keep the cavity (Figure 3.2). For an ideal

cemented prosthesis it was decided to make an interior offset of 1mm, starting at the cavity surface, to leave a gap to inject the cement during the surgical intervention.

For the standard components, Collar and Morse taper, all the bone components are needed to study the perfect fit adjustment. The custom hip prosthesis STL file is now ready to be exported to the SL machine.

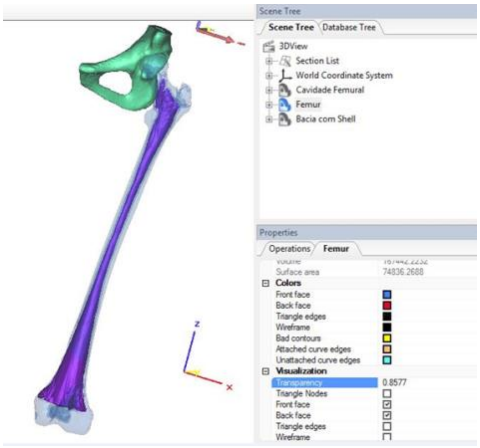

Figure 3.2 - STL files from Mimics treated in 3-Matic to study femur cavity.

3.2.2. Prototypes – SL Quickcast

Although the CAD design above described was related to a custom fit prosthesis (Figure 3.3), the following experimental work is related to several standard prostheses (Portucale) cast simultaneously (four at a time). The reason for this is that the work underway is still for validation of the casting process.

Figure 3.3 - Study developed for a custom hip prosthesis.

The STL file is treated in SolidWorks software to add a casting sink in the CAD model (Figure 3.4 a). This model is then printed in SL Quickcast (this hollow prototype enables an easy and fast calcination of the resin) (Pal *et al.*, 2006).

The SL model is coated with a slurry and sand (Figure 3.4b), dries and repeat the process until it reaches a thickness with a mechanical resistance that can withstand the following steps (usually 7-9 layers).

The shell is now submitted to a thermal shock at 1000°C during two hours (Figure 3.4c) to eliminate the SL Quickcast model(s). This step is crucial because a slow heating rate expands uniformly the resin prototype and can break the shell.

a) b) c)

Figure 3.4 - Ceramic shell manufacturing; a) Models built using CAD software; b) Sand shower to coat the SL-assembly; c) Burning process to eliminate the resin ashes.

3.2.3. Casting

The casting is done in a proprietary furnace developed at INEGI to cast reactive alloys (Figure 3.5a) with high level of details, surface quality and low oxidation. The main chamber is equipped with an 18 sector cold copper crucible. Inside each sector flows water to cool down the copper. The chamber has vacuum entries and exits to change the internal pressure (varying from atmospheric pressure to $8x10^{-3}$mbar). The chamber also has an Argon 6 injector for the controlled atmosphere.

Titanium Ti6Al4V Gr5 was placed (usually round billets) inside the chamber on the top of the copper crucible (the furnace is prepared to cast other alloys like Ti6Al4V Gr23 ELI). Once the power is on, a magnetic field is created around the coil surrounding the crucible. Due to the geometry of this coil, the magnetic field melts the TI alloy that starts to levitate (Figure 3.5b), and when ready to be casted, the power is shut down to allow

the metal to flow to the shell through a hole at the bottom of the crucible. Some metal is inevitable left behind, so it forms a titanium alloy skull, as shown in Figure 3.5c.

After casting the shell is allowed to cool down inside the furnace in an Argon controlled atmosphere, for 30 minutes, since hot Titanium can react with the oxygen from the air. The shell is then collapsed, sandblasted and prostheses are cut.

a) b) c)

Figure 3.5 - Casting furnace for reactive alloys; a) INEGI furnace apparatus to cast reactive alloys in controlled atmosphere; b) Cold crucible with Ti alloy levitating inside; c) Skull formed after casting.

3.2.4. Final custom prosthesis

The final prosthesis need now some CAD/CAM machining operations, to add a Morse taper for a perfect fit with the patient organs (Figure 3.6a). Figure also shows a fully machined non casted part that was used for production cost comparison.

The casted parts were controlled by X-ray analysis in order to detect and characterize internal casting defects like inclusions, microcracks and pores (Figure 3.6b). As one can see, the parts revealed no major defects that can affect it integrity. Although these results seems very promising, future work will eventually demand the use of Hot Isostatic Pressure (HIP) treatment to minimize the possible existence of internal defects that can cause prosthesis collapse by fatigue (Pacioga *et al.*, 2011; Pospula, 2004; Faulkner, 1998; Ni *et al.*, 2006, Maher *et al.*, 2001).

The introduction of the casting technology with cold crucible allows obtaining prosthesis 30% less expensive than fully machined ones, considering all materials needed, the time to project the part, produce the shell and cast and finishing it. The total manufacturing

time may vary, but considering the moment that the DICOM files are received it takes around one week to finish the prosthesis (see Table 3.1).

a) b)

Figure 3.6 - Final prosthesis; a) Portucale prostheses obtained by different processes: on top the casted prosthesis, in the middle machined with a Morse taper and bottom a fully machined prosthesis (not cast); b) X-Rays images of the prosthesis.

Table 3.1 - Time spent to finish a custom hip prosthesis since the DICOM files are available.

Process description	Time (days)
Project of best fit	1
Printing CAD models	1
Making shell	2-3
Casting and finishes	1
Total time	**5-6**

3.3. Conclusions

“Fit the implant to the patient, not the patient to the implant”, a sentence that is been a guide line for this research and should continue to be. The integrated presented, developed at INEGI provides prostheses with an ideal fit to the bone, excellent stability, improvement in stress transfer, in a short period of time and at a lower cost than integral machined parts.

The prostheses produced should be submitted to a new phase of tests like stress distribution, fatigue resistance and biocompatibility tests.

References

Faulkner, A., Kennedy, L.G., Baxter, K., Donovan, J., Wilkinson, M., Bevan, G., 1998. Effectiveness of hip prostheses in primary total hip replacement: a critical review of evidence and an economic model. Health Technology Assessment 2(6), 1-133.

Maher, S.A., Prendergast, P.J., Lyons, C.G., 2001. Measurement of the Migration of a Cemented Hip Prosthesis in an in Vitro Test. Clinical Biomechanics 16(4), 307-314.

McTighe, T., 1999. Design Considerations for Cementless Total Hip Arthroplasty. JISRF 11, 1-8, Terrigal, Australia.

Pacioga, A., Palade, D.D., ComŞa, S., 2011. Computational Simulation of Bone Personalized Hip Prosthesis Assembly. U.P.B. Sci. Bull., Series D, 73(2), 249-262.

Pal, D.K., Bhargava, L.S., Ravi, B., Chandrasekhar, U., 2006. Computer-aided Reverse Engineering for Rapid Replacement of Parts. Defence Science Journal 56(2), 225-238.

Pieringer, H., Labek, G., Auersperg, V., Böhler, N., 2003. The J. of Bone Joint Surgery 85-B(5), 641-645.

Pospula, W., 2004. Total hip replacement: past, present and future. Kuwait Medical Journal 36(4) 250-255.

Rahmati, S., Farahmand, F., Abbaszadeh, F., 2010. Application of rapid prototyping for development of custom – made orthopedics prostheses: an investigative study. Majlesi Journal of Mechanical Engineering 3(2), 11-16.

Ruyu, M., Wendong, X., Dongmei, W., Kerong, D., Chengtao, W., 2005. Design and manufacture of custom hip prostheses based on standard X-ray films, Springer-Verlag, London.

Ni, G.X., Lu, W.W., Chiu, K.Y., Li, Z.Y., Fong, D.Y.T., Luk, K.D.K., 2006. Strontium-containing hydroxyapatite (Sr-HA) bioactive cement for primary hip replacement: An *in vivo* study. Journal of Biomedical Materials Research Part B: Applied Biomaterials 77-B(2), 409-415.

A framework for custom design and fabrication of cranio-maxillofacial prostheses using investment casting

Article to be published in the Proceedings of the 4th International Conference on Engineering Optimization (EngOpt), Lisbon, 8-11 September, 2014.

*V. Csáky, **R. Neto**, T. Duarte, J. Lino Alves, M. Couto and M. Machado*

4. A framework for custom design and fabrication of cranio-maxillofacial prostheses using investment casting

4.1. Introduction

Medical needs for customized prostheses are derived from bone degeneration and related issues, e.g. osteoarthritis, trauma or cancer. Trauma factors are the major cause for the continuous development of custom-fit cranio-maxillofacial (CMF) prostheses (La-Salete *et al.*, 2013; Duarte *et al.*, 2011; Lantada & Morgado, 2013; Gassner *et al.*, 2003; Roccia *et al.*, 2010).

Computational advances in medical image acquisition and design methodologies enhanced the process of biomodelling and pre-surgical planning, resulting in benefits in the surgical interventions efficiency and in patients' quality of life. Custom-fit CMF prostheses increases the longevity of the implants leading to less revision surgeries and cost savings, and so represents an added value when compared with standardized prostheses (Goh *et al.*, 2010).

Regarding prostheses manufacturing, this work aims to present the fabrication of custom-fit CMF prostheses using investment casting technology for the titanium bio-alloy Ti-6Al-4V. The investment casting methodology is preferred to other foundry technologies, such as injection moulding or centrifugal casting, due to its ability to reproduce complex geometries with low surface roughness and costs, and possibility to cast a wide variety of metallic materials, which are difficult to machine or cast, such as titanium alloys and cobalt-chromium alloys that are used in medical applications (Swift and Booker, 2013).

The optimization of the design and fabrication process by means of computational tools and numerical simulation, to enhance process efficiency and patient's comfort, are the principal motivation for this work (Tsouknidas *et al.*, 2011; Aquilina *et al.*, 2013). Thus, a framework for custom design of CMF prostheses is outlined. Two distinct case-studies

are considered as demonstrative examples, a craniofacial prosthesis (I) and an orbital prosthesis (II).

4.2. Methodology

In this section, a four-step methodology for custom design and fabrication of CMF prostheses is presented, namely: *i)* image processing, *ii)* biomodelling, *iii)* fabrication and *iv)* finishing.

4.2.1. Image processing

Medical images from CT (Computed Tomography) and MRI (Magnetic Resonance Imaging) scans are available in DICOM format. Processing these images enables a 3D virtual model of the patient' anatomy and, therefore, evaluation of the damaged region. Within this work, Mimics® 16.0 software (Materialise NV, Leuven, Belgium) is used. The first step consists in importing the DICOM files into the software and segment the region of interest applying an adequate threshold range to select the grayscale intensities for the bone. The image tonalities can be visualized in grayscale or in Hounsfield scale. The second step is to improve the images' quality by applying specific filters and tools for CT noise and artifacts reduction. Using the region growing feature, structures that are not connected to the main anatomical model are eliminated. Also, artifacts can be eliminated using manual tools (e.g. draw, erase and local threshold painting options) in the image slices or in the 3D reconstructed model. Thereafter, the 3D anatomical model's surface can be smoothen and accomplished accordingly, based on the previously used tools and selected variables.

Figure 4.1 illustrates the Mimics® 16.0 interface after image processing for a craniofacial prosthesis. At this point, the 3D model can be evaluated and approved by the surgeon, determining whether there is any area demanding further investigation. Finally, an STL file consisting in a triangular mesh is exported from the software and is imported in an additive manufacturing equipment (e.g. stereolithography – SL machine) to be materialized.

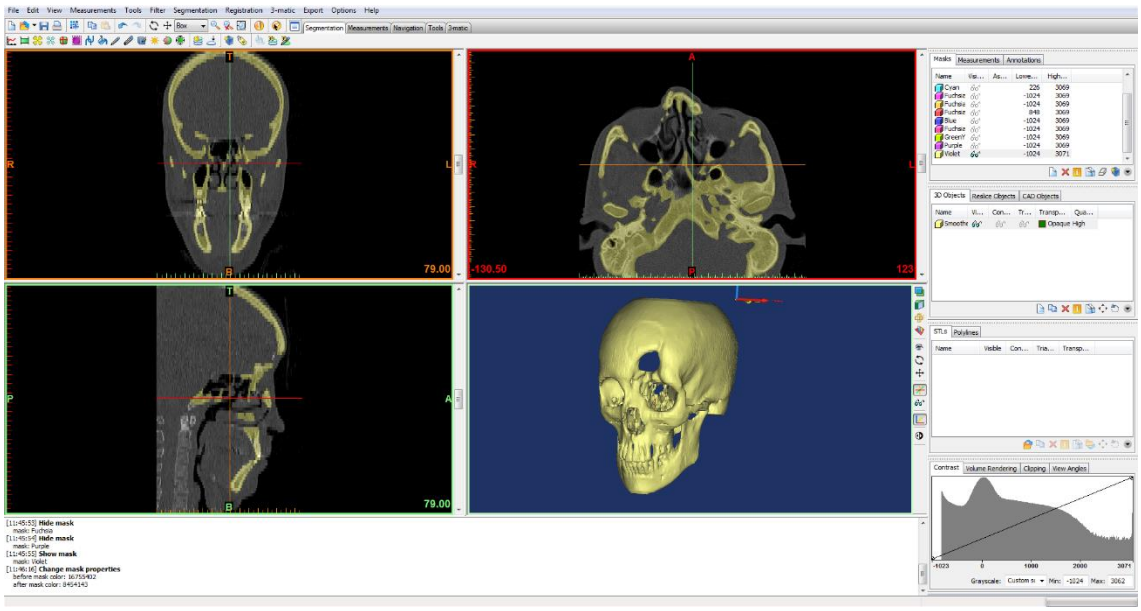

Figure 4.1 - Mimics® 16.0 interface with the imported DICOM files and 3D model of the case-study I regarding a craniofacial defect.

4.2.2. Biomodelling

The biomodelling task comprises two main steps: an evaluation of the model by means of measurements and alignment, and the prosthesis design stage itself. This tasks should be performed in a software capable of editing STL files (e.g. Materialise® 3-matic®, Geomatic® Freeform®, Blender™, etc.) due to the specific triangular mesh surface formats that are not easily modelled in CAD 3D software. For this task, the 3-matic® 8.0 (Materialise NV, Leuven, Belgium) is used. The adopted approach depends on the case-study and its complexity. For unilateral defects a symmetry plane can be considered in the anatomical model to use mirror techniques followed by Boolean operations (e.g. intersection and subtraction). In case of bilateral and/or asymmetric defects, a digital database of anatomical models is demanded.

Once the implant's design is completed, verification and reparation tools are run to certify that the geometry is valid and no entities are in conflict with each other (e.g. there are no triangles overlapping or missing in the surface shell of the model).

Thereafter, the fixation system of the implant is designed. For sake of an appropriate fixation, a bone density algorithm is used to identify the more suitable anchorage points and that will provide a reasonable higher torque in order to ensure that there will be no

significant prosthesis displacement or distortion during its lifetime that could compromise the patient's safety, comfort and health. The fixation in thick cortical bone is recommended rather than in thin cortical bone due to better strength and bone integrity during screw allocation. Furthermore, structural analysis can be performed to validate the previous selection of anchorage points and ensure that the prosthesis is well designed to withstand the mechanical stresses present in the defective region (e.g. chewing forces for a mandibular prosthesis). Thus, the fixation system design is a fundamental step to ensure the implant stability, both during the manufacturing processes and in the daily life activities.

The anatomical and prosthetic models are materialized by stereolithography (SL) for pre-validation purposes (Figure 4.2).

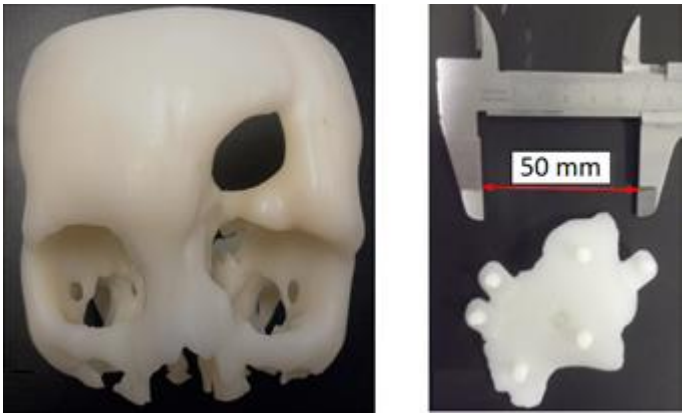

(a) (b)

Figure 4.2 - a) Anatomical model; b) Prosthesis materialized by SL.

The prosthesis assembly and its geometric tolerances can then be evaluated and corrected by redesigning whenever imperfections are reported. Thus, the design technique is an iterative process that is concluded once a multidisciplinary team of doctors and engineers agree that the assembly between the defect and the prosthesis is satisfactory. At the end of this process, the surgeon can have a 3D model of the defective anatomical region of the patient, a design project of a custom-fit prosthesis and a set of the detailed information to support the clinical intervention, including anatomical distances and the correct positioning of the implant and fixation systems.

4.2.3. Fabrication

The investment casting technology entails a set of specific steps to obtain the metallic prosthesis. To initiate the foundry process, a wax model is necessary. This model can be materialized by two ways: *i)* wax printing, that is the direct printing of the designed implant wax model using adequate additive manufacturing (AM) technology, *ii)* converting the SL model (can be obtained by other AM process) into a wax model using silicone moulds.

The first technique is faster and does not require so much labour work as the second. Although we used both processes for comparison purposes, the first method is the most recommended and that will be used in future work (INEGI bought this year a ProJet® 3510 CP, 3D Systems® Corporation).

Once this step is completed, the gating and feeding system is assembled to the model, to complete the tree for investment casting (Figure 4.3a). Thereafter, thin ceramic layers are deposited around the wax tree. The shell consists in 8 layers, being the first 2 layers called facecoat and the other ones backups. For casting reactive metals, such as titanium or cobalt-chromium alloys, a two-layer facecoat is recommended, otherwise a simple layer is enough. The first facecoat will be in contact with the wax model and then with the metal, therefore its particle size must be very thin to precisely reproduce all the details. Before the facecoat, a cleaning step is demanded to promote the slip adherence. For the first facecoat, the model is immersed in an organic binder with yttria based flour slurry (AY) and pulverized with yttria sand (125 – 150 µm). The model is then placed in a controlled atmosphere (temperature 24 ºC and humidity 40 %) with forced convection for 2 hours drying. This drying period is applied in-between immersions to promote shell solidification and strengthening. The second and subsequent facecoat layers are manufactured with coarser particles. The model is immersed in an AFAl (fumed alumina with alumina) slip and pulverized with alumina sand (60 FEPPA for the 3rd and 4th layer and 36 FEPPA for the following layers, being the first type of sand thinner than the second). In the final step the model is immersed in AFAl and dries for 12 hours in the same controlled atmosphere (Figure 4.3b). The model is now dewaxed by flash firing (1 hour at 1100°C) and the shell sintered at 1450°C for 2 hours.

a) b)

Figure 4.3 - a) Wax pattern for investment casting; b) Ceramic shell around the wax pattern.

At this point the ceramic shell is ready for metal casting. The alloy is melted and poured into the shell under a controlled atmosphere using a cold cooper crucible, i.e. cold skull induction furnace (Martins, 2008). The ceramic shell is then knocked out using a vibrating pneumatic hammer, and the gating and feeding system is removed. The metallic prosthesis (net shape) is now ready for finishing operations.

4.2.4. Finishing

The prosthesis was designed with an additional thickness to compensate models, ceramic and metal shrinkage, and finishing operations. To obtain the final desired thickness, chemical milling is performed. The thin oxygen-contaminated hard and brittle layer (α-case) created during casting is removed in this operation. The final step is a 5-axis CNC machining to smooth the surface and to drill the fixation system.

4.3. Case studies

4.3.1. Case-Study I: Craniofacial prosthesis

This case-study is of a 46 years old male with a cranial defect above the left orbit. The defect covered both the frontal zone of the skull and the upper side of the orbit. The origin of this problem was a trauma in the orbital and frontal bone of the skull. CT scans (Siemens Sensation Cardiac 64, Siemens, Germany) were acquired with the following parameters: 120 kV and 63 mAs. The DICOM set comprises 82 slices with 3 mm increment and 0.309 mm pixel size. These images provided specific data of patient's anatomical trauma defects. The DICOM files were imported Using Mimics® 16.0, the 3D model is reconstructed and exported as STL file (Figures 4.4, 4.6a).

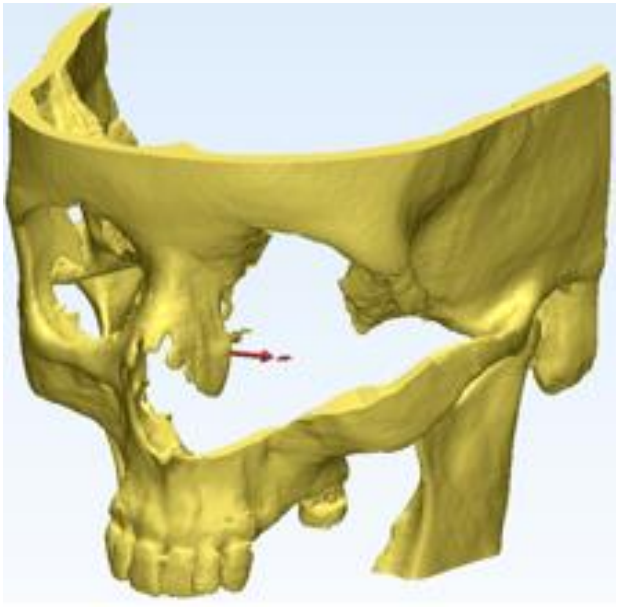

Figure 4.4 - Anatomical model of the case-study I regarding an orbital defect.

The prosthesis design is carried out using 3-matic® 8.0 software. For this case, a cranioplasty command operation of 3-matic® 8.0 is used. The first step is drawing a curve around the defect and the orbital region. An offset of 0.7 mm is applied to obtain the prosthesis' thickness and geometry. A mirror technique reproduces the healthy half skull in the defective region to trim the prosthesis excess material. The trim operation

tailored the orbital curvature in frontal view and the prosthesis' main geometry is accomplished. Figure 4.5 illustrates these sequence design steps.

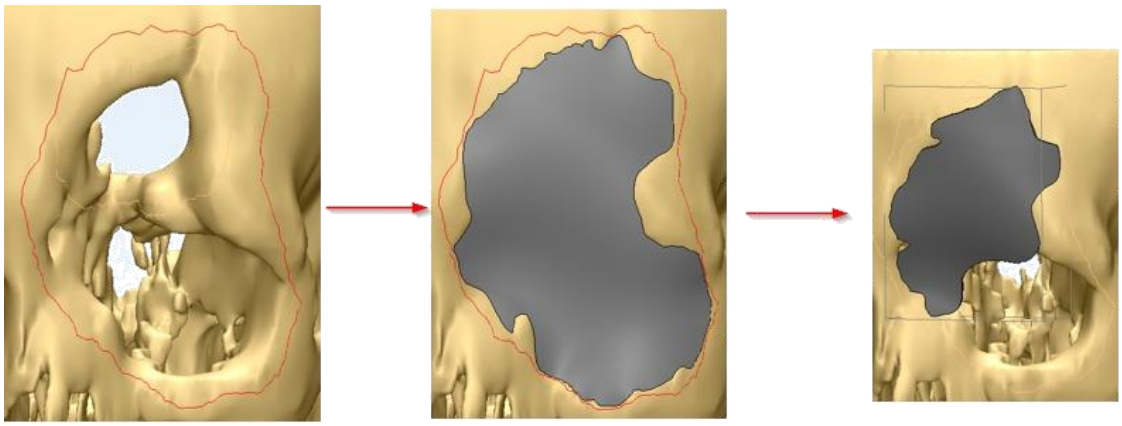

a) b) c)

Figure 4.5 - Design sequence for creating a cranioplasty prosthesis using 3-matic®: (a) Drawing a curve around the defect, (b) Applying an offset for the prosthesis' thickness & (c) Trimming the excess material in accordance to the mirrored health side of the cranium.

A bone density algorithm is used to properly choose the anchorage points. Custom sized flaps (16x8x0.5 mm) with rounded edges are designed in accordance to the skull curvature and bone density (Figure 4.6b). These flaps are used to substitute standard surgical plates, which are more expensive and liable to break when allocating screws (both in the prosthesis and in the bone). Nevertheless, the use of these plates implies 2 screws which is a more evasive technique than integrated flaps with only one fixating screw.

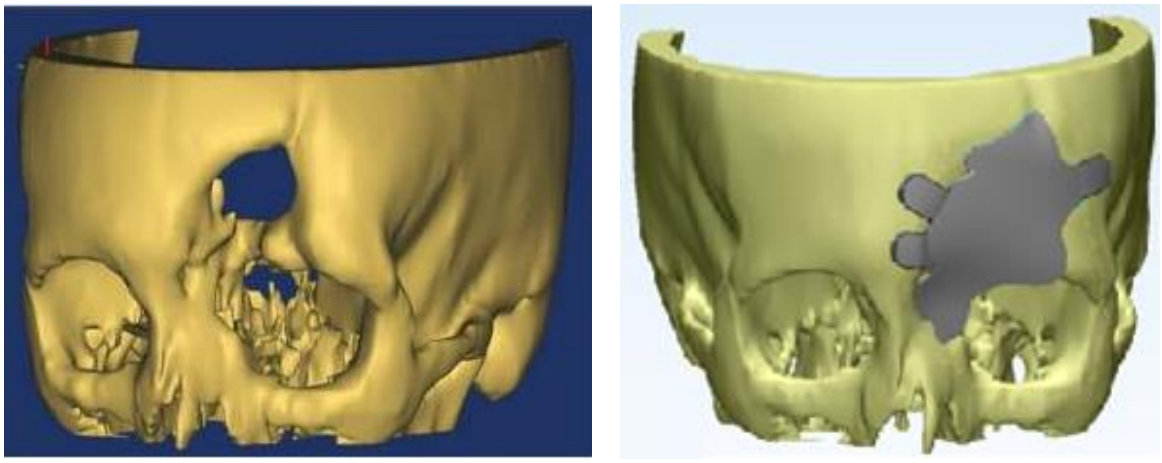

a) b)

Figure 4.6 - a) Reconstruction of the 3D model using Mimics® 16.0; b) Custom-fit design prosthesis using 3-matic® 8.0.

Finally, the skull prosthesis prototype resin model is materialized by an SL equipment (Viper™ SLA® System, from 3D Systems® Corporation, Rock Hill – SC, USA). The following steps are in accordance with the described fabrication methodology.

4.3.2. Case-Study II: Orbital prosthesis

The case-study II reports a 68 years old female with a maxillofacial deformation resulting from cancer removal. CT scans (Toshiba Aquilion, Toshiba Medical Systems, Japan), with parameters 120 kV and 90 mAs, are acquired to obtain the information about the deformation and surrounding anatomical structures. The DICOM set consists of 215 slices with 1 mm slice thickness and 0.351 mm pixel size. Similarly to the previous case-study, the 3D reconstruction is performed and the skull is materialized by SL. After analysing the model, an absence of the orbital region and superior maxilla is observed (Figure 4.7a). Later, the patient experienced a superior maxilla reconstruction surgery by bone grafting. Considering the unilateral defect, the customized prosthesis is developed using 3-matic® 8.0 employing mirroring techniques and Boolean operations. The symmetry plane was defined using the middle sagittal plane. Finally, using trimming options the final geometry of the prosthesis and fixation flaps are designed based on the bone density algorithm (Figure 4.7b). A second version of this prosthesis was designed with a specific curve flap that attaches on the opposite side of the maxilla bone. This design is demanded due to the chewing forces involved. Also, another specific fixation flap is developed to adapt in the zygomatic arch (Figure 4.7c). Thereafter, the prostheses are fabricated by the described investment casting technology. The parts are now in the cast phase.

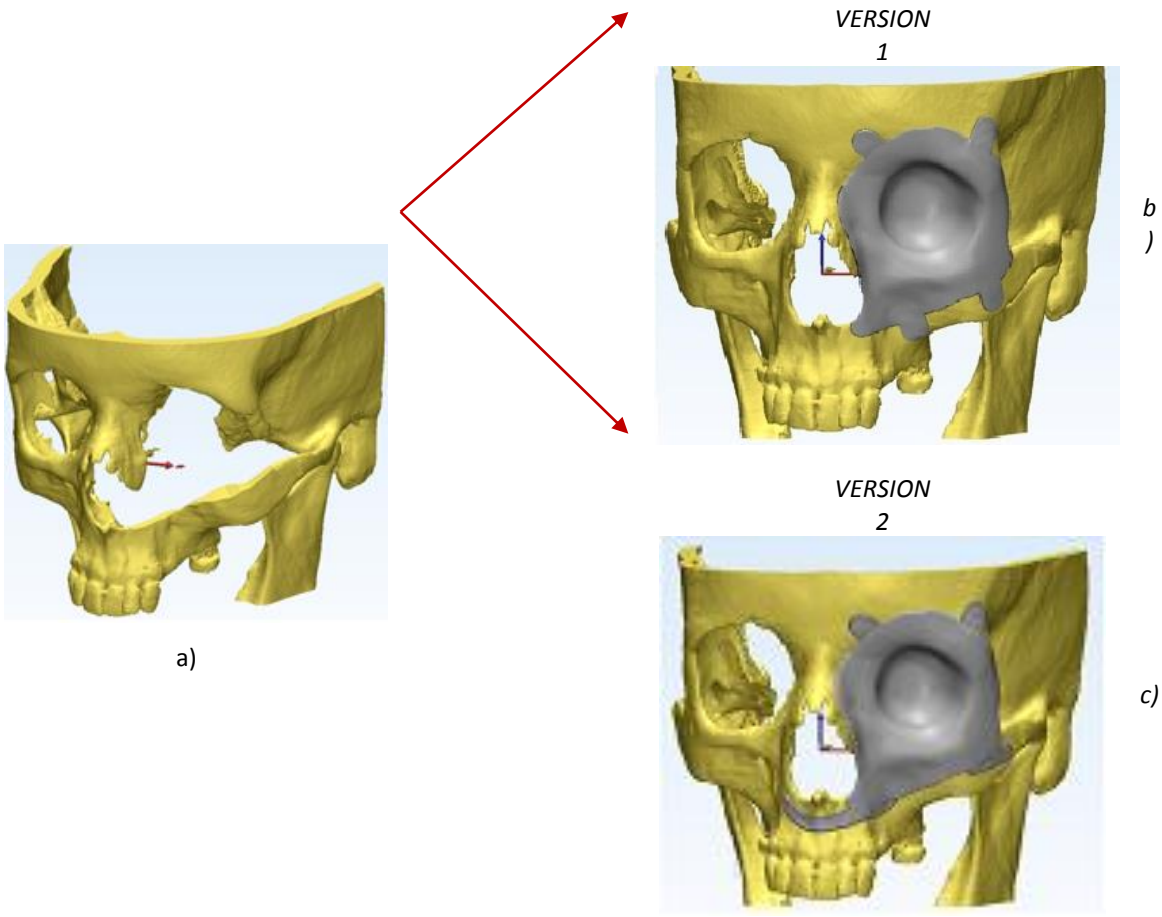

Figure 4.7 - a) 3D model reconstructed with visible defective orbital region; b) First version of the designed orbital prosthesis; c) Second version of the prosthesis' design. All design methodologies were performed using 3-matic® 8.0.

4.4. Conclusions

Custom-fit cranio-maxillofacial prosthesis (CMF) enhances patients' quality life and increases the longevity of the prosthesis, resulting in less follow-up interventions. Patient specific implants assures the correct positioning and fixation in the cortical bone, enhancing the surgical approach and respective preoperative planning. The proposed methodology for 3D reconstruction and biomodelling offers several advantages for orthopaedic surgeons, such as effective evaluation of the defective region, measurements capacity and possibility of studying different approaches to the case, including the visualization of the final result.

Investment casting represents the most efficient and direct method among the foundry industry to fabricate custom-sized CMF prostheses. The possibility to use a wide range of materials, including reactive metal such as titanium or cobalt-chromium alloys,

associated with the freeform geometry and thin details that can be reproduced, turns this process a preferred option in foundry. Finishing techniques such as chemical milling to reduce the prostheses' thickness and α-case, hence, improve the surface finishing, and 5-axis CNC machining to smooth the surface and drill the fixation system, open great opportunities for more efficient and cost-effective prosthesis.

In this work two distinct case-studies are considered as demonstrative examples of application. The required steps to develop tailored prosthesis are the evaluation of the defective region, the selection of the appropriate tools in the biomodelling software and the design of the fixation system according to surrounding bone density and required structural stability to the prosthesis. In both cases, the prostheses are materialized by SL in order to proceed with their fabrication by investment casting. The corresponding skulls are also materialized by SL for pre-validation and final assembly with the metallic prostheses.

As future work, a topology optimization is recommended based on finite element methodologies. This kind of analysis may lead to an enhancement of the fixation system and also to more lightweight prostheses without compromising their structural stability. In the foundry process, a filling and solidification simulation is pointed out to optimize the process and reduce wastes.

References

Aquilina, P., Chamoli, U., Harr, W.C.H., Clausen, P.D., Wroe, S., 2013. Finite element analysis of three patterns of internal fixation of fractures of the mandibular condyle. British Journal of Oral and Maxillofacial Surgery 51(4), 326-331.

Duarte, T., Neto, R., Lino, J., Félix, R., 2011. Projeto e fabrico de próteses maxilo-faciais metálicas à medida do paciente - parte I. O molde, revista da CEFAMOL: Associação nacional da indústria de moldes.

Gassner, R., Tarkan, T., Oliver, H., Ansgar, R., Hanno, U., 2003. Cranio-maxillofacial trauma: a 10 year review of 9543 cases with 21 067 injuries. Journal of Cranio-Maxillofacial Surgery 31(1), 51-61.

Goh, R.C.W., Chang, C., Lin, C., Lo, L., 2010. Customised fabricated implants after previous failed cranioplasty. Journal of Plastic, Reconstructive & Aesthetic Surgery 63(9), 1479-1484.

La-Salete, A., Sousa, M., Gomes, E., 2013. Análise retrospetiva de 186 casos de traumatismos maxilofaciais por acidentes de viação. Revista Portuguesa de Estomatologia, Medicina Dentária e Cirurgia Maxilofacial 54(4), 179-184.

Lantada, A.D., Morgado, P.L., 2013. Handbook on Advanced Design and Manufacturing Technologies for Biomedical Devices. Springer, Madrid.

Martins, F., 2008. Desenvolvimento de um Forno de Indução para Fusão e Vazamento de ligas de Titânio Ti e Outras Ligas Reactivas com Reprodutibilidade. MSc Dissertation, Faculty of Engineering of University of Porto, Portugal.

Roccia, F., Francesca, B., Emanuele, Z., Giulia, T., Guglielmo, R., 2010. Characteristics of maxillofacial trauma in females: A retrospective analysis of 367 patients. Journal of Cranio-Maxillofacial Surgery 38(4), 314-319.

Swift, K.G., Booker, J.D., 2013. Manufacturing Process Selection Handbook. Oxford: Butterworth-Heinemann.

Tsouknidas, A., Maropoulos, S., Savvakis, S., Michailidis, N., 2011. FEM assisted evaluation of PMMA and Ti6Al4V as materials for cranioplasty resulting mechanical behaviour and the neurocranial protection. Biomed Mater Eng 21(3), 139-147.

An engineering-based approach for design and fabrication of a customized nasal prosthesis

Article published in Prosthetics and Orthotics International, 4 June 2014, pp. 1-7 (0309364614535232)

***R. Neto**, A. Costa-Ferreira, N. Leal, M. Machado and A. Reis*

5. An engineering-based approach for design and fabrication of a customized nasal prosthesis

5.1. Background and aim

Facial defects resulting from neoplasms, burns, congenital malformations, trauma or other diseases, particularly when involving partial or total loss of an external organ, can be functionally and emotionally devastating. Although tissue reconstruction is currently provided by modern surgery with grafts or flaps, it might not always be applicable due to several constrains related to advanced age, medical conditions or excessive treatment costs involved. In such cases, defects can be restored with external prosthesis. The detail level achieved on such prosthesis is determinant for the re-establishment of patient confidence (Amarante *et al.*, 2006; Costa-Ferreira *et al.*, 2007; Horta *et al.*, 2009; Seçilmiş and Öztürkb, 2007; Sun *et al.*, 2011; Sun *et al.*, 2013; Wang *et al.*, 2011).

There are two main approaches to fabricate these external prosthetics: the conventional method and the digital method (Seçilmiş and Öztürkb, 2007). Fabrication of conventional prosthesis is based on the uptake of the failing part shape directly from the patient's body. Plaster and ordinary hand tools are used by an anaplastologist to obtain a prosthesis whose shape fits the patient satisfactorily (Feng *et al.*, 2010; Sun *et al.*, 2011; Sun *et al.*, 2013). This is a time-consuming and unpredictable process, because it is highly dependent on the skill level of the technician. Moreover, this method is particularly stressing for the patient as he or she should be kept immobilized in order to minimize distortion (Feng *et al.*, 2010; Kai *et al.*, 2000). In order to overcome such limitations, the digital method was introduced, which relies on advanced methods of reverse engineering.

The digital method has fewer process steps than the conventional method but requires access to several technologies. In a broad sense, the digital method entails three main steps, namely, data acquisition, computer-aided design (CAD) and additive manufacturing (AM)-based technologies. In the last two decades, several authors have attempted to apply the digital method in the design and manufacturing of facial

prostheses. However, the increase in the number of patients and the cost constraints request a further investigation of this approach in order to increase the efficiency, reduce the delivery times and costs and improve the quality of the final product (Ciocca *et al.*, 2010; Fantini *et al.*, 2013; Feng *et al.*, 2010; Kai *et al.*, 2000; Palousek *et al.*, 2013; Sun *et al.*, 2011; Sun *et al.*, 2013; Wang *et al.*, 2011). This demand motivates the present study. Therefore, a full engineering-based approach for producing custom-made nasal prosthesis is outlined.

The main contribution of this study is the completeness of the description of the proposed methodology. Indeed, the fabrication of custom-made nasal prosthesis entails several key points, which are widely discussed, such as the retention system, the aesthetic features, the patient comfort and the costs and time demands. Furthermore, the proposed approach is wide-ranging, which means that with a few adjustments, it can be applied to fabricate silicone prostheses of other soft-tissues structures (e.g. ears).

Figure 5.1 - Nasal prosthesis's design and manufacturing steps: (a) 3D reconstruction of patient's face by CT images, (b) direct face scanning to create a digital nose database, (c) selection and alignment of virtual nose model, (d) surface fitting and trimming of the virtual prosthesis model, (e) smoothing and cutting operations to create functional nostrils on the prosthesis, (f) virtual model of outer mould, (g) plastic model of outer mould, (h) wood box, (i) silicone casting inside the wood box, (j) silicone mould, (k) virtual model of inner mould, (l) plastic model of inner mould, (m) plastic model of inner mould inside the silicone mould, (n) silicone nose prosthesis, (o) silicone nose prosthesis on the prototyped plastic model of the patient's face, (p) CAD model of the substructure, (q) plastic model of the substructure, (r) CAD assembly of the substructure with the eyeglasses and (s) silicone nose prosthesis with the eyeglasses.

5.2. Technique

An 80-year-old woman with a total defect of the nose is considered as case-study. The patient had been submitted to a total rhinectomy for treatment of an advanced squamous cell carcinoma involving the full thickness of the nose. Also, she was admitted to adjuvant radiotherapy and is free of disease at 3 years follow-up. The medical team does not recommend surgical reconstruction due to patient's advanced age and technical complexity (at least 3 surgeries with bone transfer from the skull or rib).

The nasal defect was evaluated to identify possible restorative limitations regarding retention and aesthetics. Several alternatives of prosthetic rehabilitation were discussed with the patient. The fabrication of a silicone nasal prosthesis was planned, and the expectations of this treatment were explained to the patient (Kai *et al.*, 2000).

Regarding the retention system, a non-invasive solution was recommended by the medical team. With the patient being an eyeglasses user, a substructure combining her eyeglasses and the nasal prosthesis was projected.

This system takes advantage from the nose cavity for prosthesis retention and the eyeglasses for support and placement.

An engineering-based approach for design and fabrication of a customized nasal prosthesis is presented throughout this study. Figure 5.1 depicts some steps of the proposed methodology, which includes the following six main tasks:

1. Data acquisition;
2. 3D reconstruction;
3. Prosthesis design;
4. Moulds fabrication;
5. Prosthesis manufacturing;
6. Final fittings.

For sake of prosthesis's endurance and hygiene, it is recommended to the patient to have a second prosthesis, which can be fabricated by repeating the last two tasks (steps 5 and 6).

It is noteworthy that, to perform this study, ethical approval was granted from the local ethics committee of the author's institute, and informed consent was obtained from the patient.

5.2.1. Data acquisition and 3-D reconstruction

Computed tomography (CT) scans (SOMATOM Sensation Cardiac 64, SIEMENS AG, Forchheim) were acquired for clinical purposes. Thus, the resultant set of DICOM images, which comprises a total of 176 slices with 1 mm of increment (i.e. axial thickness) and a pixel size of 0.283 mm, is utilized in this project. MIMICS 16.0 (Materialise, Leuven) is used for image segmentation and, therefore, for virtual reconstruction of patient's face (Figure 5.1a). The output of this task is a STL file of a three-dimensional (3D) model of the patient's face. It is important to mention that if imagiologic data are not available in the patient's clinical records, an optical-based method should be used for data acquisition of patient's face, because it is a less novice and less expensive technique.

For the reconstruction step, in cases of single and/or asymmetric organs such as the nose, the natural shape of a suitable donor must be used. There are several typologies of noses, such as the Roman, the Greek, the Cogitative and so on (Palousek *et al.*, 2013; Fantini *et al.*, 2013). Thus, a digital database of nose models was constructed. The nose models were acquired by direct face scanning of some individuals (Figure 5.1b) using a structured light scanner (ATOS III Triple Scan, GOM mbH, Braunschweig). This reverse engineering system has two high-resolution cameras (8,000,000 pixels), and it allows for exporting the 3D models in STL format. Prior to the direct face scanning, the individuals were made up to minimize the optical distortion features of the skin surface such as reflection, transparency and brightness. A prototype of patient's face is built by SL-stereolithography (Viper™ SLA® System, 3D Systems® Corporation, Rock Hill, SC). Within this study, a distance of 0.05 mm between layers was adopted in each SL-stereolithography operation. All plastic models are submitted to a post-processing treatment, which includes a three-step cleaning procedure, two steps of 2 h in water and one of 5 min in alcohol, and then a cure of the plastic model into an ultraviolet (UV) chamber. From time to time, the samples are sanded to remove layer steps and to smooth out contours.

5.2.2. Prosthesis design

From the digital database, a nose model was chosen, taking into account the patient's defect (Figure 5.1c) and previous photographs. Afterwards, using in 3-matic 8.0 (Materialise), the modelling task is carried out. This software allows the manipulation of the digital nose model (move, rotate, align, etc.) until the best-fit between the patient's face and the nose model is achieved. The design process entails several modelling operations: (a) alignment of the nose with patient's face (Figure 5.1c), (b) adjustment of the nose to the patient's face in terms of shape and adhesion to the skin surface (Figure 5.1d) and (c) surface fitting, trimming and smoothing (Figure 5.1d and 5.1e).

5.2.3. Moulds fabrication and prosthesis manufacturing

The design process of the moulds (outer and inner moulds) was performed in 3-matic software (Figure 5.1f and 5.1k). During the design process of the inner mould (core), two cylinders were placed inside the nose nostrils in order to produce a functional prosthesis (Figure 5.1e). Also, a small cut was carried out at the rhinion region aimed at providing a support for the prosthesis assembly inside the nose cavity (Figure 5.1e).

The moulds and prosthesis are manufactured using a standard procedure of silicone processing that entails the following steps:

1. SL-stereolithography of the outer and the inner moulds (Figure 5.1g and 5.1l);
2. Constructing of the wood box (Figure 5.1h);
3. Placing of the prototyped model of the outer mould in a central position and covering the casting surfaces with release agent (Figure 5.1h);
4. Casting the silicone (silicone rubber VTX 950), curing and subsequent removal of the prototyped model (Figure 5.1i and 5.1j).
5. Prosthetic silicone vacuum casting and insertion of the prototyped model of the inner mould (Figure 5.1m). The prosthetic silicone (Dragon skin®, Smooth-On) colour is matched to the patient's skin;

6. Curing and subsequent removal of the prototyped model of the inner mould (core) to obtain the silicone nasal prosthesis (Figure 5.1n).

5.2.4. Final fittings

Figure 5.2 illustrates the patient with the prosthesis, which has a substructure as retention system that links the prosthesis to patient's eyeglasses (Figure 5.1r and 5.1s). This substructure was designed in 3-matic software (Figure 5.1p) and fabricated by SL-stereolithography (Figure 5.1q). To be ready for delivering, the prosthesis is submitted to an extrinsic colouring in order to get a more realistic appearance.

5.3. Discussion

The proposed methodology was validated experimentally with the assembly of the prosthesis on the prototype of patient's face (Figure 5.1o) and later *in vivo* by means of the prosthesis application on patient (Figure 5.2). For sake of discussion, three parameters were analysed, namely, the retention system, the aesthetics outcomes and the time demands and costs.

5.3.1. Retention system

The preliminary retention system test (on prototype of patient's face) demonstrated sufficient retention strength, appropriate fitting (by the internal silicone support) and easy placement (and replacement). The material properties are also good for cleaning. Within this first evaluation, the retention system was considered to be ready for the in vivo test.

The results of retention system tested on the patient confirm the preliminary results. The anatomical shape of the retention system fits well on nose cavity that permits a correct placement of the prosthesis, leaving no open margins in the contact region. The eyeglasses, combined with the prototyped substructure, provide support and promote

the vertical placement. As a consequence, the patient did not have to use skin adhesives to retain the prosthesis, which are uncomfortable and costly.

5.3.2. Aesthetic outcomes

The aesthetics outcomes include several characteristics such as fitting (shape and proportion), accuracy (position and alignment), colour and resolution (reproduction of folds, wrinkles and/or textures).

In terms of fitting, the marginal integrity of the prosthesis against the patient's face surface reveals satisfactory results, that is, the prosthesis boundary matches with face's prototype. To assess the degree of fit, the evaluation protocol proposed by Sun *et al.* (2013) was adopted, which Downloaded from entails distance measurements and a nasal–facial proportion test (see Figure 5.2). The obtained results are listed in Table 5.1. The distance measurements and nasal–facial proportion test confirm the good fit of the nasal prosthesis.

The accuracy of soft-tissue prosthesis is essentially a subjective visual assessment. The prosthesis should be convincing in restoring the appearance of the patient. In this case, it is assumed that the prosthesis has the correct size, position and anatomical shape, capable of restoring the fault limb. The agreement between the standard values and the distance and nasal–facial proportion measurements (Table 5.1) also support this conclusion.

The nasal prosthesis presents a skin colour similar to the patient's skin tone. However, it is not able to reproduce the specificity of some facial features as delicate skin folds, wrinkles, texture, among others. An extrinsic colouring may give a valuable help on this matter, therefore further work needs to be done.

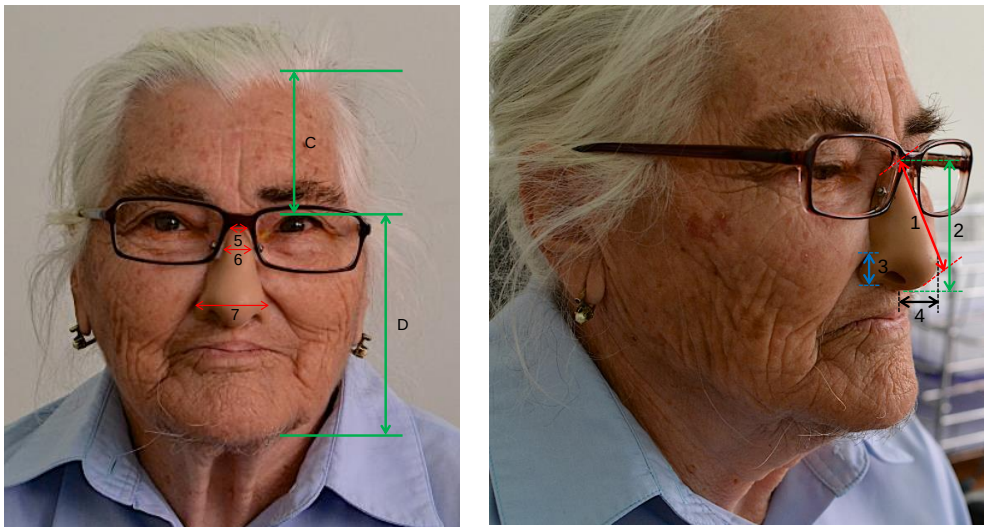

Figure 5.2 Patient with the prosthesis before extrinsic colouring (with patient's permission).

Table 5.1 Distance measurements and nasal–facial proportion measurement.

	Item	Developed Prosthesis [mm]	Prosthesis of Sun et al.[6] [mm]	Standard Value [mm]
Distance Measurements	1 Nose length	48.89	52	48-53
	2 Nose height	54	56.2	54-58
	3 Nasal ala height	13.11	13.1	13.2
	4 Nose protrusion	17	19	17-19
	5 Nasal root breadth	10	10.2	≈ 10
	6 Nasal tip breadth	13.33	13.0	12
	7 Nose width	36	39.0	37.6 ± 1.31
Nasal-facial Proportion	$\frac{C}{D}$	$\frac{70}{108.22} = 0.647$	$\frac{78.75}{129.87} = 0.606$	≈ 0.618
	$\frac{Nose\ width}{Nose\ height}$	$\frac{36}{54} = 0.667$	$\frac{39}{56.2} = 0.693$	≈ 0.618

5.3.3. Time demands and costs

Table 5.2 lists the minutes required to perform each task and also the costs associated with it. In comparison to recent studies, that indicate delivery times of 19 h, 11 min and 27 h, 20 min (Fantini *et al.*, 2013), the presented approach demonstrated to be

remarkable as it offers competitive delivery times (21 h, 39 min). Regarding costs, the proposed methodology leads to cost savings in contrast to the manual procedure, which has a total cost of approximately €651 per prosthesis (Fantini *et al.*, 2013).

5.3.4. Patient satisfaction

According to patient's report, she is very satisfied with the prosthesis in several aspects: aesthetic, local attachment, cleanliness and usage. The patient mentioned that the nasal prosthesis brought significant improvements to her quality of life and enhancements to her social life, where no one looks anymore at her as an aberration or with any discrimination. To conclude, the patient expressed her gratitude, and confessed that she never thought that having an ordinary appearance again could make her so happy. Now, her grandchildren no more fear her and enjoy being with her.

Table 5.2 Costs and time demands.

Steps	**Time (minutes)**	**Costs (€)**
1. Digital nose library	**30** (*Structured light scanning*) **60** (*STL files manipulation*)	**60** (by an engineer)
2. 3-D Reconstruction	**12** (*3-D modelling: MIMCS/3-matic*) **240** (*SL-stereolithography*: *patient's face*)	**8** (by an engineer) **160** (SL service)
3. Prosthesis Design	**60** (*3-D modelling*: *3-matic*)	**40** (by an engineer)
4. Moulds Fabrication	**60** (*3-D modelling*: *3-matic*) **240** (*SL-stereolithography*: *moulds*) **15** (*Constructing of the wood box*) **10** (*Silicone casting*) **240** (*Cure*)	**40** (by an engineer) **160** (SL service) **7.5** (silicone and other consumables)
5. Prosthesis Manufacturing	**10** (*Vacuum casting*) **240** (*Cure*)	**2.5** (silicone and other consumables)
6. Final Fittings	**12** (*SL-stereolithography*: *substructure*) **10** (*Assembly with substructure and eyeglasses*) **60** (*Extrinsic Colouring*)	**8** (substructure) **15** (eyeglasses) **150** (by an artist)
Total	**1299**	**651**

5.4. Key points

- The proposed methodology revealed encouraging results in comparison with the conventional method (manual procedure by an anaplastologist) since it saves time, reduces costs, and at the same time allows the attainment of prosthesis with the minimum contact and discomfort for the patient, disclosing excellent results in terms of aesthetic and function.
- The adopted retention system presents an anatomical shape that fits well on nose cavity allowing the correct placement of the prosthesis without any open margins around the contact region. The vertical placement of the prosthesis is ensured by the eyeglasses.
- Studies on methods for improving the surface resolution of the nasal prosthesis are pointed out as upcoming developments. Manual sculpting of plastic molds could be a solution to achieve silicone prostheses with customized skin features, such as folds, wrinkles and textures. Nonetheless, alternative techniques with some level of automation are preferable.

References

Amarante, J., Reis, J., Costa-Ferreira, A., Malheiro, E., Silva, A., 2006. Head and neck reconstruction: a review of 117 cases. Microsurgery 26(7), 519–523.

Ciocca, L., Fantini, M., De Crescenzio, F., Persiani, F., Scotti, R., 2010. New protocol for construction of eyeglasses-supported provisional nasal prosthesis using CAD/CAM techniques. J. Rehabil. Res. Dev. 47(7), 595–604.

Costa-Ferreira, A., Reis, J., Rebelo, M., Natividade-Silva, P., Amarante, J., 2007. 'Non-microsurgical' ear replantation – Baudet's technique revisited. J. Plast. Reconstr. Aes. 60(3), 325–327.

Fantini, M., De Crescenzio, F., Ciocca, L., 2013. Design and rapid manufacturing of anatomical prosthesis for facial reconstruction. Int. J. Interact. Des. Manuf. 7, 51–62.

Feng, Z., Dong, Y., Zhao, Y., Bai, S., Zhou, B., Bi, Y., Wu, G., 2010. Computer-assisted technique for the design and manufacture of realistic facial prostheses. Br. J. Oral Maxillofac. Surg. 48, 105–109.

Horta, R.M., Barbosa, R., Marques, M., Rebelo, M., Ferreira, A., Reis, J.C., Amarante, J.M., 2009. Reconstruction of the middle third of face with the temporal flap. Ann. Plast. Surg. 63(3), 288–291.

Kai, C.C., Meng, C.S., Ching, L.S., Teil, L.S., Aung, S.C., 2000. Facial prosthetic model fabrication using rapid prototyping tools. Integrated Manuf. Syst. 11, 42–53.

Palousek, D., Rosicky, J., Koutny, D., 2013. Use of digital technologies for nasal prosthesis manufacturing. Prosthet. Orthot. Int. 38, 171–175.

Seçilmiş, A., Öztürkb, A.N., 2007. Nasal prosthesis rehabilitation after partial rhinectomy: a clinical report. Eur. J. Dent. 2, 115–118.

Sun, J., Xi, J., Chen, X., Xiong, Y., 2011. A CAD/CAM system for fabrication of facial prostheses. Rapid Prototyping J. 17(4), 253–261.

Sun, J., Chen, X., Liao, H., Xi, J., 2013. Template-based framework for nasal prosthesis fabrication. Rapid Prototyping J. 19(2), 68–76.

Wang, J-X., Liao, S-H., Zhu, X-H., Wang, Y., Ling, C-X., Ding, X., Fang, Y-M., Zhang, X-H., 2011. Real time 3D simulation for nose surgery and automatic individual prosthesis design. Comput. Meth. Prog. Bio. 104, 472–479.

V

Conclusions

1. Conclusions

Industrially-driven research, even compromising scientific publications and limiting knowledge dissemination, has an extraordinary impact in promoting productive economy, as long as the opportunities created are fully and properly exploited.

The challenge in early 2005 of contra-gravity casting of aluminium alloys in plaster moulds, which is an extremely closed technology, was partially and successfully implemented at industrial level in Zollern & Comandita Portugal (ZCP). The build-up of a large team of highly qualified human resources with complementary competences, specific knowledge and advanced methodologies was clearly the main driving force for this very ambitious project.

The leading edge titanium casting process for compressor wheels allowed the development and operationalization of a complex melting and pouring system with vacuum-controlled atmosphere and ceramic and copper crucibles. This system was successfully used for the technology development of the casting of nickel alloys and titanium aluminides for turbocharger and turbo reactor applications, as well as cobalt chromium alloys and titanium alloys for knee prosthesis applications and other medical prosthesis.

The main innovation of the furnace operating at INEGI since 2008, still commercially unavailable, is its high frequency power source, proper for the low stirring of the melted alloys, promoting soft melting and reduced contamination by inclusions, oxygen and oxide films that usually occur due to the erosion of the ceramic crucibles, as well as its semi-levitation capacity with copper cooled crucibles. The operation of this furnace was an extraordinary milestone for INEGI and ZCP, because it was revealed crucial for the foundry research program in the field of reactive alloys. After 7 years of active research for automotive industry, this equipment proved also to be crucial for the INEGI's research group in other important industrial sectors. Although having own furnaces, ZCP still continues to use INEGI furnace to test some castings in different frequency conditions or just for time saving in their mass production furnaces.

This multi system furnace, with versatility for ceramic and copper crucibles, are now being used with success for leading edge technology of final steps development of casting solutions for titanium aluminides turbines using ceramic crucibles and ceramic shell moulds, as well as for casting conventional titanium Ti6Al4V for medical custom-fit and standard prostheses. Titanium aluminides turbines are in the final step of development at Zollern and industrial implementation of titanium prostheses production are also possible to be implemented.

Yttria-based face-coat and alumina-based back formulations for shells were successfully developed for conventional titanium alloys and titanium aluminides, but cheaper solutions for the later are still demanded to bring raw materials and sintering costs closer to that of the traditional investment casting. These alternative solutions are expected to be easily implemented when the turbocharger market asks for mass production.

A complex solution for face-coats to cast combustion chamber heat-shields for turbo reactors was developed, and is being used for industrial limited series production, based on the experience and sensitivity acquired during the work above mentioned.

The third generation of cold skull contra-gravity casting furnace, already fully operational, is promising, but collides with an already published patent, so it can only be used for internal purposes. However, its development enhanced the development of special brazing techniques with controlled atmosphere for the repairing and manufacture of cold skull copper crucibles, which can be very interesting in the point of view of reducing operational cost in the future.

In order to scientifically support these melting and pouring developments, numerical tools based on own numeric models and experimental validation were intensively used, accelerating the development process. INEGI also acquired the commercial ProCAST software for the design of gating and risering systems, both for internal work on reactive alloys and for ZCP, complementing their own Magma Soft software. Currently, simulation is an established virtual tool in both institutions, reducing experimental casting trials to define fine mould layouts and casting parameters, saving time and money.

Driven by the needs of extending expensive experimental facilities and highly qualified human resources, it was demonstrated that investment casting technology combined with software for medical images manipulation is a powerful solution for the production of custom fit prosthesis, a methodology supported on the AM of wax printing, alternatively to milling and direct metal laser sintering or other AM metal processes. This was also benefits the series production of standard prostheses for OEM', as demonstrated in the ongoing Medcast project with ZCP .

For low thickness prosthesis, like craniomaxilofacial parts, the casting followed by chemical milling is also promising, in alternative to the 5-axis direct milling, recently installed at INEGI, or to the incremental sheet forming of titanium alloys (ongoing project at INEGI). Chemical milling is a traditional way to remove alpha-case but it can also be used to reduce thickness to a level impossible to produce by direct casting.

Medical prostheses market is very difficult to explore because it is dominated by well-established entrepreneurs. However, as demonstrated by the actual potential ZCP clients in the field of cobalt-chromium alloys, having technology, even as an OEM supplier, is always a good way to enter the market (may be the best one).

The methodology developed for titanium prosthesis, combined with reverse engineering, with some cases of clinical success, proved to be extremely useful to manufacture parts for extra-oral applications, and requiring highly skilled artisans only for finishing characterization. Extra oral prosthesis is not a large market, but at least, for humanitarian and some economic reasons, the work already developed at INEGI can be helpful on making it available where the people needs them. These methodologies, considered a priority at INEGI, created a set of highly qualified human resources that can offer to the market a differentiated technology platform. In the future, a full engineered process could be designed to address the final manufacturing of soft bio-compatible external prosthesis, and even potentially including living cells. Such engineering platform could be developed from the human, technical and dissemination resources already available at INEGI.

2. Future work

The aim is to continue top-level industry-driven research and overcame the limited scientific dissemination, in order to attract more researchers for the current research fields, promoting knowledge and be internationally recognized to enhance access to international partnerships.

Based on all the previous work, the following topics can be expected for its future development:

- Regarding metal refractory reactions, economic alternatives based on zircon, zirconia and mixtures with low cost fine yttria can be a cheaper solution for ceramic moulds face-coats. In this field, an extended work must be done to solve problems of hot tearing of the castings and some lack of permeability that reduces the alloy fluidity. In what considers furnaces, to study and prepare investments in large capacity melting and pouring based on cold skull induction furnace, to overcome the melting capacity limitations and be closer to the real world of industrial implementation. This option can be extremely useful for continuing leading-edge developments on the promising world of titanium alloys and titanium aluminides casting process for turbo reactor, and also for the highest quality world of turbocharger applications. Research should also focus on alternatives for the ceramic shells and ceramic crucible formulations, and on manufacture methodologies for other clients than Zollern, owner of the current solutions, pushing for projects with other industrial companies particularly international, since the investment casting sub-sector in Portugal is limited to Zollern. Due to the global sustainability concerns of the common material for slurries and stuccos, zircon, one of the most used material for sanitary bathrooms applications and ceramic floors and tiles in the world, which demands are growing exponentially, is fundamental to find good technical and economic alternative solutions for investment casting industry. Alumina-based slurries and stuccos seem to be the most feasible alternatives.

  To enter in the world of metal-additive manufacturing, considered a key-technology towards sustainability and energy optimization and the only way to produce topologically optimized parts, namely prostheses. This must be done considering that

these processes are excellent product development tools and small series production for customized products, and that they must be compared with more conventional technologies of casting and milling, among others. Once having limited but extraordinary experimental facilities, two main areas demand research:

- Development of metal-matrix composites processes based on casting, and processes close to it, like squeeze casting infiltration of ceramic fibres and gas infiltration processes, for aerospace and automotive applications;
- Development of manufacturing processes for metallic foams products with controlled porosity, based on casting process for normal and topologically optimized products, namely for prostheses and other applications like fuel cells membranes.

VI

Publications

1. Publications

Neto, R., Marques, T., Marta, M., Leal, N., Couto, M., Machado, M., 2015. *Digital-based engineering tools for tailored design of medical implants*. Proceeding of the 5th European Conference on Mechanisms Science (EUCOMES), Guimarães, September 16-20, 2014.

Csáky, V., **Neto, R.**, Duarte, T., Alves, J.L., Couto, M., Machado, M., 2015. A framework for custom design and fabrication of cranio-maxillofacial prostheses using investment casting. Proceedings of the 4th International Conference on Engineering Optimization (EngOpt), Lisbon, 8-11 September, 2014.

Neto, R., Costa-Ferreira, A., Leal, N., Machado, M., Reis, A., 2014. An engineering-based approach for design and fabrication of a customized nasal prosthesis. *Prosthetics and Orthotics International*, pii: 0309364614535232.

Silva, P.F., Leal, N., **Neto, R.J.**, Lino, F.J., Reis, A., 2012. Custom hip prostheses by integrating cad and casting technology. *AIP Conference Proceedings 1479 - Numerical Analysis and Applied Mathematics* (ICNAAM 2012), 1596-1599.

Oliveira, I., Leal, N., Silva, P., Ferreira, A.D., **Neto, R.**, Lino, F.J., Reis, A., 2012. Advanced engineering tools for design and fabrication of a custom nasal prosthesis. *AIP Conference Proceedings 1479 - Numerical Analysis and Applied Mathematics* (ICNAAM 2012), 1592-1595.

Reis, A., Xu, Z., Tol, R.V., **Neto, R.**, 2012. Modelling feeding flow related shrinkage defects in aluminum castings. *Journal of Manufacturing Processes* 14(1), 1-7.

Duarte, T.P., **Neto, R.**, Félix, R., Lino, F.J., 2008. Optimization of Ceramic Shells for Contact with Reactive Alloys. *Materials Science Forum* 587-588, 157-161.

Lino, F.J., Vasconcelos, P.V., **Neto, R.J.**, Paiva, R., 2008. Stereolitography, the front edge of Rapid Prototyping. *Materials Science Forum* 587-588, 998-1002.

Cunha, A., Macedo, H., Lino, F.J., Vasconcelos, P.V., **Neto, R.J.L.**, 2007. Freedom of creation lighting objects using rapid prototyping. *IV International Materials Science*, Porto, Portugal.

Lino, F.J., Baptista, A.M., **Neto, R.J.L.**, 2006. Tribological behaviour of epoxy based composites for rapid tooling. *Wear* 260, 30-39.

Vasconcelos, P.V., Lino, F.J., Magalhães, A., **Neto, R.J.L.**, 2005. Impact fracture study of epoxy-based composites with aluminium particles and milled fibres. *Journal of Materials Processing Technology* 170, 277-283.

Lino, F.J., **Neto, R.J.L.**, Paiva, R., Moreira, A., 2004. Rapid prototyping and rapid tooling applied in product development of ceramic components. *Materials Science Forum* 455-456, 835-838.

Vasconcelos, P.V., Lino, F.J., van Hattum, F.W.J., **Neto, R.J.L.**, 2004. Mathematical models for particulate filled and milled fibre reinforced composites. *Materials Science Forum* 455-456, 742-745.

Vasconcelos, P.V., Lino, F.J., **Neto, R.J.L.**, Henrique, P., 2004. Contribution of the phase-matrix interface to the behaviour of aluminium filled epoxies. *Materials Science Forum* 455-456, 635-638.

Duarte, T.P., Lino, F.J., Barbedo de Magalhães, A., **Neto, R.**, Ferreira, J.M.F., 2004. Conversion of rapid prototyping models into metallic tools by ceramic moulding - an indirect rapid tooling process. International Journal of Materials and Product Technology 4, 317-330.

Vasconcelos, P.V., Lino, F.J., **Neto, R.J.**, Teixeira, A., 2003. Glass and Carbon Fibre Reinforced Hybrid Composites for Epoxy Tooling. Article Contest on Preparation of Composite Materials. *Struers Journal of Materialography, Struers* 40, 3-5.

Vasconcelos, P.V., Lino, F.J., **Neto, R.J.L.**, 2002. The importance of rapid tooling in product development. Key Engineering Materials 230-232, 169-172.

Santos, A.D., Ferreira Duarte, J., Reis, A., Barata da Rocha, A., **Neto, R.**, Paiva, R., 2001. The use of finite element simulation for optimization of metal forming and tool design. Journal Of Materials Processing Technology 119(1-3), 152-157.

Vasconcelos, P., Lino, F.J., **Neto, R.J.**, 2001. O fabrico rápido de ferramentas ao serviço da engenharia concorrente. *Tecnometal*.

Lino, F.J., Vasconcelos, P.V., Paiva, R., **Neto, R.J.**, 2004. Rapid Tooling for Plastic Injection Moulding Using Indirect Rapid Tooling Processes. *13th International Conference on Processing and Fabrication of Advanced Materials* (PFAM XIII), 664-698.

2. Guidance of Graduation Final Projects

Alves, Bruno Miguel Matos, 2004. *Desenvolvimento do Processo de Fabrico de Impulsores para Turbocompressores de Automóveis.* Mechanical Engineering Degree – Injection Molding Option, Faculty of Engineering of University of Porto.

Costa, Paulo Miguel Oliveira, 2004. *Estudo do Efeito de Defeitos na Vida à Fadiga de Componentes em Ferro Fundido Nodular.* Mechanical Engineering Degree – Manufacturing and Mechanical Technology Option, Faculty of Engineering of University of Porto.

Ala, Pedro Miguel da Fonseca, 2003. *Fabrico Rápido de Ferramentas por Conversão Indirecta com Silicones.* Mechanical Engineering Degree – Manufacturing and Mechanical Technology Option, Faculty of Engineering of University of Porto.

Begonha, Gonçalo Botelho Gomes, 2003. *Introdução ao Estudo e Desenvolvimento do Processo de Fundição de Ligas de Magnésio para a Indústria Automóvel.* Mechanical Engineering Degree – Manufacturing and Mechanical Technology Option, Faculty of Engineering of University of Porto.

3. Guidance of MSc Dissertations

Torres, Francisco Faria Ricca de Ancede, 2014. *Otimização do processo de obtenção de peças em aluminetos de titânio por fundição de precisão*. MSc in Mechanical Engineering, Faculty of Engineering of University of Porto.

Soares, Pedro André de Castro Moura, 2014. *Desenvolvimento do processo de laser cladding com metais para fabrico aditivo*. MSc in Mechanical Engineering, Faculty of Engineering of University of Porto.

Rocha, Marieta da Sousa, 2014. *Desenvolvimento do processo de produção de próteses crânio-maxilofaciais por processos alternativos à fundição*. MSc in Mechanical Engineering, Faculty of Engineering of University of Porto.

Pires, Nuno Leite De Sousa Da Silva, 2014. *Projeto e otimização de sistemas de alimentação e gitagem para peças em aluminetos de titânio*. MSc in Mechanical Engineering, Faculty of Engineering of University of Porto.

Moreira, Luís Filipe Minhava Peixoto Morais, 2014. *Desenvolvimento da metodologia de fabrico de protótipos de torneiras pelo processo de cera perdida*. MSc in Mechanical Engineering, Faculty of Engineering of University of Porto.

Mendes, Bárbara Flávia Carvalho Teixeira, 2014. *Desenvolvimento de metodologia digital para projeto e fabrico de próteses extraorais*. MSc in Mechanical Engineering, Faculty of Engineering of University of Porto.

Melo, Pedro Fernandes de Ataíde, 2014. *Estudo do processo de baixa pressão para ligas de cobre.* MSc in Mechanical Engineering, Faculty of Engineering of University of Porto.

Leite, João Miguel Castro, 2014. *Desenvolvimento da metodologia de projeto e fabrico de próteses articulares*. MSc in Mechanical Engineering, Faculty of Engineering of University of Porto.

Homem, Ricardo António Coimbras, 2014. *Estudo do processo de maquinagem de ligas de titânio*. MSc in Mechanical Engineering, Faculty of Engineering of University of Porto.

Gomes, Frederico Alpoim Da Silva, 2014. *Comparação de processos de fabrico aditivo que utilizam metais.* MSc in Mechanical Engineering, Faculty of Engineering of University of Porto.

Duarte, Ruben Miguel Monteiro, 2014. *Desenvolvimento do processo de fundição por baixa pressão para a obtenção de puxadores em ligas de alumínio*. MSc in Mechanical Engineering, Faculty of Engineering of University of Porto.

Csaky, Viktor, 2014. *Desenvolvimento do processo de produção de próteses crânio-maxilofaciais fundidas*. MSc in Mechanical Engineering, Faculty of Engineering of University of Porto.

Cortez, Pedro Manuel Araújo, 2014. *Estudo microestrutural da superliga de níquel GTD-111 durante o seu envelhecimento e após tratamentos térmicos de rejuvenescimento.* MSc in Mechanical Engineering, Faculty of Engineering of University of Porto.

Ribeiro, José Ricardo Faria, 2013. *Desenvolvimento e otimização do processo de obtenção de cavidades moldantes fundidas em aço*. MSc in Mechanical Engineering, Faculty of Engineering of University of Porto.

Gonçalves, João Pedro da Silva, 2013. *Melhoria do processo de obtenção de peças em ligas de titânio por fundição por cera perdida*. MSc in Mechanical Engineering, Faculty of Engineering of University of Porto.

Gomes, João Nuno Moniz, 2013. *Projeto de Equipamento para Soldadura Automática de Cera.* MSc in Mechanical Engineering, Faculty of Engineering of University of Porto.

Campos, Hugo Rogério Carvalho, 2013. *Otimização do processo de injeção de ceras no processo de fundição por cera perdida.* MSc in Mechanical Engineering, Faculty of Engineering of University of Porto.

Barrigana, Tiago Gradiz, 2013. *Estudo da reatividade de ligas de titânio e aluminetos de titânio fundidos com refratários de carapaças cerâmicas*. MSc in Mechanical Engineering, Faculty of Engineering of University of Porto.

Serôdio, João Pedro Ribeiro, 2012. *Desenvolvimento do processo de obtenção de turbinas em ligas de titânio e inconel.* MSc in Mechanical Engineering, Faculty of Engineering of University of Porto.

Magalhães, Álvaro Miguel Santos, 2012. *Desenvolvimento do processo de fundição de turbinas para turbocompressores em aluminetos de titânio*. MSc in Mechanical Engineering, Faculty of Engineering of University of Porto.

Fonseca, Bruno Pinheiro da, 2012. *Endurecimento estrutural de peças em ligas de alumínio injetadas*. MSc in Mechanical Engineering, Faculty of Engineering of University of Porto.

Silva, Sara Amorim da, 2011. *Aproveitamento sustentável da borracha proveniente dos pneus usados / Ecodesign uma nova abordagem no design de mobiliário urbano.* MSc in Industrial Design, Faculty of Engineering of University of Porto.

André, Gustavo Maria Mendes, 2011. *Desenvolvimento do processo de fusão e vazamento de ligas de níquel e aluminatos de titânio*. MSc in Mechanical Engineering, Faculty of Engineering of University of Porto.

Andrade, José Maria de Moncada Côrte-Real Freire de, 2011. *Desenvolvimento de um forno para fusão em cadinho frio e vazamento em contra-gravidade.* MSc in Mechanical Engineering, Faculty of Engineering of University of Porto.

Silva, Luís Pedro Freitas da, 2010. *Desenvolvimento de um forno para fusão em cadinhos frios e optimização das arquitecturas de moldações por simulação numérica*. MSc in Mechanical Engineering, Faculty of Engineering of University of Porto.

Leal, Nuno Emanuel Ferreira, 2010. *Desenvolvimento do processo de fabrico de próteses humanas em silicone para substituição de orgãos em tecidos moles*. MSc in Mechanical Engineering, Faculty of Engineering of University of Porto.

Gonçalves, Carlos Manuel Ribeiro, 2010. *Desenvolvimento da metodologia de projecto e fabrico de próteses à medida do paciente.* MSc in Mechanical Engineering, Faculty of Engineering of University of Porto.

Rocha, Bruno Adão da Silva, 2009. *Desenvolvimento do processo de produção de próteses em ligas de titânio*. MSc in Mechanical Engineering, Faculty of Engineering of University of Porto.

Marques, Flávio Dias Ferreira, 2009. *Desenvolvimento do processo de vazamento em coquilhas rotativas.* MSc in Mechanical Engineering, Faculty of Engineering of University of Porto.

Ferreira, José Pedro Mimoso, 2009. *Novos materiais para lavatórios, torneiras e puxadores.* MSc in Mechanical Engineering, Faculty of Engineering of University of Porto.

Martins, Bruno António Fernandes, 2008. *Desenvolvimento de um forno de indução para fusão e vazamento de ligas de titânio ti e outras ligas reativas com reprodutibilidade*. MSc in Mechanical Engineering, Faculty of Engineering of University of Porto.

Félix, Rui Manuel Carvalho, 2008. *Desenvolvimento de um forno de indução para fusão e vazamento de ligas de titânio ti e outras ligas reativas com reprodutibilidade*. MSc in Mechanical Engineering, Faculty of Engineering of University of Porto.

Costa, José Alberto Monteverde Loureiro, 2008. *Aumento da fiabilidade de moldes de fundição injetada*. MSc in Mechanical Engineering, Faculty of Engineering of University of Porto.

Alves, Bruno Miguel Matos, 2008. *Desenvolvimento do processo de fabrico de ferramentas de fundição elastoméricas para o processo de moldação em gesso*. MSc in Mechanical Engineering, Faculty of Engineering of University of Porto.

Antas, Ana Filipa Felgueiras, 2007. *Utilização das tecnologias de prototipagem rápida na área médica*. MSc in Industrial Design, Faculty of Engineering of University of Porto.

Pereira, Acácio José Viegas, 2006. *Desenvolvimento de novos produtos em vidro utilizando as tecnologias de prototipagem rápida*. MSc in Industrial Design, Faculty of Engineering of University of Porto.

Moutinho, Manuel José Pontes, 2006. *Desenvolvimento do processo de produção de componentes de magnésio em moldações não permanentes*. MSc in Mechanical Engineering, Faculty of Engineering of University of Porto.